TECHNISCHE UNIVERSITÄT DRESDEN

Technische Universität Dresden

Fakultät Mathematik und Naturwissenschaften

Fachrichtung Biologie

Dissertation

zur Erlangung des akademischen Grades

„Dr. rer. nat"

HEDGEHOG SIGNALING REGULATES MECHANICAL TENSION ALONG THE ANTEROPOSTERIOR COMPARTMENT BOUNDARY IN THE DEVELOPING *DROSOPHILA* WING

Vorgelegt von: **Diplom Biologin Katrin Rudolf**

Geboren am 27.01.1988 in Offenbach a.M.

Tag der Verteidigung: 04.08.2014

Gutachter: **Prof. Dr. rer. nat. Christian Dahmann**

Prof. Dr. rer. nat. Frank Jülicher

Bearbeitungszeitraum: 15.10.2011-12.06.2014

Dedicated to my grandparents

Hildegard Ueckert

Maria Rudolf

Ludwig Rudolf

1 ABSTRACT

The interplay between biochemical signals and mechanical processes during animal development is key for the formation of tissues and organs with distinct shapes and functions. An important step during the formation of many tissues is the formation of compartment boundaries which separate cells of different fates and functions. Compartment boundaries are lineage restrictions that are characterized by a straight morphology. Biochemical signaling across compartment boundaries induce the expression of morphogens in the cells along the boundaries. These morphogens then act at long-range to direct growth and patterning of the whole tissue. Compartment boundaries stabilize the position of morphogens and thereby contribute to proper tissue development. The straight morphology of compartment boundaries is challenged by cell rearrangements caused by cell division and tissue reshaping. Physical mechanisms are therefore required to maintain the straight morphology of compartment boundaries. The anteroposterior (A/P) compartment boundary in the developing *Drosophila melanogaster* wing is established by biochemical signals. Furthermore, mechanical processes are required to maintain the straight shape of the A/P boundary. Recent studies show that mechanical tension mediated by actomyosin motor proteins is increased along the A/P boundary. However, it was not understood how biochemical signals interact with mechanical processes to maintain the A/P boundary. Here I provide the first evidence that Hedgehog signaling regulates mechanical tension along the A/P boundary. I was able to show that differences in Hedgehog (Hh) signal transduction activity between the anterior and posterior compartments are necessary and sufficient to maintain the straight shape of the A/P boundary, which is crucial for patterning and growth of the adult wing. Moreover, differences in Hh signal transduction activity are necessary and sufficient for the increase in mechanical tension along the A/P boundary. In addition, differences in Hh signal transduction activity are sufficient to generate smooth borders and to increase mechanical tension along ectopic interfaces. Furthermore, the differential expression of the transmembrane protein Capricious is sufficient to increase mechanical tension along ectopic interfaces. It was previously suggested that mechanical tension is generated by an actomyosin-cable through which the increase in mechanical tension is transmitted between the junctions along the A/P boundary. Here I show that mechanical tension is generated locally at each cell bond and not transmitted between junctions by an actomyosin cable. My results provide new insights for our understanding of the interplay between biochemical signals and mechanical processes during animal development.

2 TABLE OF CONTENTS

3 TABLE OF FIGURES

4 LIST OF ABBREVIATIONS

- Δci^{94}	Loss-of function allele of *ci*
- A	Anterior
- Ā	Apical cross section area
- A/A	Interface between anterior cells
- A/P boundary	Anteroposterior compartment boundary
- Abl	Abelson kinase
- ant	anterior
- Ap	Apterous
- ATP	Adenosine triphosphat
- Boi	Brother of Ihog
- *bsk*	basket (gene)
- C1	First row inside the clone parallel to the clonal interface
- CALI	Chromophore –assisted laser inactivation
- *caps*	Capricious (gene)
- Caps	Capricious (protein)
- CD2	Cluster of differentiation 2
- *ci*	cubitus interruptus (gene)
- Ci	Cubitus interruptus (protein)
- ci^{-}	Loss-of function allele of *ci* (Δci^{94})
- ci^{PKA4}	constitutively active allele of *ci*
- Ci^{rep}	Cubitus interruptus (Repressor)
- Cos2	Costal2
- d	distance
- D	Dorsal
- D/V boundary	Dorsoventral compartment boundary
- DAH	Differential Adhesion Hypothesis
- DE-cadherin	Drosophila E-cadherin
- DITH	Differential Interfacial Tension Hypothesis
- Dl	Delta
- Dpp	Decapentaplegic
- *dpp*	Decapentaplegic (gene)
- Ds	Dachsous
- *en*	Engrailed (gene)
- En	Engrailed (protein)
- en^{-}	Loss-of function allele of *engrailed* (en^{E})
- en^{E}	loss-of function allele of *engrailed*
- F-actin	Filamentous actin
- FLP	Flippase
- Fng	Fringe
- FRT	Flippase Recognition Site
- Fu	Fused
- Fz	Frizzled
- GAL	Yeast transcription activatior protein
- GFP	Green fluorescent protein
- GFP-gpi	Membrane-anchored GFP
- *hh*	Hedgehog (gene)
- Hh	Hedgehog (protein)
- hh^{ts2}	Temperature-sensitive allele of Hedgehog
- HSC	Hedgehog signaling complex

- I — Pixel intensity
- Ihog — Interference Hedgehog
- JNK-pathway — c-Jun NH(2)-terminal kinase pathway
- L — average cell bond length
- MHB — Mid-hindbrain boundary
- MyoII — Myosin II
- *omb* — Optomotorblind (gene)
- P — Posterior
- P/P — Interface between posterior cells
- PCP — Planar cell polarity
- PKA — Protein kinase A
- post — posterior
- PS boundary — Parasegment boundary
- Ptc — Patched
- ROCK — Rho-kinase
- SEM — Standard deviation of the mean
- Ser — Serrate
- Smo — Smoothened
- SuFu — Suppressor of Fused
- *tkv* — thickveines (gene)
- Trn — Tartan
- UAS — Upstream activating sequence
- ubi — ubiquitous
- V — Ventral
- v_0 — Initial velocity
- *w* — Roughness
- W1 — First row of wild-type cells around the clone parallel to the clonal interface
- W2 — Second row of wild-type cells around the clone parallel to the clonal interface
- Wg — Wingless
- Wnt — Wint
- β-Gal — Beta-Galactosidase
- ϕ — Vertex angle

5 INTRODUCTION

5.1 ANIMAL DEVELOPMENT

Animal development is one of the most complex processes in nature during which a fully functional organism has to be built up from one single cell. The formation of highly specialized tissues and organs requires precise cell communication to orchestrate proliferation, differentiation, movement and, sometimes, cell death. Cells can communicate via secreted signalling molecules received by neighboring cells which regulate their pattern of gene expression and thereby their behavior. The regulation of gene expression is important for the cells to produce only those proteins which are necessary to conduct the cell's function at a certain time and place. In addition, during its development the embryo undergoes dramatic shape changes, which depend on mechanical forces, mediated by cytoskeletal motor proteins. Therefore, biochemical and mechanical processes have to act jointly to shape the embryo. However, the knowledge about the interplay between biochemical signals and mechanical processes during animal development is still very fragmentary. Understanding developmental processes in detail is of great importance since defects in biochemical signaling and mechanical processes are often involved in the emergence of human diseases.

5.2 CELL SORTING IS AN IMPORTANT PROCESS DURING DEVELOPMENT

The formation of tissues and organs with distinct functions is a crucial aspect of development. Tissues consist of cells with similar identities and functions. Implementation of biochemical signals by altering the pattern of gene expression can determine cell identities. Cells of a certain identity are able to recognize the cells of a different identity and actively sort out from them. Mechanisms of cell sorting are based on the cognition of cell identities. However, it is poorly understood how cell identities regulate cell sorting to ensure the formation of different tissues and organs. Different theories were phrased about how cell sorting is regulated and executed during development. In 1955 Townes and Holtfreter formulated the hypothesis that cells with different identities have different affinity properties and therefore sort out from each other (Townes and Holtfreter 1955). This was based on observations made on dissociated cells of the *Xenopus* embryo.

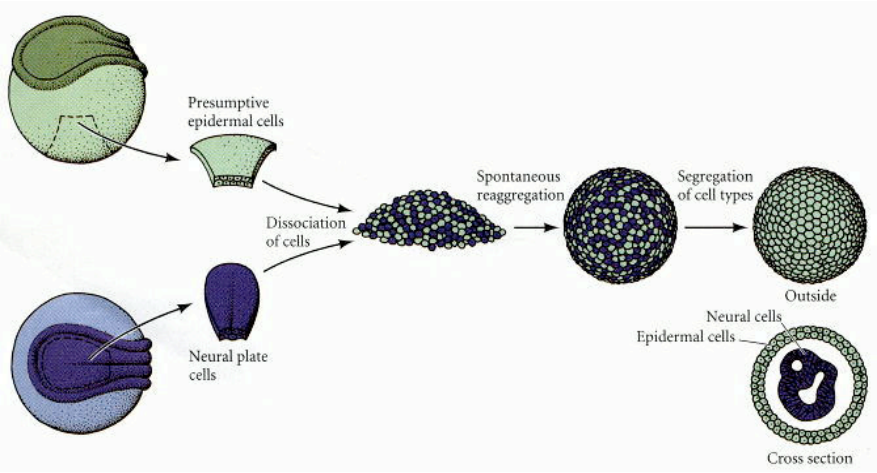

Figure 1: Cell sorting experiment by Townes and Holtfreter (Townes and Holtfreter 1955) in the *Xenopus laevis* embryo.
Tissue explants of the presumptive epidermis (green) and neural plate (blue) were dissociated using an alkaline solution and mixed with each other. The cells of both origins mixed in the spontaneously formed aggregate. Later the epidermal cells build up a sheath around the neural cells, which formed an aggregate in the center (Gilbert 2000).

The authors explanted tissue fragments from different regions of a *Xenopus* embryo during neurula stage. The explants taken from the presumptive epidermis and neural plate were dissociated to single cells and mixed with each other. After a while, the cells of both origins first reassembled and formed an aggregate again. Later on, they sorted out. Epidermal cells formed a layer at the periphery that enveloped neural plate cells in the centre of the aggregate (Figure 1). From these observations Townes and Holtfreter concluded that cells of different origin have different affinity properties. Considering the fact that neural cells always sorted to the centre of the aggregate, Townes and Holtfreter reasoned that the neural cells might have a stronger affinity to each other than epidermal cells. Malcolm Steinberg proposed in 1963 that differential adhesive properties mediate cell sorting. In his “Differential Adhesion Hypothesis” (DAH) he suggested that tissues behave like liquids and have a certain degree of surface adhesion (Steinberg 1963). Two adjacent tissues with different adhesive properties will sort out by minimizing the contact to each other. The strength of adhesion is mediated by the quantity of adhesion molecules. The contact between the cells with a similar quantity of adhesion molecules is thermodynamically more stable than the contact between the cells with different adhesion properties (Figure 2). Steinberg’s DAH was experimentally supported by measuring cell surface tension. The level of cell adhesion molecules proved to directly regulate the tissue surface tension of cells *in vitro.* Furthermore, this difference lead to cell sorting (Foty and Steinberg 2005). However, the contribution of differential adhesion properties to cell sorting events during embryonic development is still subject of discussion.

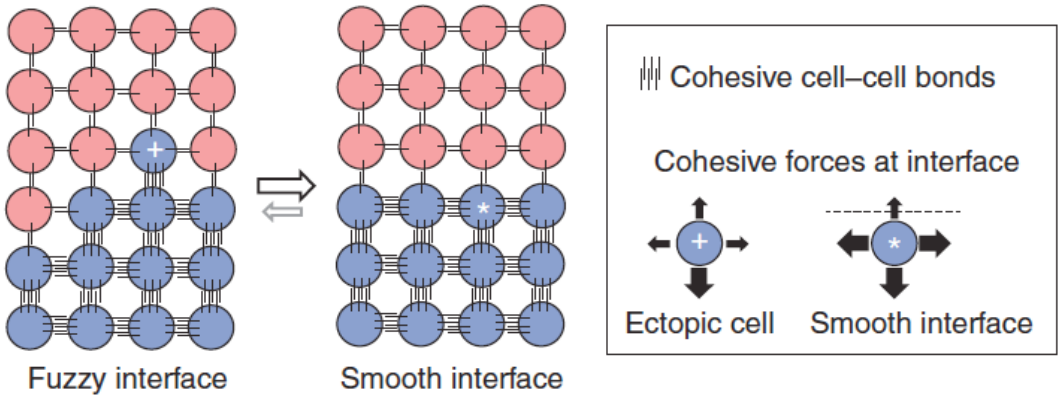

Figure 2: Differential Adhesion Theory by Malcom Steinberg (Steinberg 1963).
Different cohesive forces of cells are due to the quantity of adhesion molecules. Cells with similar cohesive forces tend to maximize the contact with each other because this connection is thermodynamically more stable than the connection to the cells with less adhesion molecules. This leads to cell sorting and thereby to smooth interfaces between adjacent groups of cells (modified after Batlle and Wilkinson 2012).

In a critique to Steinberg's theory, Harris proposed in 1976 that groups of cells are much more complex than liquids and that the DAH does not completely explain cell sorting events in animal development. One of his suggested alternative theories was the Differential surface contraction hypothesis (Harris 1976). Following this theory, sorting behavior would be due to differential surface contraction mediated by contractile molecules. Furthermore, the surface contraction between two groups of different identities is higher than between cells of the same identity, therefore mixing is prevented. Brodland combined Steinberg's and Harris's theories to the Differential Interfacial Tension Hypothesis (DITH) (Brodland 2002) by suggesting that differential cell adhesion and surface contraction lead to surface tension that mediates cell sorting.

5.3 CADHERINS AS MEDIATORS OF CELL ADHESION AND CELL SORTING

Cadherins were found to be mediators of cell adhesion. The calcium-dependent adhesion molecules are part of the adherens junctions and connect epithelial cells with each other at the apicolateral membrane of the cell. Through their experiments *in vitro* Takeichi and Nose showed in 1987, that cadherins form homophilic interactions and are connected to actin filaments (Takeichi, Atsumi et al. 1981, Nose and Takeichi 1986, Takeichi, Shirayoshi et al. 1986, Hirano, Nose et al. 1987). The intracellular domains of cadherins are connected to the actomyosin cortex via α- and β-catenin. E-cadherin is the main cadherin in epithelial tissues and forms homodimers to ensure the epithelial integrity of epithelial cells. In the *Drosophila* ovary, DE-cadherin (*Drosophila* E-cadherin) was found to be important for the correct sorting of the oocyte to the posterior pole of the egg chamber. The egg chamber consists of 15

nurse cells that provide the oocyte with nutrients and a sheath of somatic follicle cells covering the nurse cells and the oocyte. During development the oocyte has to move to the posterior pole of the egg chamber. The posterior follicle cells and the oocyte express higher levels of E-cadherin than the nurse cells or the other follicle cells (Godt and Tepass 1998). The strong adhesion between the oocyte and the posterior follicle cells maintains the posterior position of the oocyte. If E-cadherin is removed from the oocyte or the posterior follicle cells, the oocyte fails to position correctly (Godt and Tepass 1998). Differential expression of cadherins was additionally found to be involved in cell sorting processes in vertebrates (Price, De Marco Garcia et al. 2002). However, the precise contribution of the differential expression of cadherins to cell sorting during animal development is still unclear.

5.4 CELL SORTING ALONG COMPARTMENT BOUNDARIES

The formation of functional organs does not only require cell sorting between cells of different tissues but also the subdivision into adjacent groups of cells within a tissue, called compartments. Partitioning the tissue into compartments leads to the formation of boundaries between them, which are an important model system to study cell sorting in animal development. Compartment boundaries are lineage interfaces between two adjacent groups of cells that do not intermix (Garcia-Bellido, Ripoll et al. 1973; Lawrence 1973). Compartment boundaries have a straight and sharp morphology, which is important since they provide positional information for organizer structures which pattern the tissue and orchestrate growth to develop a correctly formed and functional adult organ (Basler and Struhl 1994; Capdevila and Guerrero 1994; Tabata, Schwartz et al. 1995; Zecca, Basler et al. 1995). Compartment boundaries were first discovered in the *Drosophila* wing. X-ray induced recombination was used to generate marked cells in the developing wing. The progeny of these marked cells grew to a clone later in development. Observing the localization of clones within the adult tissue revealed the existence of an invisible boundary between anterior and posterior cells, the A/P boundary (Figure 3 b). The clones never crossed this boundary and exhibited a straight interface when they abutted the A/P boundary but a wiggly interface towards other cells in the tissue (Garcia-Bellido, Ripoll et al. 1973; Garcia-Bellido 1975; Morata and Lawrence 1975). Compartment boundaries also exist for example in the *Drosophila* embryo between the anterior and posterior compartments within segments (Figure 3 a), as well as between the dorsal and ventral compartments in the wing (D/V boundary) (Figure 3 c). The D/V boundary, in opposition to the A/P boundary, is visible in the adult wing as it gives rise to the wing margin. The concept of compartment boundaries preventing cell mixing between adjacent groups of cells seems to be evolutionary conserved, since they exist in vertebrates as well. The embryonic vertebrate brain consists,

amongst others, of the midbrain and the hindbrain, which is subdivided into rhombomers (Figure 3 e,f). The mid-hindbrain boundary (MHB), as well as the boundaries between the rhombomers are compartment boundaries which are important for the correct patterning of the vertebrate brain (Fraser, Keynes et al. 1990; Langenberg and Brand 2005).

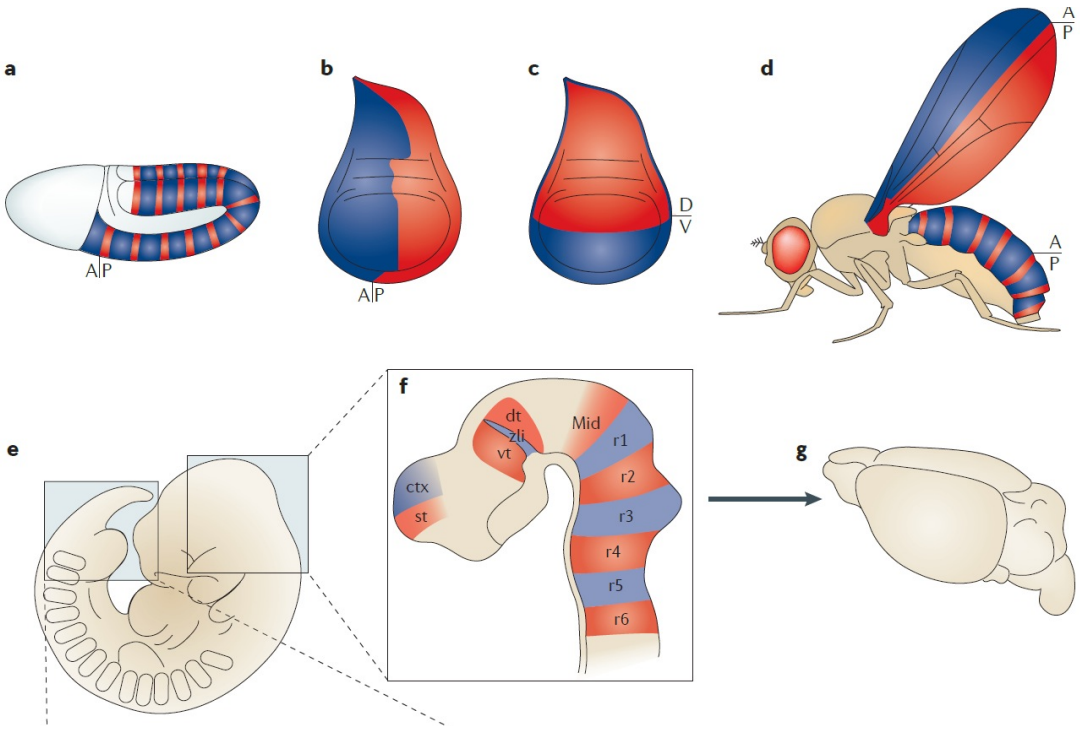

Figure 3: Compartment boundaries in insects and vertebrates.
Compartment boundaries subdivide segments in the *Drosophila* embryo (a). Between the anterior and posterior (b), as well as dorsal and ventral cells in the precursor of the adult wing (c), both of which are crucial for the correct development of adult structures (d). The compartment boundaries in the embryonic mouse brain between the mid- and the hindbrain and the rhombomers are important for the structure of the adult brain (g) (modified after Dahmann, Oates et al. 2011).

Eph-ephrin signalling was found to be required for boundary formation and the prevention of cell mixing along the compartment boundaries in the vertebrate hindbrain, (Mellitzer, Xu et al. 1999; Xu, Mellitzer et al. 1999). Eph-receptors which are receptor tyrosine kinases and the ephrin ligands are expressed alternating in odd and even rhombomers (Figure 4). Binding of Eph-receptors and ephrin ligands directly influences the cytoskeleton (Gale and Yancopoulos 1997; Kalo and Pasquale 1999) which leads to repulsion between cells of different compartments and increased adhesion between cells of the same segment (Kemp, Cooke et al. 2009). However, it is not yet fully understood how cell sorting is ensured along compartment boundaries and how their straight shape is maintained during development in insects and vertebrates.

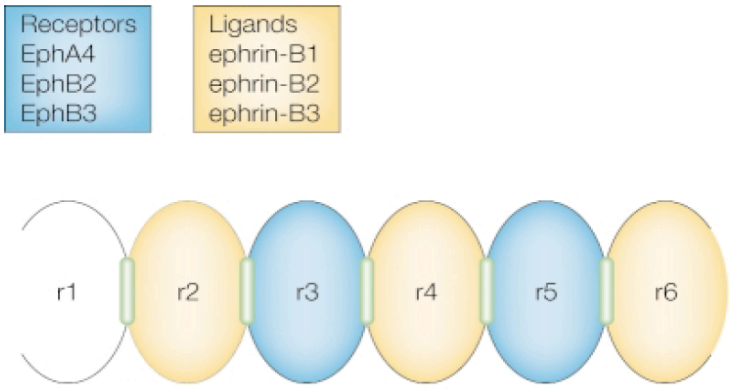

Figure 4: Eph-ephrin signalling mediates compartmentalization and cell sorting in the vertebrate hindbrain.
Eph-receptor tyrosine kinases and their ligands, ephrins, are expressed alternating in rhombomers in the vertebrate hindbrain. The receptors like EphA4 are expressed in odd- and ephrin-ligands in even-numbered rhombomers (modified after McNeill 2000).

5.5 *DROSOPHILA AS* A MODEL TO STUDY COMPARTMENT BOUNDARIES

Drosophila melanogaster is one of the most important model organisms for geneticists and developmental biologists since the early 20th century. The genome of *Drosophila*, which is completely sequenced, consists of about 14,000 genes located on four chromosomes. The dipteran insect has numerous advantages, like a short generation cycle, easy handling and a large number of progeny. After fertilization the embryo develops within 24h inside the egg before it hatches as a larva. The larva undergoes three stages, called instars, which are separated by three molting events. The first two instars last 24h and the third instar lasts 48 (at 25˚C). Late third instar larvae stop feeding at some point and crawl up from the food to pupate. During pupation metamorphosis takes place and after 5-6 days the adult fly hatches. It becomes fertile around 4 hours after hatching and can give rise to a new generation.

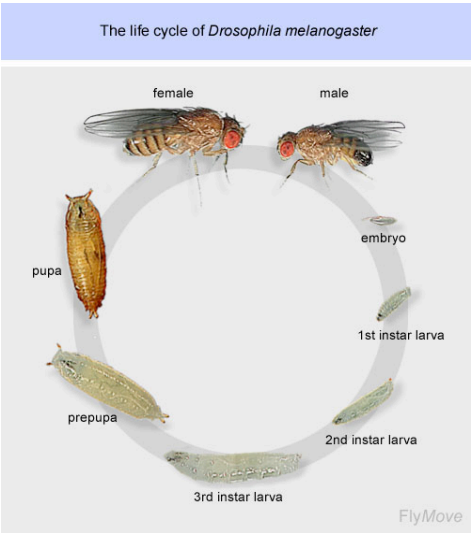

Figure 5: Life cycle of *Drosophila melanogaster.*
The embryonic development of *Drosophila melanogaster* lasts 24h after fertilization before the larvae hatch. Three larval stages, instars, separated by moltings last 24hrs for the first two and 48hrs for the third instar (at 25°C). The adult hatches after following 5-6 days before the larva pupates. (modified after Weigmann, Klapper et al. 2003).

During larval development the future appendages are preformed inside the larval body as epithelial monolayers, imaginal discs. Imaginal discs exist for the mouthparts, the antennae and eyes, legs, wings, halteres and genitalia. They form out of epithelial cells in the embryo, founder cells which are given a certain identity via the expression of selector genes (Garcia-Bellido, Ripoll et al. 1973; Lawrence 1973; reviewed by Lawrence and Struhl 1996). The early embryo is subdivided into parasegments (Martinez-Arias and Lawrence 1985) and the expression of selector genes depends on the position within parasegments. Two sets of founder cells from parasegment 4 and 5 form the anterior and posterior compartments of the wing imaginal disc (Garcia-Bellido 1975; Garcia-Bellido and Moscoso del Pradio 1979; Jiang and Levine 1993). Cells of the posterior compartment are determined by the expression of the selector gene *engrailed* (Morata and Lawrence 1975). Subsequently, a shortrange morphogen, Hedgehog, is expressed only in posterior cells (Lee, von Kessler et al. 1992; Mohler and Vani 1992; Tabata, Eaton et al. 1992). Hedgehog then activates the long-range morphogen Dpp (Decapentaplegic), a member of the TGF-ß family which patterns the tissue in both compartments, which is important for the formation of the adult wing structure (Padgett, St Johnston et al. 1987; Basler and Struhl 1994; Tabata and Kornberg 1994; Zecca, Basler et al. 1995).

5.6 PATTERN FORMATION DURING WING IMAGINAL DISC DEVELOPMENT

The compartment boundary between the anterior and posterior compartments in the *Drosophila* wing imaginal disc is an excellent model to study cell sorting. The anteroposterior compartment boundary (A/P boundary) is set up by biochemical signals and organises the wing patterning. Cells in the first rows of the anterior compartment receive the Hh signal, since they express the receptor Patched (Basler and Struhl 1994; Tabata and Kornberg 1994; Zecca, Basler et al. 1995).

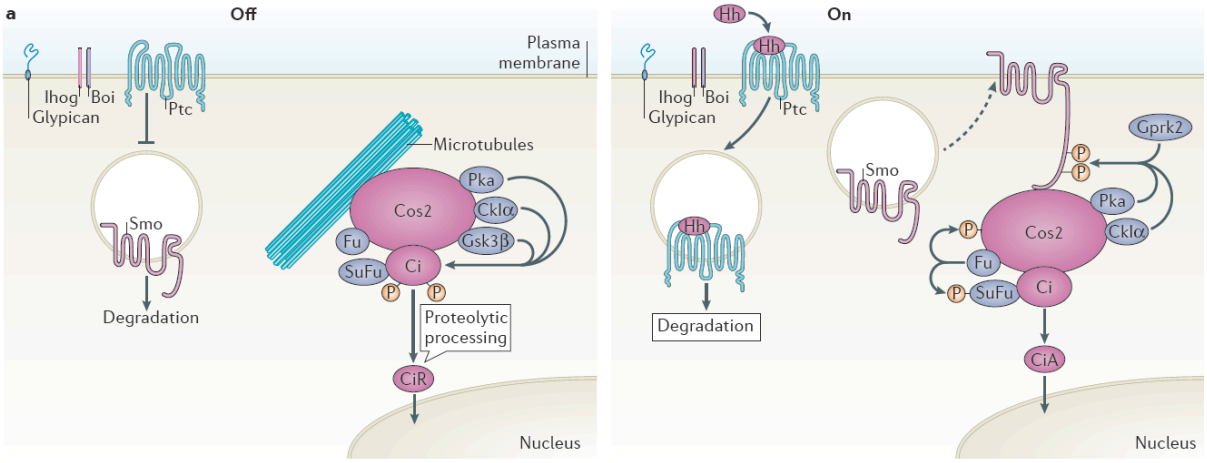

Figure 6: Hedgehog signaling pathway in *Drosophila melanogaster*

Left panel: Without Hh, Patched (Ptc) prevents the transport and incorporation of Smoothened (Smo) to the plasma membrane. The Hedgehog signaling complex (HSC) consists of Cos2, which binds Ci, and the kinases PKA, CkIα and Gsk3ß, Fused (Fu) and Supressor of Fu (SuFu). The HSC is bound to and can move along microtubules by the kinesin-motor function of Cos2. Ci gets phosphorylated and proteolytically processed to Ci^{rep}, which represses target gene expression. **Right panel:** Binding of Hh to the Ihog-Boi-Ptc receptor complex leads to degradation of Ptc and the translocation of Smo to the plasma membrane. Smoothened gets activated by phosphorylation via PKA, CkIα and Gprk2. Subsequently, Smo binds to the HSC with its cytoplasmic tail. Fused is activated and phosphorylates SuFu and Cos2. Thereby, proteolytic cleavage of Ci is prevented and full-length Ci can induce target gene expression in the nucleus (modified after Briscoe and Therond 2013).

Patched is a transmembrane protein (Hooper and Scott 1989; Nakano, Guerrero et al. 1989). Patched forms a receptor complex together with Ihog (Interference Hedgehog) and Boi (Brother of Ihog). Without Hh, Patched inhibits the transmembrane protein Smoothened (Smo) from being incorporated into the plasma membrane (Figure 6) (reviewed by Briscoe and Therond 2013). Binding of Hh to Patched results in accumulation of Smo presumably either by an increase in its transport by vesicles or by increasing its stability (Denef, Neubuser et al. 2000; Li, Chen et al. 2012; Xia, Jia et al. 2012). In the absence of Hh, the cytoplasmatic tails of Smo are in an inactive, closed conformation. With Hh, Smo is converted to an open form that is essential for the localisation on the plasma membrane and signal transduction (Zhao, Tong et al. 2007; Chen, Li et al. 2010). Smoothened regulates the activity of the zinc-finger transcription factor Ci (Cubitus interruptus). Without Hh, Ci is bound to a Hedgehog signaling complex (HSC) which consists of Costal 2 (Cos2) and binds Ci and negative and positive regulators of Ci activity (Robbins, Nybakken et al. 1997; Kalderon 2004). Kinases, like PKA (protein kinase A), Gsk3ß and CkIα phosphorylate the C-terminal region of Ci, which triggers proteolytic cleavage leading to the removal of the transactivation domain. This truncated form of Ci, Ci^{rep}, enters the nucleus and represses the expression of target genes, like *dpp* or *ptc* (Zhang, Zhao et al. 2005). When Smoothened is activated by binding of Hh to Patched, the cytoplasmatic tail of Smo is phosphorylated by PKA, CkIα and Gprk2. Additionally, Fused (Fu) is activated by dimerization and phosphorylates Cos2 and SuFu (supressor of fused). As a consequence, full-length Ci can dissociate from the complex and activate target gene expression (Ruel, Gallet et al. 2007; Shi, Li et al. 2011; Zhang, Mao et al. 2011; Zhou and Kalderon 2011). The expression of *ci* is inhibited in posterior cells by Engrailed (Eaton and Kornberg 1990).

5.7 BIOCHEMICAL SIGNALS MEDIATE CELL SORTING ALONG THE A/P COMPARTMENT BOUNDARY

Engrailed and Hh signal transduction activity are required for the cell sorting along the A/P compartment boundary (Garcia-Bellido, Ripoll et al. 1973; Morata and Lawrence 1975; Garcia-Bellido, Ripoll et al. 1976; Kornberg, Siden et al. 1985). It was postulated that the difference in Engrailed leads to different adhesion properties between anterior and posterior cells and by this to cell sorting via minimizing the contact towards the cells of the other compartment (Garcia-Bellido 1975; Morata and Lawrence 1975; Lawrence and Struhl 1982; Blair 1995; Lawrence and Struhl 1996). Rodriguez and Basler, as well as Blair and Ralston, showed that cell sorting along the A/P boundary is rather mediated indirectly by Engrailed through Hh signal transduction than by lineage based different adhesion properties between A and P cells (Blair and Ralston 1997; Rodriguez and Basler 1997). They analysed the sorting behavior of *smo* mutant clones (*smo*$^{-}$), in which Hh signal transduction activity was blocked and found that those clones moved towards the posterior compartment when abutting the A/P boundary. They sorted out from anterior cells but failed to mix with posterior cells as well, which was indicated by the formation of smooth clonal boundaries towards anterior and posterior cells (Blair and Ralston 1997). They concluded, that the sorting of *smo*$^{-}$ clones from anterior cells is due to the differential expression levels of *ci* and independent of Engrailed. However, the differential expression levels of Engrailed between *smo*$^{-}$ clones and posterior wild-type cells appear to induce cell sorting behavior as well (Blair and Ralston 1997; Rodriguez and Basler 1997). Moreover, considering the fact that Hh forms a gradient in the anterior compartment, it was predicted that an abrupt difference in Hh signal transduction activity between two groups of cells is needed to lead to a sudden difference in cell adhesion and is therefore sufficient for sorting behaviors (Rodriguez and Basler 1997; reviewed by Dahmann and Basler 1999). This assumption was confirmed by experiments investigating the sorting behavior of clones that lacked either *ci* or *en* or both (Dahmann and Basler 2000). In the anterior compartment, Ci was found to be necessary for the mixing with anterior cells. Clones mutant for *ci* of anterior origin often crossed the A/P boundary and formed smooth boundaries towards anterior and posterior cells in the vicinity of the A/P boundary because of the difference in expression levels of Ci and Engrailed compared to anterior respectively posterior cells. Dahmann and Basler reasoned that Hh signal transduction acts via a transcriptional response, mediated by Ci in anterior cells. Clones mutant for *en*$^{-}$ of posterior origin, which abutted the boundary, sorted from posterior towards the anterior compartment and mixed with anterior cells (Morata and Lawrence 1975; Blair and Ralston 1997). Since *ci* expression is normally repressed by Engrailed in posterior cells, *en*$^{-}$ clones of posterior origin expressed Ci and could therefore mix with anterior cells.

Dahmann and Basler concluded from this, that the segregation of *en*$^-$ clones from posterior cells is mediated by the differential expression of Ci rather than by Engrailed (Dahmann and Basler 2000). Clones double mutant for *en* and *ci* that crossed the A/P boundary formed smooth borders towards anterior (A) and posterior (P) cells, independent from their origin. Moreover, *en*$^-$*, ci*$^-$ double mutant clones, which originated from the posterior compartment built up smooth boundaries to P cells. Therefore it is assumed that Engrailed controls cell sorting along the A/P boundary in an Hh-signaling dependent, via Ci, and in an Hh–signaling independent manner, but the Hh dependent way outvotes the Hh-independent way. This could also explain why the expression of Engrailed in anterior cells next to the A/P boundary in late third instar wing discs does not impair the shape and function of the A/P boundary (Blair 1992). Furthermore, Dahmann and Basler showed that the differential expression of DE-cadherin leads to cell segregation along clonal boundaries, presumably because of differential cell adhesion. However DE-cadherin does not play a role in cell sorting along the A/P boundary. Instead it is hypothesized, that Engrailed and Hedgehog regulate cell sorting along the A/P boundary by transcriptional regulation of a single, yet unknown, adhesion molecule (Dahmann and Basler 2000). Because of the assumption that a c*i*-mediated transcriptional output regulates cell sorting along the A/P boundary, the role of the *ci*-target *dpp* in maintaining the A/P boundary was examined. Dpp signaling in anterior cells was found to be important for the maintenance of the A/P boundary, as clones mutant for the Dpp-receptor *thickveines (tkv),* as well as for *basket (bsk)* (part of the *Drosophila* JNK-pathway, which has to be inactivated as *tkv*$^-$ clones undergo JNK-mediated apoptosis) crossed the A/P boundary (Shen and Dahmann 2005). Because Hh signal transduction was not altered in *tkv*$^-$*/bsk*$^-$ mutant clones the displacement of such clones is not due to the loss of Hh signal transduction. Furthermore, the expression of the Dpp target *omb* (*optomotorblind*) in anterior cells is required for the maintenance of the straight A/P boundary and may act downstream or in parallel with Ci (Shen and Dahmann 2005). Still, it remained unclear whether Hh-signaling-mediated cell sorting along the A/P boundary leads to differential expression of an adhesion molecule. The cadherin Cad99C was found to be specifically expressed in an anterior stripe of cells along the A/P compartment boundary and being regulated by Hh signalling. However, Cad99C is not necessary for maintaining the straight shape and the cell sorting along the boundary (Schlichting, Demontis et al. 2005). Even though the biochemical signals building up and maintaining the A/P compartment boundary are well-known, the mechanical processes contributing to the cell segregation between A and P cells are still unknown.

5.8 BIOCHEMICAL SIGNALS MEDIATE CELL SORTING ALONG THE D/V COMPARTMENT BOUNDARY

The compartment boundary subdividing the dorsal and ventral compartment (D/V boundary) in the *Drosophila* wing imaginal disc is established via biochemical signaling as well. In contrast to the A/P boundary, the D/V boundary is established later in development, during the second larval instar. The LIM-homeodomain transcription factor Apterous is expressed in cells of the dorsal compartment and acts as a selector gene defining the dorsal identity (Blair 1993; Diaz-Benjumea and Cohen 1993). It induces the expression of the Notch-ligand Serrate (Couso, Knust et al. 1995; Diaz-Benjumea and Cohen 1995) as well as of the glycoslytransferase Fringe. Fringe modulates the Notch receptor in the dorsal compartment to be less affine to Serrate and more affine to the Notch-ligand Delta, which is expressed in the ventral compartment (Doherty, Feger et al. 1996; Klein and Arias 1998). The Notch receptor in the ventral compartment becomes more affine to Serrate (Irvine and Wieschaus 1994; Panin, Papayannopoulos et al. 1997). This bidirectional Notch signalling leads to *wingless* expression in a stripe in dorsal and ventral cells along the D/V boundary (Couso and Martinez Arias 1994; Kim, Irvine et al. 1995; Rulifson and Blair 1995) (Figure 7). Wingless (Wg), a *Drosophila* Wnt molecule, is expressed in early stages in the whole wing disc tissue, where it was thought to act as a morphogen (Williams, Paddock et al. 1993; Couso, Knust et al. 1995; Ng, Diaz-Benjumea et al. 1996; Zecca, Basler et al. 1996; Neumann and Cohen 1997; Martinez Arias 2003). High levels of Wingless in the first cell rows of the dorsal and ventral compartment lead to the expression of *senseless*, which is important for the formation of the wing margin (Couso, Bishop et al. 1994; Nolo, Abbott et al. 2000; Jafar-Nejad, Tien et al. 2006). Farther away from the D/V boundary, Wg promotes growth (Giraldez and Cohen 2003; Baena-Lopez, Franch-Marro et al. 2009) via the expression of *vestigial, distal-less* and *frizzled-3* (Zecca, Basler et al. 1996; Neumann and Cohen 1997; Sato, Kojima et al. 1999; Sivasankaran, Calleja et al. 2000). It was, however, suggested in recent studies that Wg does not act as a morphogen as they could show that the spreading of Wg throughout the tissue is not required for the appropriate growth and patterning of the wing (Alexandre, Baena-Lopez et al. 2014).

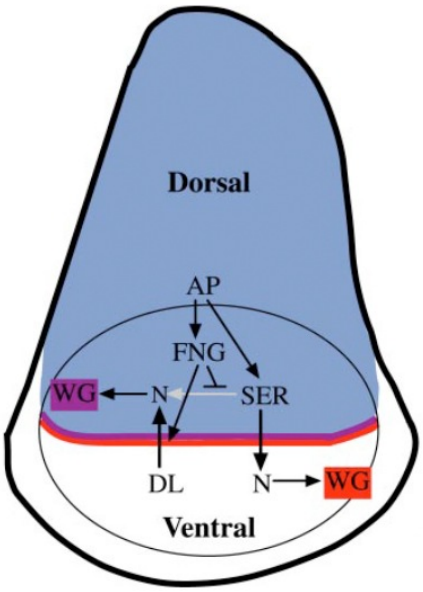

Figure 7: Apterous induces Notch signaling along the D/V compartment boundary in the *Drosophila* wing disc.
The selector gene *apterous* (AP) is expressed in the dorsal compartment (blue). It induces the expression of the Notch-ligand Serrate (SER) and the glycosyltransferase Fringe (FNG). Fringe regulates the affinity of the Notch receptor (N) to its ligands Serrate and Delta (DL). Notch receptors in the dorsal compartment become less affine to Serrate and Notch receptors in the ventral compartment become more affine to Delta. Binding of the ligands to Notch results in *wingless* (WG) expression in a stripe along the D/V boundary in both compartments (purple and red line) (modified after Irvine and Rauskolb 2001).

Apterous also induces the expression of the LRR (leucin-rich-repeat) –transmembrane proteins Capricious (Caps) and Tartan (Trn) (Milan, Weihe et al. 2001). In the early second instar, the time the D/V boundary is established, Capricious and Tartan are exclusively expressed in the dorsal compartment. Later in development, the expression of Caps and Trn is localized at the lateral region in the dorsal and ventral compartment (Milan, Weihe et al. 2001). Capricious and Tartan are important for the formation of the D/V boundary and Capricious is sufficient to maintain the boundary in *apterous* mutant wing discs (Milan, Weihe et al. 2001). Moreover, clones overexpressing Capricious have a smoother interface than control clones (Milan, Perez et al. 2002). Capricious was also shown to mediate cell-cell communication in synapse-formation (Shishido 1998; Shishido, Takeichi et al. 1998; Taniguchi, Shishido et al. 2000). However, the role of Apterous, Notch signaling and Capricious in maintaining the shape of, and preventing cell mixing along the D/V boundary is not well understood.

5.9 MECHANICAL PROCESSES MAINTAINING COMPARTMENT BOUNDARIES

Cells within tissues and organs have distinct mechanical properties, according to their function. Regulating and changing mechanical properties of cells are for example required for tissue shape changes during development. The A/P boundary in the wing imaginal disc is characterized by its straight and sharp morphology. It is already established during embryonic development and remains straight when the wing disc grows from about 50 to 50.000 cells during larval development. Maintaining the straight shape is critical for the correct patterning of the tissue to ensure the formation of an adult wing of the appropriate size and shape. The straight shape of the A/P boundary can be challenged by cell

rearrangements due to cell proliferation. Therefore, mechanisms are required for maintaining the straight shape of the A/P boundary throughout development and growth (Figure 8) (reviewed by Dahmann, Oates et al. 2011). It has been shown that cells along the A/P and D/V compartment boundaries in the wing imaginal disc have different mechanical properties, compared to cells away from the boundaries (Major and Irvine 2005; Major and Irvine 2006; Landsberg, Farhadifar et al. 2009; Monier, Pelissier-Monier et al. 2010; Aliee, Roper et al. 2012). Major and Irvine proposed in 2005 and 2006 that changes in the mechanical properties of boundary cells could lead to the formation of a “fence” along the compartment boundary, which could be such a mechanism. They proposed that such a “fence” is formed by the cortical actomyosin meshwork underlying the apical side of epithelial cells. Epithelial cells, like in the wing imaginal disc, are tightly connected via E-cadherin junctions. E-cadherin molecules form homotypic connections between neighbouring cells. Intracellular, they are connected to α-and β-catenins and via them to actin filaments (Jamora and Fuchs 2002; Bershadsky 2004; Gates and Peifer 2005; reviewed in Lecuit and Lenne 2007). Myosin motor proteins can move actin filaments using ATP, which leads to contractile forces at the cell cortex and by this to mechanical tension (reviewed in Lecuit and Lenne 2007). Major and Irvine showed that filamentous actin (F-actin) and Myosin II are up-regulated along the D/V boundary and that Myosin II function is required for maintaining the D/V boundary, since blocking F-actin or MyoII results in an irregular D/V boundary (Major and Irvine 2005; Major and Irvine 2006). DE-cadherin, α- and ß-catenin were however not increased. Thus, in the opinion of Major and Irvine, the “fence”-mechanism could be a sufficient boundary mechanism, rather than differential adhesion between cells of different compartments (Major and Irvine 2006). They suggested that actin-myosin based tension could maintain the straight and sharp morphology and prevent cell mixing along the D/V compartment boundary.

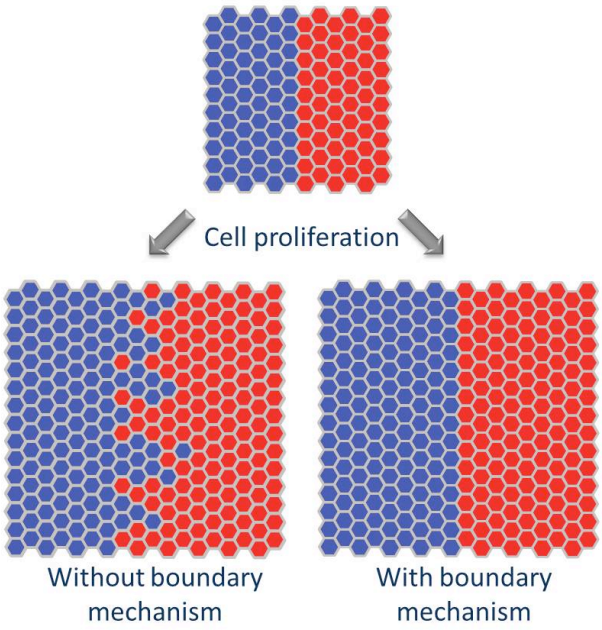

Figure 8: Cell proliferation challenges tissue interfaces.
When a tissue, that is subdivided in two groups of cells (blue and red), undergoes massive cell proliferation, the interface between the adjacent groups is challenged. Without any boundary mechanism (left) the interface eventually becomes very irregular and cell mixing occurs. However, if a boundary mechanism is active, the boundary remains straight and no cell mixing is visible (modified after Dahmann, Oates et al. 2011).

This “fence”-model was supported by studies at the parasegment (PS) boundaries in the early *Drosophila* embryo (Monier, Pelissier-Monier et al. 2010). Cells along the PS boundary formed a straight boundary and F-actin and MyoII were increased along the PS boundary at cell bonds of both, anterior and posterior boundary cells in a cable-like structure. Inhibiting MyoII function by blocking the phosphorylation by ROCK (Rho-kinase) with the drug Y-27632 resulted in a wiggly boundary and cell mixing (Monier, Pelissier-Monier et al. 2010). They tested whether the actomyosin cable can prevent cell mixing using CALI (chromophore-assisted laser inactivation) to inactivate Myosin II molecules locally along the PS boundary *in vivo*. By tracking of dividing cells along the boundary and inhibiting Myosin II, it was revealed that cells invaded the other compartment. They concluded that cortical tension via the actomyosin cable along the PS boundary is required to correct cell rearrangements and thereby prevent cell mixing following cell divisions (Monier, Pelissier-Monier et al. 2010). Though the increase in mechanical tension mediated by an actomyosin mediated “fence”-mechanism was proposed to be a possible boundary mechanism, it was not tested yet whether mechanical tension is increased along compartment boundaries.

5.10 INCREASED MECHANICAL TENSION ALONG THE A/P AND D/V BOUNDARY IN THE *DROSOPHILA* IMAGINAL WING DISC

An actomyosin based contraction could lead to an increase in mechanical tension along the compartment boundaries in the *Drosophila* wing imaginal disc and thereby prevent cell mixing. In turn the increase in mechanical tension could lead to cell shape changes (Garcia-Bellido and Moscoso del Pradio 1979; Brodland and Chen 2000; Farhadifar, Roper et al. 2007). Signatures of an increase in mechanical tension are widened vertex angles between junctions along the A/P boundary as well as an increase in F-actin and Myosin. Recent studies analysed the shape of the boundary and the morphological signatures of the cells along the A/P boundary to test whether mechanical tension is increased along the A/P boundary. The cells along the A/P boundary showed a larger apical cross section area than the other cells in the tissue and the angles between cell junctions along the A/P boundary were increased compared to the tissue away from the boundary (Landsberg, Farhadifar et al. 2009). Landsberg et.al. concluded from these results that these morphological signatures of cells along the A/P boundary are caused by the apposition of cells from different compartments. Clones, mutant for *smo* and expressing Hh, which differed in their Hh signal transduction activity from surrounding anterior cells exhibited a smooth interface as well as an increased apical cross section area of cells and widened bond angles between boundary cells along the clonal interface. A difference in Engrailed expression was sufficient to increase the bond angles along en^{-},ci^{-} clones localized in the posterior compartment, as well for the increase in apical cross section area of cells along the clonal boundary. Landsberg et.al. reasoned from these findings that differences in Hh signal transduction activity and Engrailed are sufficient to induce the morphological signatures of the cells along the A/P boundary (Landsberg, Farhadifar et al. 2009). Laser ablation of single cell bonds was used to test whether these signatures are consistent with an increase in mechanical tension along the A/P boundary. Relative mechanical tension was quantified by measuring the vertex displacement after laser ablation of cuts along the A/P boundary and cuts away from it. They could show that mechanical tension is increased 2.5-fold along the A/P boundary. When Myosin II activity was blocked by using the Rho-kinase inhibitor Y-27632 (Uehata, Ishizaki et al. 1997; Winter, Wang et al. 2001), mechanical tension was decreased in the entire tissue (Landsberg, Farhadifar et al. 2009). Computer simulations, based on a vertex model (Farhadifar, Roper et al. 2007) of a growing tissue which is subdivided into two groups of cells was used to test whether the increase in mechanical tension could be sufficient for ensuring cell sorting along compartment boundaries. When tension was equal all over the tissue in the simulation, the interface between the two groups became very irregular and cell

mixing occurred. However, a 2.5 fold increase in mechanical tension at bonds along the A/P boundary was sufficient to maintain the straight shape of the boundary and to prevent cell mixing (Landsberg, Farhadifar et al. 2009).

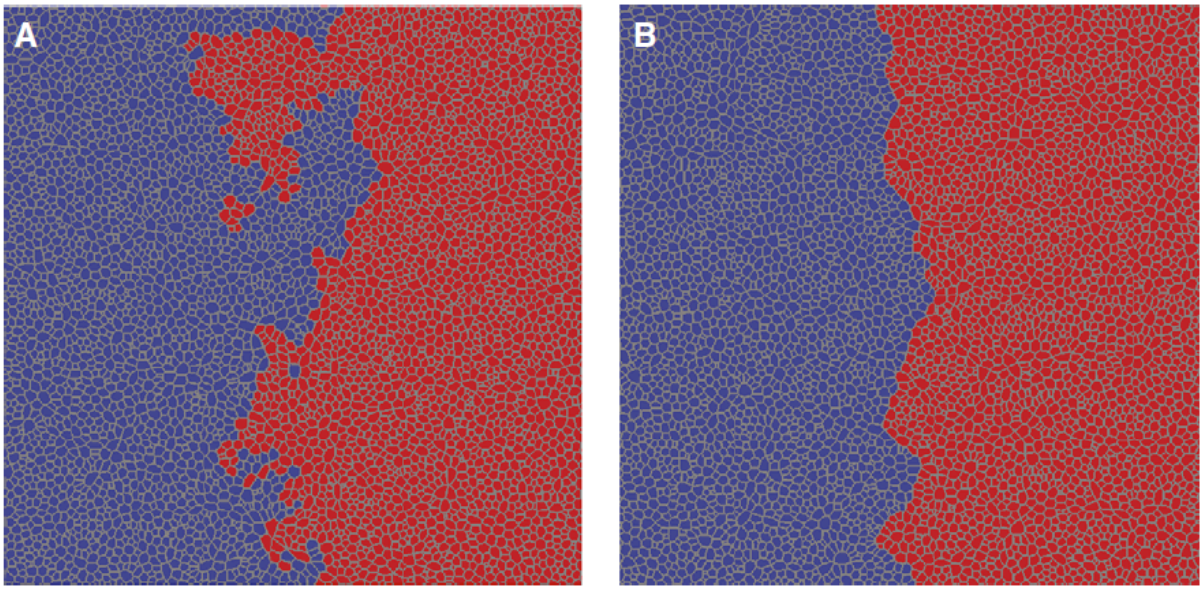

Figure 9: The increase in mechanical tension is sufficient to maintain the straight shape of a tissue interface *in silico*.
Computer simulations of growing tissues that are subdivided into two groups of cells, using the vertex model. **Left panel:** If mechanical tension is equal all over the tissue, the interface between two groups of cells that were originally separated by a straight boundary becomes irregular and cell mixing occurs. **Right panel:** If mechanical tension is increased 2.5-fold at the interface between blue and red cells, during growth the interface maintains relatively straight and cell mixing is prevented (modified after Landsberg, Farhadifar et al. 2009).

Mechanical tension is increased along the D/V compartment boundary as well (Aliee, Roper et al. 2012) and thus could present a general mechanism to prevent cell mixing. For the D/V boundary, additional mechanisms were found to have an influence on boundary shape. These included oriented cell division and cell elongation, which are caused by anisotropic forces in the tissue (Aliee, Roper et al. 2012). Mechanical tension, mediated by actomyosin motor proteins is a physical mechanism to prevent cell mixing along the compartment boundaries in wing imaginal discs. However, it remains unclear how mechanical tension along the A/P and D/V boundary is increased in response to biochemical signals.

6 AIMS

The aim of my project was to investigate the interplay between the biochemical signals and mechanical processes along the A/P compartment boundary in the *Drosophila* wing imaginal disc. By using genetics, laser ablation of single cell bonds, immunostaining and quantitative image analysis, I examined whether the difference in Hedgehog signal transduction activity between anterior and posterior cells along the A/P boundary is necessary and sufficient to maintain the straight shape of the boundary and the morphological signatures of boundary cells. I was also interested in whether the difference in Hedgehog signal transduction activity along the A/P boundary is necessary and sufficient for the increase in mechanical tension. Furthermore, I tested whether the difference in Engrailed and Hh signal transduction activity is required and sufficient to induce smooth borders and to recapitulate the morphological signatures of boundary cells along ectopic boundaries. Additionally, I tested whether differences in Engrailed and Hedgehog signal transduction activity are sufficient to increase mechanical tension along ectopic boundaries. Other than Engrailed and Hh signal transduction activity, the LRR-transmembrane protein Capricious was found to be involved in cell segregation along the D/V compartment boundary in the imaginal wing disc. Therefore, I tested whether the differential expression of Capricious is sufficient to create smooth borders, to recapitulate the morphological signatures of boundary cells and to increase mechanical tension along ectopic interfaces. It was suggested that an actomyosin cable, which mediates the increase in mechanical tension, separates anterior and posterior cells. Following this hypothesis I tested whether mechanical tension is transmitted between junctions along the A/P boundary.

The results of this project will give new insights into the interplay between biochemical signals and mechanical processes in mediating cell sorting along tissue interfaces.

7 MATERIAL AND METHODS

7.1 ANTIBODY STAINING OF WING IMAGINAL DISCS

7.1.1 Antibody staining of wing imaginal discs

Larvae were dissected in PBS (phosphate buffered saline) and the carcasses (turned inside-out) were fixated in PBS containing 4%Formaldehyde and 0.4% Triton-X-100 for 35-40'. After fixation the larvae were washed 3x for 10' in PBS. The primary antibodies were added to the larvae in 200µl PBT (PBS containing 0.1% Bovine serum albumin), followed by incubation over night at 4˚C. The larvae were washed again 3x 10' in PBS. The secondary antibodies respectively phalloidin were diluted in 200µl PBT and added to the larvae, following incubation for 2hrs at room temperature. After that, the larvae were washed again 3x for 10' before mounting. For mounting the wing imaginal discs were separated from the larval carcasses and transferred to an objective slide into a drop of PPDA (p-Phenylenediamine). Cover slips with selected witdh (170µm±5) were used (modified from protocol by Karin Schlichting, 2009).

7.1.2 Primary antibodies

- Mouse-anti β-Galactosidase, 1:1000 (Promega (no. Z378A))
- Rat-anti-DE-cad, 1:50 (Developmental Studies Hybridoma Bank, University of Iowa (DCAD2))
- Mouse anti- CD2, 1:1000 (AbD Serotec (MCA154))
- Rabbit anti- GFP, 1:2000 (Santa Cruz Biotechnology®, Inc (sc-8334))
- Mouse-anti Patched, supernatant, 1:100 (Developmental Studies Hybridoma Bank, University of Iowa (Apa1))
- Mouse- anti Engrailed, supernatant, 1:100 (Developmental Studies Hybridoma Bank, University of Iowa (4D9))

7.1.3 Secondary antibodies

- Donkey anti-mouse IgG (H+L) Alexa Fluor 555, 1:200 (Molecular Probes®, Invitrogen (A31570))

- Donkey anti-rat Cy5 IgG (H+L), 1:200 (Jackson ImmunoResearch Laboratories, Inc. (712-175-153)
- Goat anti rabbit IgG (H+L) conjugate, Alexa Fluor 488, 1:200 (Molecular Probes®, Invitrogen (A11008))

7.1.4 Fluorophore coupled dyes

- Alexa Fluor 488 phalloidin, 1:200 (Molecular Probes®, Invitrogen (A12379))
- Rhodamine phalloidin, 1:200 (Molecular Probes®, Invitrogen (R-145))

7.2 FLY STOCKS

Fly stocks were taken from the stock collection of Prof. Christian Dahmann.

- *yw*
- *D751: yw hs-flp; UAS-GFP-gpi/ CyO (y^+); hh^{ts} / TM6B*
- *D752: yw hs-flp; en-GAL4, ubi DE-cad-GFP/ CyO (y^+); hh^{ts} / TM6B*
- *D776: ; enGal4, ubiDE-Cad-GFP/CyO; UAS-GFP-gpi/TM6B*
- *;enGal4/CyO; UAS-GFP-gpi/TM6B* (derived from D776)
- *D19: yw;; UAS-ci^{PKA4}*
- *yw hs-flp; enlacZ/CyO; hh^{ts}/TM6B* (Caroline Sonnabend, Caro1)
- *D11: yw hs-flp; en-lacZ/ CyO; Act5c>CD2>GAL4*
- *D777: yw hs-flp; ubi-DE-cad-GFP/ CyO(y+); UAS-GFP-gpi/ TM2*
- *D196: yw hs-flp; FRT42 en^E/ CyO(y^+)*
- *yw hs-flp; FRT42, ΔECadGFP/ CyO(y^+)* (from Daiki Umetsu)
- *yw hs-flp; FRT42D, en^E/CyO;; ci^{94}/Dp(y^+)* (Methot and Basler 1999) (from Marco Milan)
- *yw hs-flp; FRT42D, ubiGFP(ci^+)/CyO;; ci^{94}/Dp(y^+)* (from Marco Milan)
- *D773: yw hs-flp;UAS-caps*
- *D145: yw hs-flp; Sp/CyO; MKRS/TM6B*
- *yw hs-flp; UAS-GFP-gpi/CyO; hh^{ts}, UAS-Ci^{act}/TM6B* (derived from D19 and D751)
- *yw hs-flp; ubi-DECad-GFP/CyO; Act5c>CD2>GAL4,UAS-GFP-gpi* (derived from D11 and D777)
- *yw hs-flp; Sp/CyO; UAS-Ci^{act}* (derived from D19 and D145)

7.2.1 Phenotypic markers

- *yw* yellowish body color, white eyes, yellowish larval mouth parts
- *w* white eyes
- y^+ dark body color
- *CyO* curled wings, balancer for 2nd chromosome
- *Sp* multiple stenopleural bristles, balancer for 2nd chromosome
- *TM2* *ubx,* size of halteres is increased, balancer for 3rd chromosome
- *MKRS* *stubbled*, shortened bristles all over the body, balancer for 3rd chromosome
- *TM6B* *humeral* (multiple humeral bristels), *tubby* (larvae are shorter and thicker than normal larvae), balancer for 3rd chromosome

7.3 IMAGE ACQUISITION

7.3.1 Olympus FV1000

The inverse confocal laser scanning microscope Olympus FV1000, at the MPI-CBG in Dresden was used for image acquisition from January 2012 till June 2012. The following objectives were used: Olympus UPlanApo 10x 0.4NA, Olympus UPlanApo 40x 1.35NA oil and Olympus UPlanApo 60x 1.35NA oil. The following laser lines were used: HeNe 633nm, DPSS 561 and Argon 488 to detect the following dyes: Alexa488 (Ex:495nm, Em:519nm), Alexa 555 (Ex:555nm, Em:565nm), Cy5 (Em:650nm, Em:670), Alexa Fluor® 488 phalloidin (Ex:496nm, Em:519) and Rhodamine phalloidin (Ex:540nm, Ex:565nm). Image acquisition was done with the software FV-ASW 1.7. Image resolution: 800x800, 1µm=3.774pxl. The 488 and Cy5 channel were detected at the same time; the channel for Rhodamine-phalloidin or 555 was detected separately. Images were taken as a Z-stack, step size: 0.5-1µm. (http://www.biodip.de/wiki/CO1_-_Olympus_Fluoview_1000)

7.3.2 LSM 780, upright, CRTD

The upright laser scanning microscope LSM 780, located at the CRTD Dresden, was used for image acquisition for images taken from January 2013 till June 2014. The following objectives were used: Zeiss Plan-Apochromat 10x 0.45NA and Zeiss Plan-Apochromat 40x 1.4NA oil. The following lasers were used: Argon Multiline: 458nm, 488nm, 514nm; DPSS 561nm and HeNe 633nm to detect the following dyes: Alexa488 (Ex:495nm, Em:519nm), Alexa 555 (Ex:555nm, Em:565nm), Cy5 (Em:650nm, Em:670), Alexa Fluor® 488 phalloidin (Ex:496nm, Em:519) and Rhodamine phalloidin (Ex:540nm, Ex:565nm). Software: ZEN

2010. The LSM780 contains two PMTs, which can detect 32 PMT (GaAsP= Gallium Arsenide Phosphide) channels. Image resolution: 1024x1024 pixel; 1µm=4.818pxl. The 488 and Cy5 channel were detected at the same time; the channel for Rhodamine-phalloidin or 555 was detected separately. Images were taken as a Z-stack, step size: 0.5µm. (http://www.biodip.de/wiki/LSM_780,_upright,_CRTD)

7.3.3 Image processing with Fiji

Image stacks of the format .oib (Olympus) or .lsm (Zeiss) were loaded into the open-source image processing software Fiji (Image J 1.48 b). Multi-color image stacks were separated into channels. The images of each channel were projected, according to the level of adherens junctions or nuclei. Brightness and Contrast levels were modified for better visibility, but not for analysis of pixel intensities. Scale bars were added with Fiji.

7.4 LASER ABLATION OF SINGLE CELL BONDS

7.4.1 UV-laser ablation system

Laser ablation experiments were performed using the UV-laser ablation system of Prof. Dr. Stephan Grill at the Max-Planck-Institute for Cell Biology and Genetics (MPI-CBG) in Dresden. The instrument consists of an inverted Zeiss Axio Observer.Z1 confocal imaging system and a laser ablation unit. The confocal imaging system consists of a Nipkow spinning disc confocal head (CSU 10, Yokogawa), three laser lines (488nm, 561nm, 594nm) and a EM-CCD (electron multiplying charge-coupled device) camera. The laser ablation unit consists of a Q-switched, third harmonic Nd:YAG laser (PowerChip, JDS Uniphase) (λ=355nm, pulse energy 10µJ). A Zeiss C-Apochromat 63x 1.2NA water immersion objective was used for ablation (Oswald 2010).

- Software for image acquisition: Labview (National Instruments) “Zeissmicromulticolor-felix-final” (Oswald 2010)
- Adjustments for live imaging: Laser/CSU: Target temperature -70˚C, laser line: 488nm (20-30%), filter: 525/50nm, spinning speed: 5000, exposure time=0.15s, frame rate= 1s, reflector: UV/ablation, no optovar
- EM-CCD camera: Gain max.200, Pre-Amp-Gain: 1.00
- Imaging: exposure time=0.15s, frame rate=0.2s (actual frame rate=0.25), Filter 525nm
- Cutting: Single cell bonds were ablated after 80-120 frames with the following parameters: 5 pulses per shot, Intensity=1.5, Piezo height 1.8, length of laser line 6µm, line area density 2 shots/µm
- Laser alignment: x-center:175, y-center: 255

- Scale: 1pxl=0.14µm
- Images were recorded 80-120 frames before and 450-550 frames after ablation

7.4.2 Preparation of wing imaginal wing discs for laser ablation

Larvae were dissected in Schneider's S2 Medium (life technologies, Gibco®) right before imaging and transferred to an objective slide. Double-sided tape was used as a spacer to prevent squeezing of wing imaginal discs. Cover slips with selected width (170µm±5) were used.

7.4.3 Quantification of vertex displacement after laser ablation

Image stacks were loaded to Fiji and converted to RGB. The point selection tool (tick 1 pixel, auto-measure, auto next-slice, label points) was used to track the verticies one after the other throughout the movie. The measured vertex positions ($x_{1,2}$, $y_{1,2}$) were copied to Excel and aligned by time. Frame rate=250ms. Vertex distance was calculated by =SQRT((x_2-x_1)^2+(y_2-y_1)^2) and normalized to the average cell bond length in the wing disc (1.69855102µm (Landsberg, Farhadifar et al. 2009)). The vertex distance increase was calculated by substracting the average bond length 10s before the cut from all bond lengths. The distance was converted from pxl to µm by dividing it by 4.608 (4,608 pxl equal 1µm). This was repeated for all cuts of a certain time. Average distance increase and SEM were calculated. The average vertex distance increase and SEM were plotted with Excel in a xy-scatter plot as a function of the time relative to ablation (-10 – 50s) (modified after protocol by Dr.Jens-Christian Röper).

7.4.4 Quantification of initial velocity of vertex displacement

The initial velocity (v_0) was calculated by v_0 [µm/s]= ((vertex distance increase $_{0.25s}$ – vertex distance increase$_{0s}$)/0.25s)*1.69855102µm.

7.5 STATISTICS

The T-Test function of Microsoft®Excel® 2011 (version 14.4.2) was used for calculating the p-values for the clonal roughness (=TTEST(array1,array2,2(two-tailed-distribution),2 ($\mu_1 \neq \mu_2$)). The p-values for the other datasets were calculated with "calculating means (t-test) function of the software Statplus:mac LE 2009. In both cases, a t-test for two-tailed distributions was performed testing the Hypothesis, that values are inequal from each other ($H_0=\mu_1 \neq \mu_2$). Significance levels: $p<0.05$ (*), $p<0.01$(**), $p<0.001$(***).
Average values and SEM (Standard error of the mean=STDEV/SQRT(n)) were calculated with Excel.

7.6 IMAGE ANALYSIS

7.6.1 Software for image analysis

1. Fiji (Schindelin, Arganda-Carreras et al. 2012)
2. Packing Analyzer (Aigouy, Farhadifar et al. 2010)
    a. Packing Analyzer v6.5 (Copyright 2007-2013 by Aigouy, Benoit)
        i. containing plug-in for quantifying clonal roughness by Maryam Aliee
    b. Packing Analyzer v4.0 (Copyright 2007-2011 by Aigouy, Benoit)
        i. containing plug-in for measuring vertex angles between cell junctions
3. R (R.app GUI 1.53 (6335 Leopard build 32-bit), S. Urbanek & H.-J. Bibiko, ©R Foundation for Statistical Computing, 2012)

7.6.2 Quantification of roughness of the A/P boundary

The roughness of the A/P boundary was quantified as follows:

1. Opening image stack with Fiji
    a. Image - Color - Split Channels
    b. Creating z-projections: Image - stack - z-stack (use slices according to DE-cadherin signal intensity)
    c. Image - Type - RGB color
2. Creating composite:
    a. z-projection of channel to analyse
    b. eventually z-projection of a second channel (like betaGal-Staining to mark the compartment boundary)
    c. Image - colour - merge channels
    d. saving the composite
    e. Eventually saving the z-projection of separate channel, to segment the image (i.e. E-Cadherin)
    f. Save as - .tif
3. Opening image with Packing Analyzer v6.5
4. Segmenting the image with “Segmentation” and “Correction”
    a. When done for the E-Cadherin channel, loading the composite image to PA and segmenting it as well, so that PA creates a folder for the image
    b. Copy the file “HandCorrection” from the folder of the channel used for segmentation to the folder of the image to analyse
    c. Click: Post Process -> Recenter (Fake recentering)-> Tracking (track cells) -> Tracked bonds (track bonds) -> Virtual cloning
5. “Virtual cloning”

a. “Show tracks”
b. Labeling of all cells with a red dot, which should belong to the same “clone” along the interface to measure the pixel intensity of
c. “Track clone”
d. Same for the row of cells on the other side of the interface; the command “autodetect clone” can be used as well but some corrections migth need to be done
e. “Edit clone mode”
f. Checking if the two clones generated share the interface to look at and making sure that each cell belongs to one clone only

6. “Plots”
    a. Plot clone info
        i. for each clone (i.e. 0 and 1)
        ii. plot bonds of clone cells
        iii. clonal_interface
        iv. Fill in the ID's for the clones you want to look at and click “ok”
7. Folder which PA generated for file of interest
    a. Choosing bond_length_in_and_out_clones_000_and_001.csv
        i. Opening in Excel
        ii. Sorting the table for the column “Is Interface”, so that TRUE is up
        iii. Deleting everything which is “FALSE” in this column
        iv. Calculating the average bond length
        v. This value tells the average bond length along the interface of two clones in Pixel - copying this value
        vi. Back to PA
        vii. Click “Clonal_interface” and enter the value to “Scale”
        viii. File “Roughness_between_clone_000_and_001”
        ix. Open the file with Excel
        x. Table with “Scale” (1 means one average cell bond length) and “roughness”
8. Plotting roughness values with Excel
    a. Calculating average and SEM for the roughness values for all images of a certain type
    b. xy-scatter with logarithmic scales (base=10)
    c. Average values for roughness w normalized to the average cell bond length along the A/P boundary of each image of a certain type that was analysed

and SEM as a function of the scale L normalized to the average cell bond length (1L=1 average cell bond length).

7.6.3 Quantifying the ratio of F-actin pixel intensity

The ratio of pixel intensity of F-actin was calculated from the pixel intensity along the interface between two groups of cells (A1,P1 for the A/P boundary and C1,W1 for clonal interfaces respectively) and the average pixel intensity of all cell bonds of the boundary cells. (Figure 10).

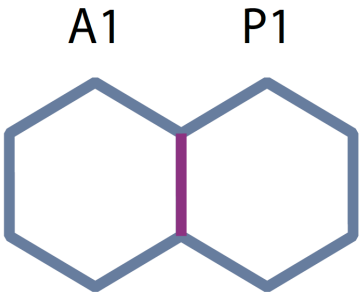

Figure 10: Ratio of pixel intensity.
The ratio of pixel intensity was calculated from the pixel intensity along the interface of two cells (purple) and the average pixel intensity of all cell bonds of the cells A1 and P1 (blue and purple).

Quantifying F-actin pixel intensity with PA

1.-6. like 7.6.2

9. “SQLite DB”
    a. DB generator
    b. DB editor
    c. table names
        i. cells - export table to csv - save file as: cells_table.csv
        ii. bonds: bonds_table.csv
        iii. tracked_cells: tracked_cells_table
        iv. tracked_bonds: tracked_bonds_table
    d. OK
10. Calculating pixel intensity with R
    a. open R
    b. open bond_intensity_for_Katrin.r (by Daiki Umetsu)
    c. drag and drop folder to R to “dir”
    d. check if the clone numbers are the right ones
    e. select channel
    f. R will output a file “puter_bonds_relative_intensity.csv
    g. Open the fil

h. If the value is
    i. <1 – decrease
    ii. =1 - equal intensity
    iii. >1 - increase of the signal

7.6.4 Quantification of apical cross section area Ā (with PA)

The apical cross section area of boundary cells was quantified as follows:

1.-6. like 7.6.2

7. Open file “plot-clone_cells_’nb of clone’.csv” for each virtual clone to analyse in Excel
    a. Calculating average from column “flood area”
    b. Calculating SEM
8. A/P boundary: Open file “plot_all_cells_.csv”
    a. Calculating average area from column “flood area” of all cells from each image
    b. Calculate SEM
9. Clonal interface: Select cells in the second row of wild-type cells around the clonal interface (w2)
    a. Open in Excel: “plot_clone_cells_’nb of clone for w2 cells’.csv”
    b. Calculate average value and STDEV and SEM for area of w2 cells
10. Deviation of apical cross section area:
    a. A/P boundary: Calculate ratio of $\bar{A}$ of A1 respectively P1 cells to $\bar{A}$ of all cells in the distinct image: $((\bar{A}_{A1,P1} - \bar{A}_{all\ cells}) / \bar{A}_{all\ cells}) * 100$ in [%]
        i. Plot in a column-chart with SEM
    b. Clonal interface: Calculate ratio of $\bar{A}$ of C1 respectively W1 cells to $\bar{A}$ of W2 cells in the distinct image: $((\bar{A}_{W1,C1} - \bar{A}_{W2}) / \bar{A}_{W2}) * 100$ in [%]
        i. Plot in a column-chart with SEM

7.6.5 Quantification of deviation of the vertex angle

The deviation of the vertex angle was quantified as follows:

1.-6. like 7.6.2

7. Open image in Packing Analyzer v.4.0
8. Plots- “Clonal interface angles”
9. open “Angles_at_interface_between_clone_nb1_nb2.csv” in Excel
10. Calculate average and SEM from column “corrected angle”

11. Calculate deviation of vertex angle ϕ between junctions along the A/P or clonal interface from the average vertex angle <ϕ>=119.8 (Landsberg, Farhadifar et al. 2009): $=((\phi_{AP}-<\phi>)/<\phi>)*100$ in [%]
12. Plot in column chart with SEM

7.6.6 Quantification of clonal roughness

The algorithm for calculating clonal roughness was developed by Maryam Aliee, (unpublished). The clonal roughness was quantified as follows:

1.-6. like 7.6.2

7. "Virtual cloning"- mark all cells in the clone
8. "Clonal roughness"
9. Open 'Clonal_roughness_clonenb.csv' in Excel.
10. Two columns: 1.'L', 2.'s'
11. Calculate s-L
12. Calculate Average and SEM for clonal roughness values of clones of certain type
13. Plot in xy-scatter (logarithmic scale, base=10) as a function of L.

7.7 EXPERIMENTAL SETUP

7.7.1 Using the Gal4-UAS-system for tissue-specific expression

The GAL4-UAS system was used for tissue-specific expression of transgenes (Brand and Perrimon 1993).

7.7.2 Mosaic analysis

The FLP-FRT-system (Golic and Lindquist 1989; Golic 1991) was used for heat-shock induced stochastic recombination, followed by formation of clones which are genetically different from the surrounding wild-type cells (Used for 8.11-.17).

7.7.3 Inactivating Hh protein in the anterior compartment by making use of a temperature sensitive allele of Hh

The following cross was performed and larvae were raised as follows:

1. Cross : D751 *yw hs-flp; UAS-GFP-gpi/ Cyo (y+); hh^{ts2} / TM6B* X
   D752 *yw hs-flp; en-GAL4, ubi DE-cad-GFP/ CyO (y+); hh^{ts2} / TM6B*
2. *F1: yw hs-flp; UAS-GFP-gpi/ en-Gal4, ubi DE-cad-GFP; $hh^{ts\ 2}$/ hh^{ts2}*
3. Raise larvae at 18°C
4. Shift larvae to 29°C before wandering stage for 24-26h

5. Dissecting wandering stage larvae for laser ablation and/or antibody staining
    a. Experiment: dissect green, non-tubby (homozygous for hh^{ts2}) larvae
    b. Control: green, tubby (heterozygous for hh^{ts2}) larvae
6. For 8.2: Antibody staining was done to detect Patched intensity
    a. 1st antibodies:
        i. mouse-anti-Patched
        ii. rabbit-anti-GFP (to mark the posterior compartment)
    b. 2nd antibodies:
        i. anti-mouse-Alexa555
        ii. anti-rabbit-Alexa488

7.7.4 Analyzing the shape of, and the morphological signatures of the cells along the A/P boundary in hh^{ts2}/hh^{ts2} and $hh^{ts2}/+$ wing imaginal discs

Used fly stock: yw hs-flp; en-lacZ / CyO; hh^{ts2}/ TM6B (from Caroline Sonnabend, Caro1)

1. Crossing flies
    a. for experiment: *yw hs-flp; en-lacZ / CyO; hh^{ts2}/ TM6B X*
    yw hs-flp; en-lacZ / CyO; hh^{ts2}/ TM6B
    b. for control: *yw hs-flp; en-lacZ / CyO; hh^{ts2}/ TM6B X*
    yw
2. Raise larvae at 18°C
3. At early to mid-third instar stage, shift larvae to 29°C for 24-36h
4. Dissect wandering stage larvae
    a. Experiment: dissect non-*tubby* larvae (homozygous for hh^{ts2})
    b. Control: dissect non-*tubby* larvae (heterozygous for hh^{ts2})

5. Antibody staining for F-Actin, DE-Cadherin and β-Gal
    a. 1st antibodies:
        i. rat anti-DE-cadherin (DCAD2)
        ii. mouse anti β-Galactosidase
    b. 2nd antibodies and dyes:
        i. anti-rat Cy5
        ii. anti-mouse Alexa 555
        iii. Phalloidin Alexa 488

7.7.5 Analysis of UAS-Ci^{PKA4} expressing clones

1. Cross D11 *yw hs-flp; en-lacZ/ CyO; Act5c>CD2>GAL4/ Act5c>CD2>GAL4* X
   a) D19 *yw hs-flp;;UAS-Ci^{PKA4}*
   b) *yw*
2. heatshock: 36˚C, 30’
3. incubate @25˚C for 3 days
4. Antibody staining
   a. 1st antibodies
      i. rat anti-DE-cadherin
      ii. mouse anti CD2
   b. 2nd antibodies:
      i. anti-rat Cy5
      ii. anti-mouse Alexa 555
      iii. Phalloidin Alexa 488

7.7.6 Generating UAS-Ci^{PKA4} expressing clones for laser ablation experiments

1. Generate stock:
   yw hs-flp; ubi-DE-Cad-GFP/ CyO; Act5c>CD2>GAL4, UAS-GFP-gpi/ TM6B
   a. Cross
      i. *D11 yw hs-flp; en-lacZ/ CyO; Act5c>CD2>GAL4/ Act5c>CD2>GAL4 X D777 yw hs-flp; ubi-DE-cad-GFP/ CyO (y+); UAS-GFP-gpi/ TM2*
      ii. F1: *yw hs-flp; ubi-DE-cad-GFP/ CyO; Act5c>CD2>GAL4/ UAS-GFP-gpi*
      iii. Select green, curly, non-TM2 female virgins
      iv. cross F1 to *yw hs-flp; Sp/CyO; MKRS/TM6B* (D145)
      v. F2: single ♂ (green, Hu, non-Sp, non-Sb, curly, dark red eyes)
      yw hs-flp; ubi-DE-cad-GFP/ CyO; Act5c>CD2>GAL4,UAS-GFP-gpi/ TM6B X
      yw hs-flp; Sp/CyO; MKRS/TM6B (D145*)*
         - Egg lay in 1st vial (to generate stock- interse)
         - Flip to 2nd vial
         - After 2-3 days, heatshock @ 36°C for 30’
         - incubation for 3 days at 25˚C
         - Dissect tubby larvae to see if clones are visible

2. Cross:

   yw hs-flp; ubi-DE-Cad-GFP/ CyO; Act5c>CD2>GAL4, UAS-GFP-gpi/ TM6B X

   y w;; UAS-Ci^{PKA4} /UAS-Ci^{PKA4} (D19)

3. Heat shock after 2-3 days of egg laying at 36°C for 30'
4. Incubate for 3 days at 25˚C
5. Dissect wandering stage larvae
   a. dissect green non-tubby larvae
   b. Perform laser ablation

7.7.7 Generating control clones for laser ablation

1. Cross

   yw hs-flp; ubi-DE-Cad-GFP/ CyO; Act5c>CD2>GAL4, UAS-GFP-gpi/ TM6B X

   yw

2. Heat shock after 2-3 days of egg laying at 36°C for 30'
3. Incubate for 3 days at 25˚C
4. Dissect wandering stage larvae
   a. dissect green non-tubby larvae
   b. Perform laser ablation

7.7.8 Generating wing discs which express UAS-Ci^{PKA4} in the posterior compartment for laser ablation

1. Cross D776 *enGAL4;ubiEcadGFP/CyO; UAS-GFP-gpi/TM6B X*
   D19 *;;UAS-Ci^{act}*

2. raise larvae @18ºC
3. Use wandering-stage larvae for laser ablation

7.7.9 Generating wing discs which express UAS-Ci^{PKA4} in the posterior compartment for analysing morphological signatures

1. Cross ;*enGAL4/CyO; UAS-GFP-gpi/TM6B X*
   D19 *;;UAS-Ci^{act}*

2. raise larvae @18ºC
3. use wandering-stage larvae for lantibody staining
4. Antibody staining:
   a. 1st antibodies:
      i. rat anti-DE-cadherin
      ii. rabbit-anti-GFP
   b. 2nd antibodies and dyes:
      i. anti-rat Cy5

ii. anti-rabbit Alexa 488
iii. Rhodamin-Phalloidin

7.7.10 Generating hh^{ts2} mutant wing discs which express UAS-Ci^{PKA4} in the posterior compartment for analysing morphological signatures

1. Establish stock: *yw hs-flp; UAS-GFP-gpi/ CyO; hh^{ts2}, UAS-ci^{PKA4}/ TM6B*
    a. Cross: *D751 yw hs-flp; UAS-GFP-gpi/ CyO; hh^{ts2} /TM6B X*
    yw hs-flp; Sp/CyO; UAS-ci^{PKA4}
        i. F1: *yw hs-flp; UAS-GFP-gpi/CyO; UAS-ci^{PKA4}/ hh^{ts2}* virgins X
        D145 yw hs-flp; Sp/CyO; MKRS/ TM6B
        ii. F2: single males *yw hs-flp; UAS-GFP-gpi/ CyO; UAS-ci^{PKA4} ,hh^{ts2}/ TM6B* X
        D145 yw hs-flp; Sp/CyO; MKRS/ TM6B virgins
2. Cross *yw hs-flp; UAS-GFP-gpi/CyO; hh^{ts}, UAS-ci^{PKA4}/ TM6B* X
    D752 *yw hs-flp; en-GAL4, ubi DE-cad-GFP/ CyO (y+); hh^{t2s} / TM6B*
    a. Raise larvae at 18˚C
    b. Temperature shift @29˚C for 24-26h
3. Dissect wandering stage larvae for antibody staining
    a. Experiment: dissect green, non-tubby (*UAS-ci^{PKA4},hh^{ts2}/hh^{ts2}*) larvae
    b. Control: green, tubby (*UAS-ci^{PKA4},hh^{ts2}/TM6B*) larvae
4. Antibody staining:
    a. 1st antibodies:
        i. rat-anti DE-cadherin
        ii. mouse-anti-Patched /mouse-anti-Engrailed
        iii. rabbit-anti-GFP
    b. 2nd antibodies:
        i. anti-rat Cy5
        ii. anti-mouse Alexa555
        iii. anti-rabbit Alexa488

7.7.11 Generating hh^{ts2} mutant wing discs which express UAS-Ci^{PKA4} in the posterior compartment for laser ablation

1. Cross *yw hs-flp; UAS-GFP-gpi/CyO; hh^{ts}, UAS-ci^{PKA4}/ TM6B* X
    D752 *yw hs-flp; en-GAL4, ubi DE-cad-GFP/ CyO (y+); hh^{t2s} / TM6B*
    a. Raise larvae at 18˚C
    b. Temperature shift @29˚C for 24-26h
2. Dissect wandering stage larvae for laser ablation

a. Experiment: dissect green, non-tubby (*UAS-ci^{PKA4},hh^{ts2}/hh^{ts2}*) larvae
b. Control: green, tubby (*UAS-ci^{PKA4},hh^{ts2}/TM6B*) larvae

7.7.12 Detectin patched and dpp expression levels in enGal4-UAS-ci^{PKA4} expressing wing imaginal discs

1. Generate stocks:
    a. *;ptc-lacZ/+;UAS-ci^{PKA4}/+*
        i. D298 *yw hs-flp; ptc-lacZ (nuclear) X*
        D19 *;; UAS-ci^{PKA4}*
    b. *;dpp[disc]-lacZ (cytoplasmatically)/+; UAS-ci^{PKA4}/+*
        i. D237 *y hs-flp; dpp[disc]-lacZ X*
        D19 *;; UAS-Ci^{PKA4}*
2. Cross (a) and (b) to ;*enGAL4/CyO; UAS-GFP-gpi/TM6B*
    a. F1: ;*enGAL4/patched-lacZ; UAS-GFP-gpi/+*
    b. F1: ;*enGAL4/dpp-lacZ; UAS-GFP-gpi/+*
3. Larvae were raised at 25˚C (a) or 18˚C (b)
4. Antibody staining:
    a. 1st antibodies:
        i. rat anti-DE-cadherin
        ii. mouse anti β-Gal
        iii. rb anti-GFP
    b. 2nd antibodies:
        i. anti-rat Cy5
        ii. anti-mouse Alexa 555
        iii. anti-rb-Alexa 488

7.7.13 Laser ablation along en$^-$/inv$^-$ clones

1. Cross: D196 *yw hs-flp; FRT42 en[E]/ CyO y+* X
    yw hs-flp; FRT42 ∆ECadGFP/ CyO y+
2. Heat-shock for 40’ at 37˚C
3. Incubation at 25˚C for 3 days
4. Dissect wanderin stage larvae for laser ablation
5. Laser ablation was done at cell bonds inside the anterior (control) and posterior compartment

7.7.14 Analysis of the morphological signatures along en⁻/inv clone

1. Cross: D196 *yw hs-flp; FRT42 en[E]/ CyO y+* X
   yw hs-flp; FRT42 ΔECadGFP/ CyO y+
2. Heat-shock for 40' at 37˚C
3. Incubation at 25˚C for 3 days
4. Dissect wanderin stage larvae for antibody staining
5. Antibody staining:
   a. 1st antibodies:
      i. rabbit-anti-GFP
      ii. rat-anti-Decadherin
   b. 2nd antibodies/dyes:
      i. anti-rabbit Alexa488
      ii. anti-rat Cy5
      iii. Phalloidin- Alexa488

7.7.15 Generating en⁻, ci⁻ double mutant clones

1. Cross: yw hsFLP; FRT42D enE/CyO;; Ci94/Dp(y+) *X*
   yw hsFLP; FRT42D ubiGFP(ci+)/CyO;; Ci94/Dp(y+)
2. Heatshock for 60' at 37˚C
3. Incubation at 25˚C for 3 days
4. Dissect *y⁻* wandering stage larvae
5. Antibody staining:
   a. 1st antibodies:
      i. rabbit anti-GFP
      ii. mouse anti-Engrailed
      iii. rat anti-DEcadherin
   b. 2nd antibodies:
      i. anti-rabbit Alexa488
      ii. anti-mouse Alexa555
      iii. anti-rat Cy5

7.7.16 Generating capricious overexpressing clones for laser ablation

1. Cross:
   yw hs-flp; ubi-DE-Cad-GFP/ CyO; Act5c>CD2>GAL4, UAS-GFP-gpi/ TM6B X
   D773 *yw; UAS-caps /UAS-caps*
2. Heat shock after 2-3 days of egg laying at 36°C for 30'
3. Incubate for 3 days at 25˚C
4. Dissect wandering stage larvae
   a. dissect green non-tubby larvae
   b. Perform laser ablation

7.7.17 Generating capricious overexpressing clones for analysis of the morphological signatures

1. Cross D11 *yw hs-flp; en-lacZ/ CyO; Act5c>CD2>GAL4/ Act5c>CD2>GAL4* X
   a) D773 *yw hs-flp;UAS-caps*
2. heatshock: 36˚C, 30'
3. incubate @25˚C for 3 days
4. Antibody staining
   a. 1st antibodies
      i. rat anti-DE-cadherin
      ii. mouse anti CD2
   b. 2nd antibodies:
      i. anti-rat Cy5
      ii. anti-mouse Alexa 555
      iii. Phalloidin Alexa 488
5. Dissect wandering stage larvae

8 RESULTS

8.1 EXPERIMENTAL DESIGN I: EXPLORING THE ROLE OF HEDGEHOG SIGNALING IN MAINTAINING THE MORPHOLOGICAL SIGNATURES OF AND THE INCREASE IN MECHANICAL TENSION ALONG THE AP BOUNDARY

The AP compartment boundary in the *Drosophila* wing disc is established via Engrailed and the Hedgehog signaling pathway. Besides these chemical signals, a local increase of mechanical tension is important to maintain the straight shape of the A/P boundary. The following experiments were performed to test whether Engrailed and Hedgehog signaling are important to maintain the straight shape of the boundary and the morphological signatures of the cells along the AP boundary. Moreover, I tested whether differences in Hh signal transduction activity regulate the increase in mechanical tension along the A/P boundary.

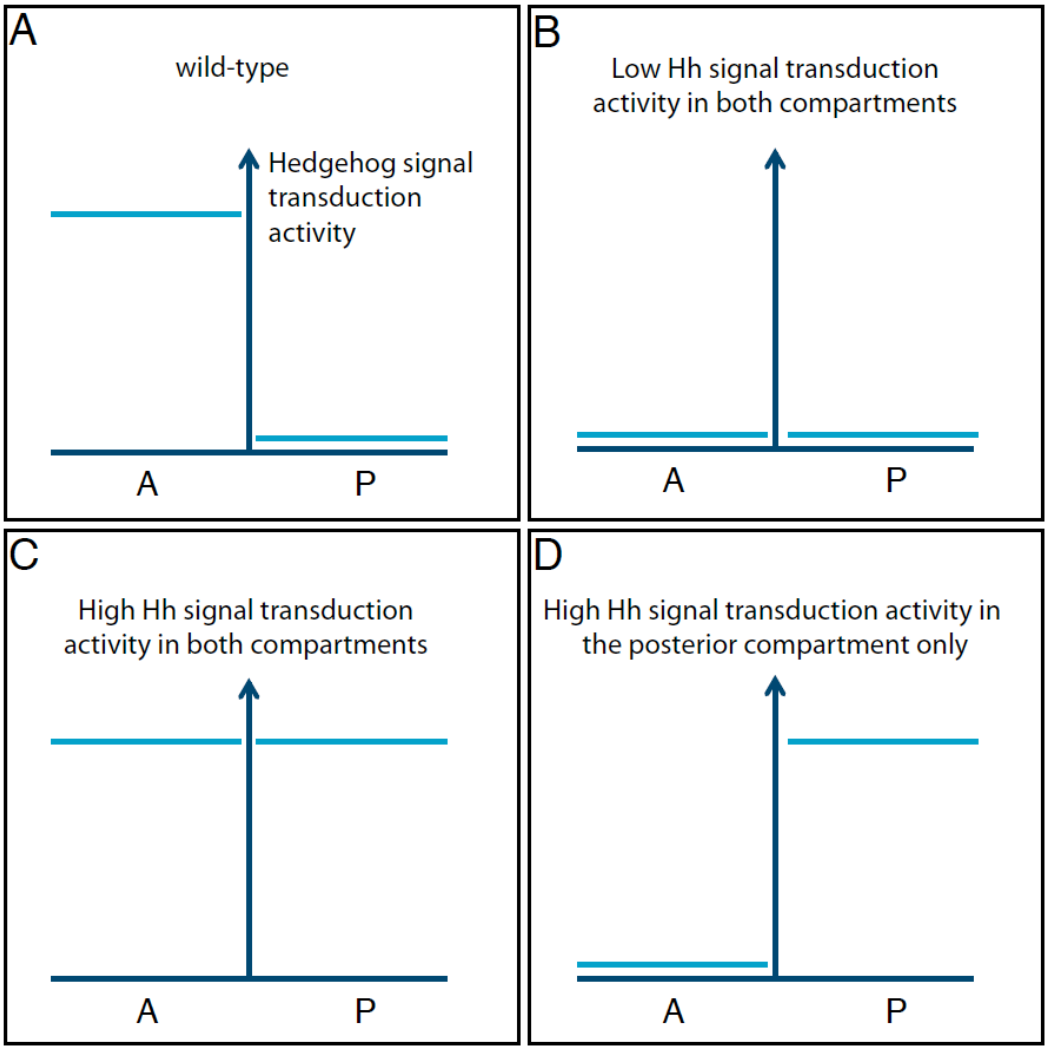

Figure 11: Experimental scenarios of differences in Hh signal transduction activity along the A/P compartment boundary in the *Drosophila* wing imaginal disc.
Different scenarios where used to test whether differences in Hh signal transduction activity are necessary and sufficient for the straight shape of, and the morphological signatures of cells along, the A/P compartment boundary in the *Drosophila* wing imaginal disc. Moreover, it was tested whether the differential expression of Hh signal transduction activity is necessary and sufficient for the increase in mechanical tension at cell bonds along the A/P boundary in these four scenarios. **(A)** Wild-type situation. Hh signal transduction activity is low in the posterior compartment and high in the anterior compartment. **(B)** Hh signal transduction activity is low in the posterior as well as in the anterior compartment. **(C)** Hh signal transduction activity is high in the posterior as well as in the anterior compartment. **(D)** Hh signal transduction activity is high in the posterior compartment and low in the anterior compartment.

The role of the Hh signaling pathway in maintaining the shape of the AP boundary and the increase in mechanical tension was examined in four different scenarios of Hh signal transduction activity in the wing disc, which were achieved by various genetic tools (Figure 11). In the wild-type condition Hh signal transduction activity is low in the posterior compartment, as it does not lead to detectable target gene expression, whereas it is high in the first cell rows of the anterior compartment (Figure 11 A). In the second scenario Hh signal transduction activity is low in both compartments. This will test the requirement of the Hh protein for maintaining the AP boundary (Figure 11 B). In the third scenario Hh signal transduction activity is high in both compartments. This will test whether a difference in Hh signal transduction activity along the AP boundary is necessary to maintain a straight A/P boundary (Figure 11 C). To test whether the difference in Hh signal transduction activity is sufficient to maintain the signatures of the AP boundary, we generated a scenario in which Hh signal transduction activity is high in the posterior but low in the anterior compartment in the last scenario (Figure 11 D). The shape of the boundary, the morphological signatures of the cells along it and the relative mechanical tension were examined in all of the four scenarios. The shape of the boundary was quantified by measuring roughness, which is defined as the deviation of the boundary line from a straight line for different average cell bond lengths (Figure 12 A).

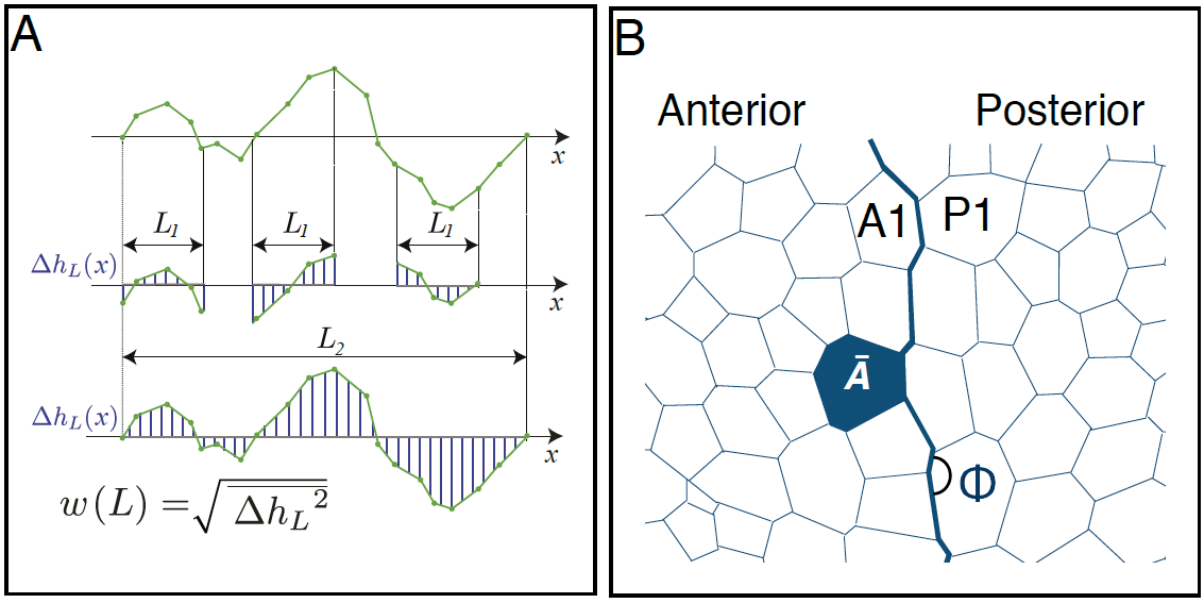

Figure 12: Roughness measurement and analysis of the morphological signatures of the cells along the A/P boundary
(A) Quantification of boundary shape by measuring roughness *w*. The deviation($\Delta h_L(x)$) for any distance (L) along the x-axis (x) of the boundary compared to a straight line within the distance L is quantified (modified from Aliee, Roper et al. 2012). **(B)** Quantification of the morphological signatures of cells along the A/P boundary. The average apical cross section area ($\bar{A}$) of cells along the A/P boundary (A1, P1) and the vertex angles (ϕ) between cell junctions along the A/P boundary were quantified (modified from Landsberg, Farhadifar et al. 2009)

The vertex angle (ϕ) between boundary cells and between cells of the same compartment, the apical cross section area ($\bar{A}$) of A1 and P1 cells and cells in the compartments and the F-actin pixel intensity between cell bonds along the boundary (Figure 12 B, bold blue line) were quantified for the different scenarios. Using laser ablation the relative increase in mechanical tension along the AP boundary was quantified (Figure 13).

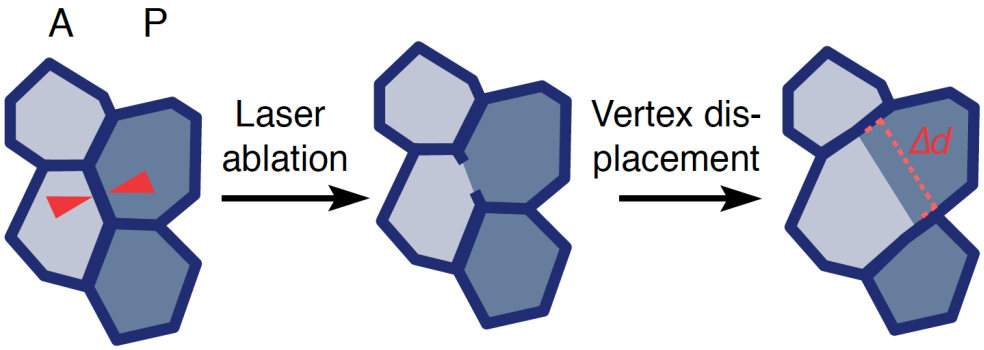

Figure 13: Quantification of vertex distance increase after laser ablation.
Vertex distance increase following laser ablation was quantified by measuring the vertex displacement for several timepoints after the cut and quantifying the distance increase (Δd) for each timepoint (see Material and Methods section) (modified from illustration by Daiki Umetsu).

The vertex distance increase after laser ablation was calculated by tracking the displacement of the vertices (Δd) before and after the cut for some time (Figure 13) and describes the long-term response to the ablation. Whereas the initial velocity is calculated by measuring the difference in vertex distance 250ms after the cut and rather describes the immediate response to the cut. Both serve as relative measurements for mechanical tension (Landsberg, Farhadifar et al. 2009).

8.2 INACTIVATING THE HEDGEHOG PROTEIN LEADS TO A LOSS IN HEDGEHOG SIGNAL TRANSDUCTION ACTIVITY IN THE WING DISC

To test whether the activity of the Hedgehog protein has an influence on the correct establishment and maintenance of the AP boundary, we sought to reduce Hedgehog signaling activity using a temperature sensitive allele of *hh* (*hh*^{ts2}) (Ma, Zhou et al. 1993). Larvae carrying the allele were raised at the permissive temperature and shifted to the restrictive temperature for 24 to 26 h, which led to a loss of function of the Hh protein. Membrane-anchored GFP (GFP-gpi), driven by the *engrailed* promoter served as a marker for the posterior compartment. The expression level of Patched served as an indicator for Hh signal transduction activity. In control wing discs, Patched was expressed in a stripe along the AP compartment boundary (Figure 14 A). No Patched expression was detectable in wing discs homozygous for *hh*^{ts2} at restrictive temperature (Figure 14 B). These results show that inactivating the Hh protein is sufficient to deactivate Hedgehog signal transduction activity.

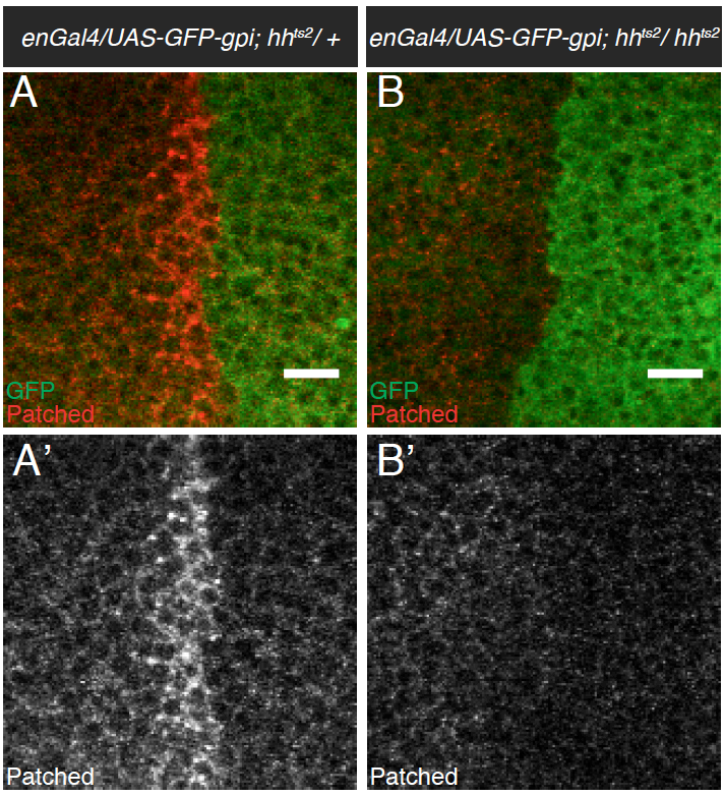

Figure 14: Inactivating Hh is sufficient to reduce the Hh signal transduction activity in the anterior compartment.
Cropped confocal images of a control wing disc **(A)** and a wing disc homozygous for hh^{ts2} **(B)** of wandering-stage larvae. Control and *hh* mutant larvae were raised for 24-26 hrs at restrictive temperature. The posterior compartment is marked by expression of *UAS-GFP-gpi* under the control of the *engrailed* promoter (*enGal4)* and antibody staining against GFP **(A,B;green).** Antibody staining against Patched was used as a readout for Hh signal transduction activity **(A,B;red and A',B')** . Scale bars represent 10µm. **(A,A')** Patched is expressed in the first cell rows of the anterior compartment in control wing discs heterozygous for hh^{ts2}. **(B,B')** Patched is not expressed anymore when Hh is inactivated.

8.3 HEDGEHOG IS IMPORTANT FOR THE STRAIGHT SHAPE AND THE MORPHOLOGICAL SIGNATURES OF THE AP BOUNDARY

To test whether the activity of the Hh protein is required to maintain the straight shape and the morphological signatures of the AP boundary, Hh signal transduction activity was reduced in the wing disc using the hh^{ts2} allele. The *engrailed-lacZ* enhancer trap was used to mark the posterior compartment. For analysing the morphological signatures of the boundary larvae were treated as described in the previous paragraph. The wing discs were stained with antibodies against DE-cadherin and β-Galactosidase (Figure 15 A and B) to recognize the apical cell membranes (green) and the posterior compartment (red). The confocal images were segmented with the Packing Analyzer Software (Aigouy, Farhadifar et al. 2010) (Figure 15 A' and B'). The red line marks the compartment boundaries. The roughness of the AP boundary was increased significantly ($p<0.01$ – $p<0.05$) for all distances L (L=1 represents the average cell bond length of one bond along the A/P boundary) in hh^{ts2}

homozygous mutant wing discs compared to heterozygous control wing discs (Figure 16 A). The average vertex angle deviation showed a significant ($p<0.001$) decrease for hh^{ts2} mutants compared to control wing discs. The deviation of the vertex angle is 8% (±0.59 SEM; n=6) in control wing discs and 2.1% (±1.12 SEM; n=4) in hh^{ts2} mutant wing discs (Figure 16, B). The apical cross section area of A1 cells is 19.9% (±2.55 SEM; n=6) and of P1 cells 25.1% (±5.3 SEM; n=6) larger compared to the average area of all cells in control wing discs. In hh^{ts2} mutants, A1 and P1 cells are significantly smaller (A1: 2.9%±6.6 SEM; n=8, P1: -0.07%±4.75 SEM; n=8) than A1 and P1 cells in the control (Figure 16 C). In the control case F-actin pixel intensity was increased (Figure 15 A'', arrowhead) along the AP boundary by 13.67% (±2.7 SEM, n=4) (Figure 16, D). F-actin pixel intensity along the AP boundary was not increased (-1.83%±0.54; n=4; $p<0.01$) in hh^{ts2} mutants (Figure 15 B''; Figure 16 D). These results show that inactivating Hh results in a rougher boundary and a loss of all morphological signatures of the AP boundary. We conclude that Hh is important to maintain the straight shape and the morphological signatures of the AP boundary.

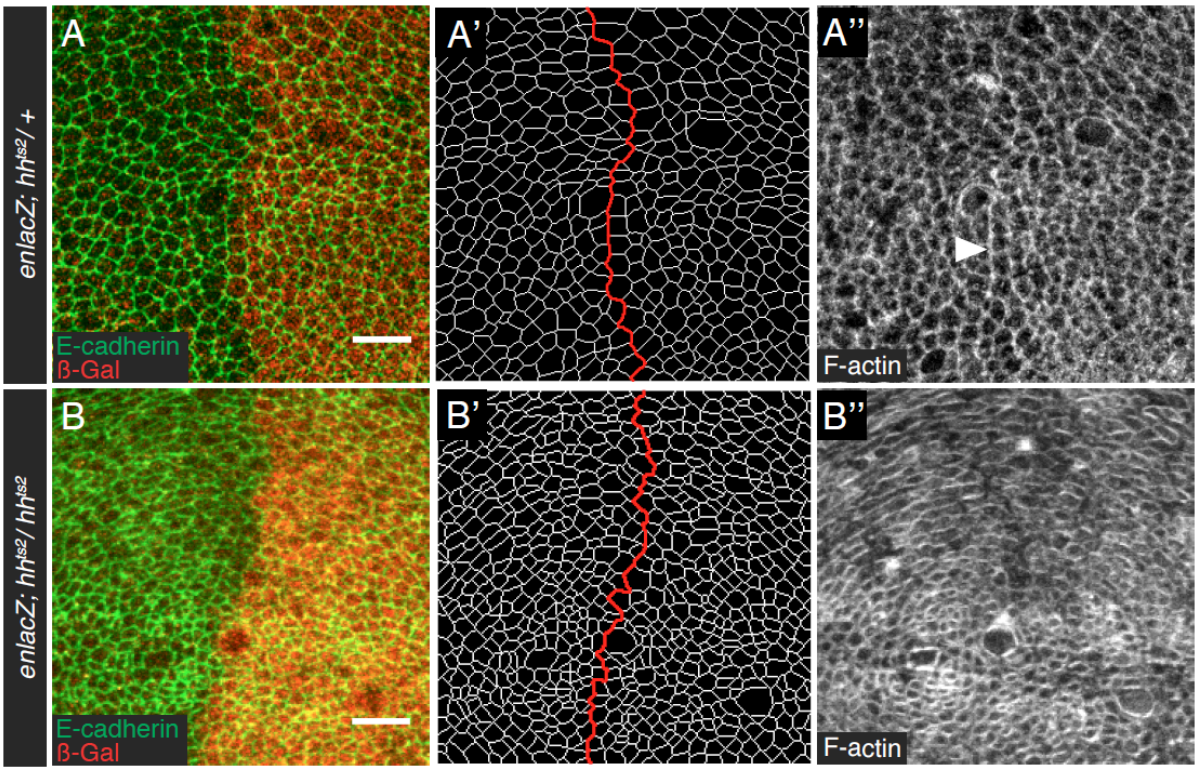

Figure 15: Hh is necessary for the straight shape of, and the increase in F-actin at junctions along, the A/P boundary.
Cropped confocal images of a control wing disc **(A)** and a wing disc homozygous for hh^{ts2} **(B)** of wandering-stage larvae. Control and hh^{ts2} mutant larvae were raised for 24-26 hrs at restrictive temperature. The posterior compartment is marked by the *enlacZ* enhancer trap and antibody staining against ß-Gal **(A,B;red).** Antibody staining against DE-cadherin was used to mark the adherens junctions **(A,B;green)**. The cell bonds on the level of adherens junctions were segmented using Packing Analyzer for quantitative image analysis. The red line marks the A/P boundary **(A',B').** F-actin was labeled using Phalloidin **(A'', B'').** Scale bars represent 10µm. **(A, A')** The A/P boundary is straight in control wing discs heterozygous for hh^{ts2}. **(B,B')** The A/P boundary is more irregular when Hh is inactivated. **(A'')** F-actin is increased at cell junctions along the A/P boundary in control wing discs (arrowhead). **(B'')** F-actin is not increased anymore when Hh is inactivated.

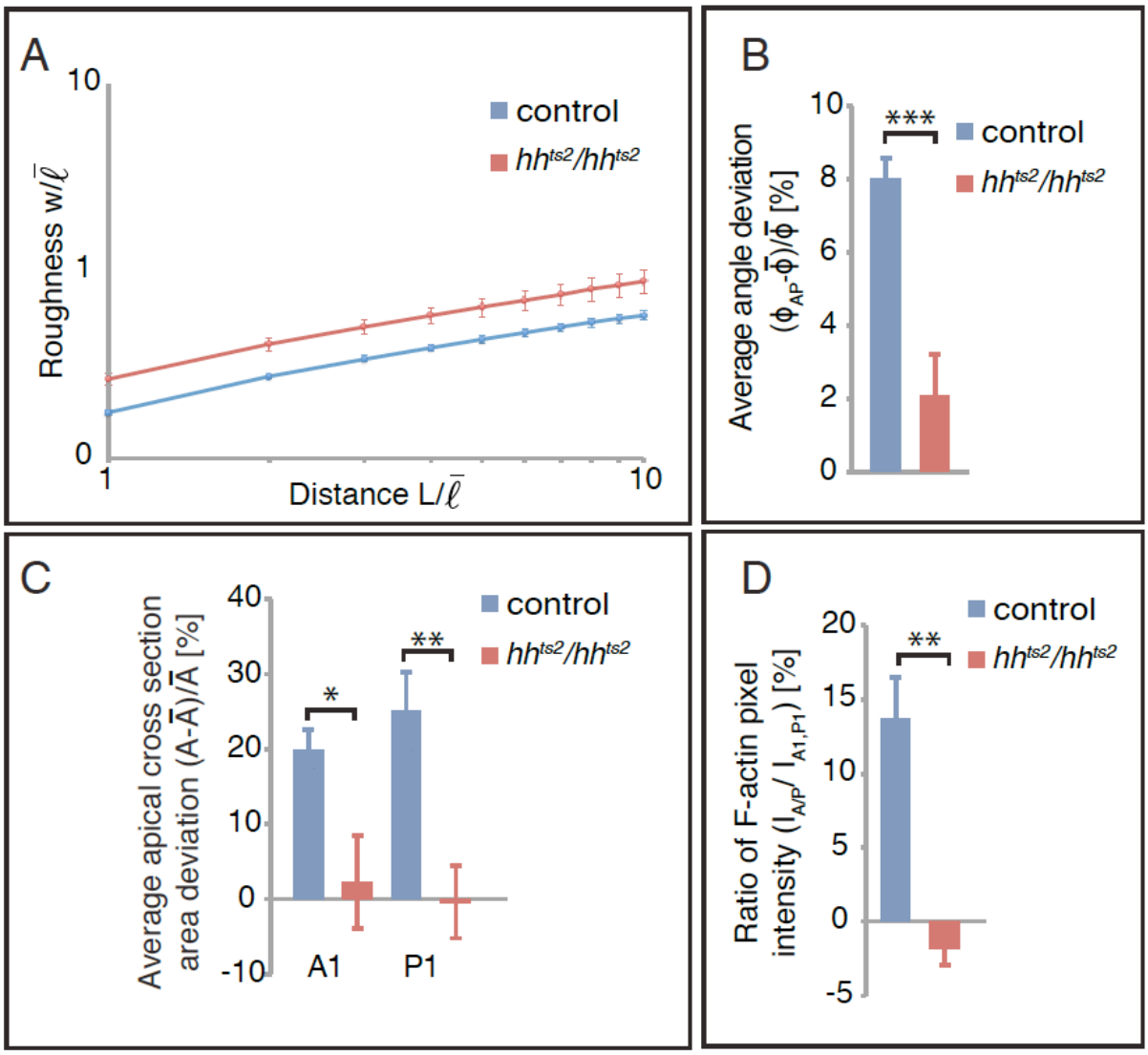

Figure 16: Hh is necessary for the straight shape of, and the morphological signatures of cells along, the A/P boundary.
(A) Roughness *w,* normalized to the average cell bond length </> for 1 to 10 average cell bond lengths (L) of the A/P boundary of control (blue) and Hh mutant (red) wing discs. Mean and SEM are shown. p<0.01-0.05 for L 1-10, n=6 for control and n=7 for Hh mutant wing discs. **(B)** Average deviation of the vertex angle between cell junctions along the A/P boundary (ϕ_{AP}) from the average vertex angle between junctions in the wing disc (<ϕ>=119,8 (Landsberg, Farhadifar et al. 2009)) for control (blue) and Hh mutant (red) wing discs in [%]. Mean and SEM are shown. p<0.001, n= 6 (control), n=4 (Hh mutant). **(C)** Apical cross section area deviation for cells in the first row anterior (A1) and posterior (P1) parallel to the A/P boundary in control (blue) and Hh mutant wing discs (red) from the average apical cross section area of cells in the wing disc (<A>) in [%]. Mean and SEM are shown. A1: p<0.05, n=6 (control), n=8 (Hh mutant wing discs). P1: p<0.01, n=6 (control), n=8 (Hh mutant wing discs). **(D)** Ratio of F-actin pixel intensity of junctions along the A/P boundary (I_{AP}) compared to cell junctions of A1 and P1 cells ($I_{A1,P1}$) in [%] for control (blue) and Hh mutant (red) wing discs. Mean and SEM are shown. p<0.01, n=4 (control), n=4 (Hh mutant wing discs).

8.4 HEDGEHOG IS REQUIRED FOR THE INCREASE IN MECHANICAL TENSION ALONG THE AP COMPARTMENT BOUNDARY

To test whether the activity of the Hh protein is required for the increase in mechanical tension at cell bonds along the AP boundary, laser ablation was performed in control and hh^{ts2} mutant wing discs. Larvae were treated as described above. An *ubi-DEcadherin-GFP* transgene was used to recognize the cell membranes on the level of adherens junctions and *enGal4* and *UAS-GFP-gpi* were used to identify cells of the posterior compartment. Single cell bonds at the AP boundary and away from it inside the compartments were ablated in control and hh^{ts2} mutant wing discs. The vertex distance increase after ablation was measured and from that the initial velocity of vertex displacement after 250ms was calculated. The vertex distance increase for cuts along the AP boundary was increased compared to cuts away from it for all timepoints after the cut in hh^{ts2}/+ control wing discs (Figure 17 A). In hh^{ts2} mutants the vertex distance increase for cuts at the AP boundary was indistinguishable to cuts away from it for all timepoints (Figure 17 B). The initial velocity of vertex displacement 250ms after the cut between cells of the same compartment in control wing discs was 1.54µm/s (±0.2,n=10) (Figure 17 C). The initial velocity was significantly increased (3.19µm/s ±0.2, n=10, $p<0.001$) for cuts along the AP boundary. Thus, mechanical tension is increased 2-fold along the AP boundary in the wild-type situation. In hh^{ts2} mutants the initial velocity was similar for cuts in the compartments (2µm/s ±0.15, n=16) and cuts along the AP boundary (1.91µm/s ±0.2, n=19) (Figure 17 D). Therefore mechanical tension is not increased along the AP boundary in hh^{ts2} mutants. These results show that Hh is important for the increase in mechanical tension along the AP compartment boundary.

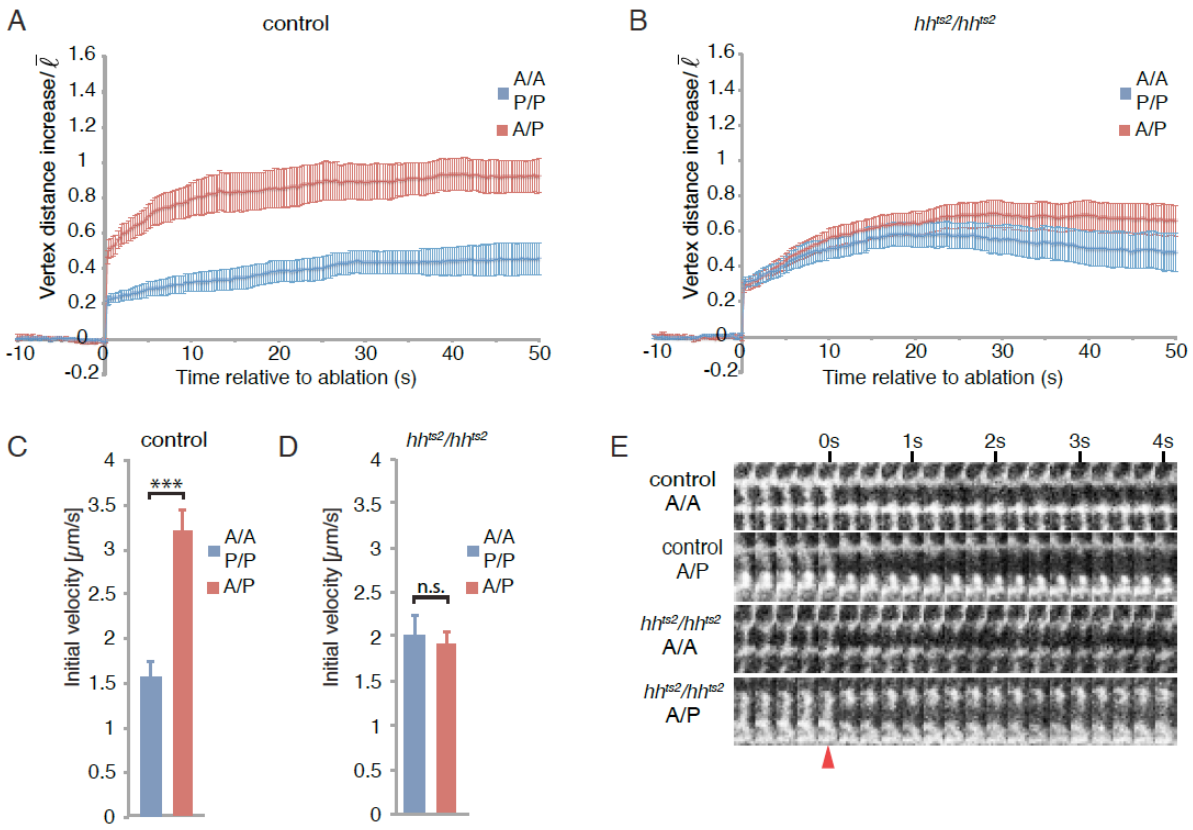

Figure 17: Hh is necessary for the increase in mechanical tension along the A/P boundary. **(A,B)** Vertex distance increase normalized for the average cell bond length in the wing disc (1.7µm (Landsberg, Farhadifar et al. 2009)) as a function of time relative to ablation. Cell bonds between cells of the same compartment (A/A,P/P; blue) and along the A/P boundary (A/P; red) were ablated and vertex displacement was measured every 250ms for 10s before and 50s after the cut. **(A)** Vertex distance increase for cuts in hh^{ts2}/+ control wing discs. Mean and SEM are shown: n=10 (A/A, P/P), n=10 (A/P). **(B)** Vertex distance increase for cuts in Hh mutant wing discs. Mean and SEM are shown: n=16 (A/A, P/P), n=19 (A/P). **(C,D)** Initial velocity [µm/s] of vertex displacement 250ms after ablation for cell bonds between cells of the same compartment (A/A, P/P; blue) and cell bonds along the A/P boundary (A/P; red). **(C)** Initial velocity for cuts in control wing discs. Mean and SEM are shown: p<0.001, n=10 (A/A, P/P), n= 10 (A/P). **(D)** Initial velocity for cuts in Hh mutant wing discs. Mean and SEM are shown: p>0.05, n=16 (A/A, P/P), n= 19 (A/P). **(E)** Kymographs for cuts of cell bonds between cells in the anterior compartment (A/A) and along the A/P boundary for control and Hh mutant wing discs for 4s after the cut. The frame rate is 4 frames/s. The red arrowhead marks the timepoint of the cut.

8.5 ECTOPIC EXPRESSION OF CI IN THE POSTERIOR COMPARTMENT LEADS TO HEDGEHOG SIGNAL TRANSDUCTION ACTIVITY IN THE ANTERIOR AND POSTERIOR CELLS

To test whether high levels of Hh signal transduction activity in both compartments (Figure 11 C) have an influence on the shape, the morphological signatures of and the increased mechanical tension at the AP boundary, the Hh-downstream transcription factor Ci was ectopically expressed in the posterior compartment. The *patched-lacZ* and *dpp-lacZ* enhancer traps were used for the read-out of the Hh signal transduction activity in the anterior and posterior compartments. The expression of *patched* is positively regulated by Ci

(Alexandre, Jacinto et al. 1996) and *dpp* is a target gene of Ci (Padgett, St Johnston et al. 1987; Basler and Struhl 1994; Tabata and Kornberg 1994; Zecca, Basler et al. 1995), therefore their expression levels are appropriate readouts of the Hh signal transduction activity. To increase Hh signal transduction activity in the posterior compartment, *UAS-ci*^{PKA4} was ectopically expressed under the control of the *engrailed* promoter. The allele *ci*^{PKA4} encodes for an isoform of Ci that cannot be phosphorylated due to the substitution of 6 serin residues by alanins. Thereby, protelolytic cleavage cannot be conducted, which results in an Hh-signaling independent activation of target gene expression by a constitutively active Ci molecule (Methot and Basler 2000).The *UAS-GFP-gpi* construct was used to mark the posterior compartment. Larvae were raised at 18˚C, dissected at the wandering stage and immunolabeled for β-Galactosidase and GFP. In control wing discs *patched* is expressed in the first 5-8 cell rows of the anterior compartment (Figure 18 A-A''). The β-Galactosidase is located in the nucleus, therefore confocal images were taken on the basal focal plane. When *ci*^{PKA4} is expressed posterior, *patched* is expressed in all cells of the posterior compartment and in the first one to two cell rows in the anterior compartment (Figure 18 B-B''). Patched in the posterior compartment may sequester most of the Hh molecules, which may lead to less Hh molecules reaching anterior cells and by that to the reduced *patched* expression in the anterior compartment. In late 3rd instar wing discs *dpp* is expressed in an anterior stripe of cells located some cell rows away from the AP boundary (Figure 18 C-C''). Dpp is not expressed directly at the A/P boundary because Engrailed is expressed when the Hh concentration is high in a few cell rows in the anterior compartment in late wing disc development (Blair 1992). It represses *dpp* (Hidalgo 1994; Sanicola, Sekelsky et al. 1995; Maschat, Serrano et al. 1998), which needs only low concentrations of Hh and thus is expressed farther away from the boundary than *patched*. When *ci*^{PKA4} is expressed in the posterior compartment, *dpp* is expressed anterior in a stripe along the AP boundary and in the lateral and to some extend in the medial region of the posterior compartment (Figure 18 D-D''). As mentioned above Engrailed represses *dpp,* which explains the low expression levels in the posterior compartment. Due to less Hh in the anterior compartment *engrailed* is not expressed in anterior cells, which leads to *dpp* expression in the first cell rows of the anterior compartment. The *dpp* expression in the anterior cells confirms that Hh signal transduction is still active in the anterior cells. These results show that ectopic expression of *ci*^{PKA4} results in increased Hh signal transduction activity in the posterior compartment.

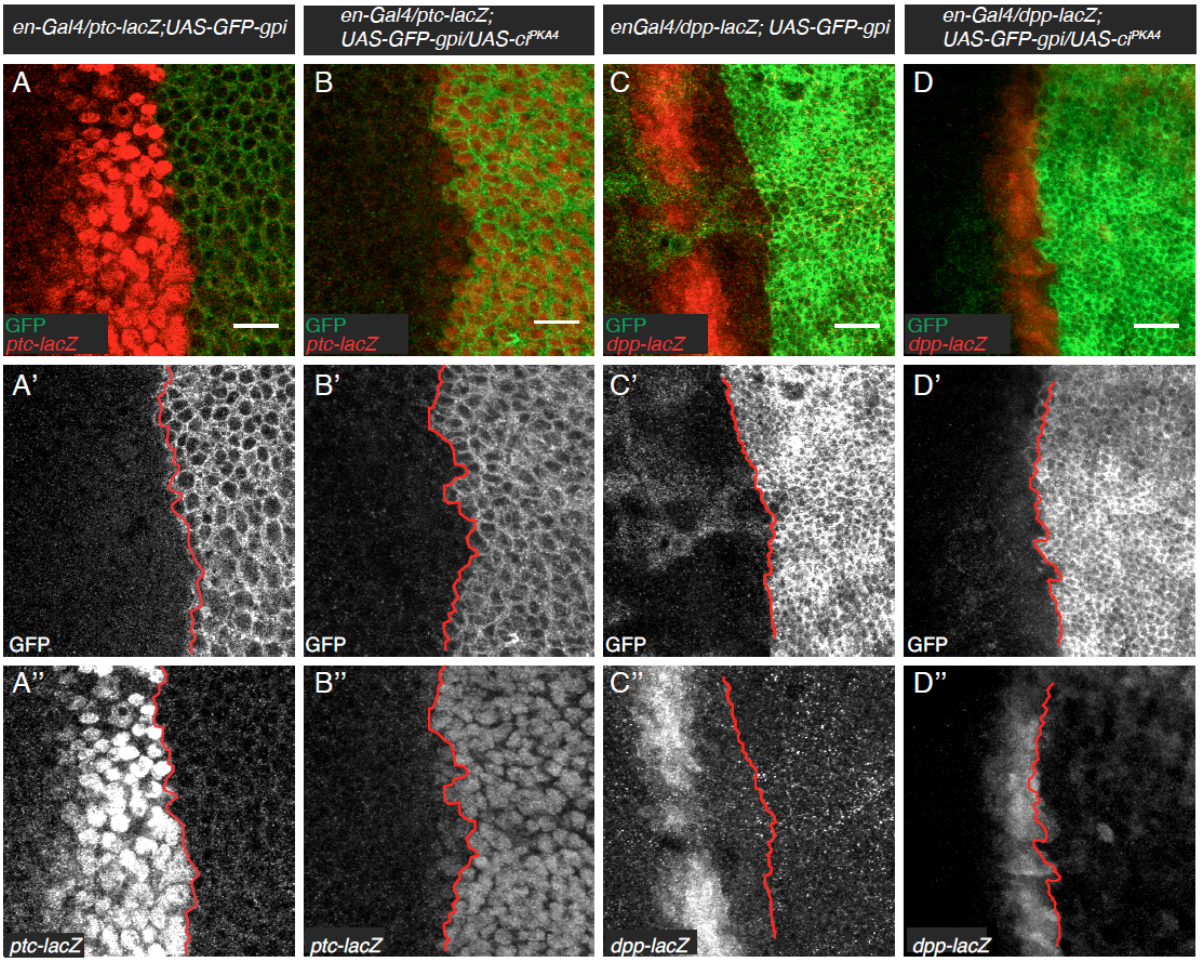

Figure 18: Ectopic expression of Ci in the posterior compartment leads to elevated levels of Hh signal transduction activity in the anterior and posterior compartment.
Cropped confocal images of control wing discs **(A,C)** and wing discs expressing *UAS-ci*^{PKA4} under the control of the *engrailed* promoter (*enGal4)* **(B,D)** of wandering-stage larvae. Larvae were raised at 18˚C (B-D) or 25˚C (A) . The posterior compartment is marked by expression of *UAS-GFP-gpi* under the control of the *engrailed* promoter and antibody staining against GFP **(A-D;green, A'-D').** The *ptc-lacZ and dpp-lacZ* enhancer-traps were used as a readout for Hh signal transduction activity **(A-D;red, A''-D'')**. The red line marks the A/P boundary **(A'-D').** Scale bars represent 10µm. **(A-A'')** Patched is expressed in the first cell rows of the anterior compartment in control wing discs. Images were taken at the basal focal plane, due to the nuclear localization of ß-Gal. **(B-B'')** When *ci*^{PKA4} is expressed in the posterior compartment, Patched is expressed in all cells of the posterior compartment and in the first 1-2 cell rows in the anterior compartment next to the A/P boundary. **(C-C'')** Dpp is expressed some cell rows away from the A/P boundary in the anterior compartment in control wing discs. Images were taken at the apical focal plane due to the cytoplasmatic localization of ß-Gal. **(D-D'')** Dpp is expressed in some cell rows next to the A/P boundary and in some cells in the posterior compartment when *ci*^{PKA4} is expressed in the posterior compartment.

8.6 A DIFFERENCE IN HEDGEHOG SIGNAL TRANSDUCTION ACTIVITY IS NECESSARY FOR THE MORPHOLOGICAL SIGNATURES OF THE AP BOUNDARY

To test whether a difference in Hh signal transduction activity is important for the shape and the morphological signatures of the AP boundary, we increased Hh signal transduction activity in the posterior compartment by expressing ci^{PKA4} under the control of the *engrailed* promoter. The posterior compartment was marked by the expression of *GFP-gpi.* The wing discs were stained with antibodies against DE-cadherin and GFP (Figure 19 A,B) to recognize the apical cell membranes (green) and the posterior compartment (red). The confocal images were segmented with the Packing Analyzer Software (Figure 19 D,E). The red line marks the compartment boundaries. The roughness of the AP boundary was increased significantly ($p<0.01$ – $p<0.05$) for all L when ci^{PKA4} was expressed posterior compared to control wing discs (Figure 20 C). The average vertex angle deviation along the AP boundary was significantly ($p<0.01$) decreased when Hh signal transduction was high in both compartments compared to control wing discs. The deviation of the vertex angle is 8% (±0.59 SEM; n=6) in control wing discs and 3.7% (±0.9 SEM; n=7) in ci^{PKA4} expressing wing discs (Figure 20 F). The deviation of the apical cross section area in ci^{PKA4} expressing wing discs was significantly (A1: $p<0.01$; P1: $p<0.001$) smaller (A1: 7.42%±2.4 SEM; n=5; P1: -4.5%±2.2 SEM; n=5) than for A1 and P1 cells in the control (Figure 20 G). F-actin is increased along the A/P boundary in control wing discs (13.67%±2.7; n=4), however, it is not significantly increased anymore ($p<0.05$) in wing discs with high Hh signal transduction activity in both compartments (6.3%±0.46; n=5). These results show that the difference in Hh signal transduction along the A/P boundary is required for the shape and the morphological signatures of the A/P boundary.

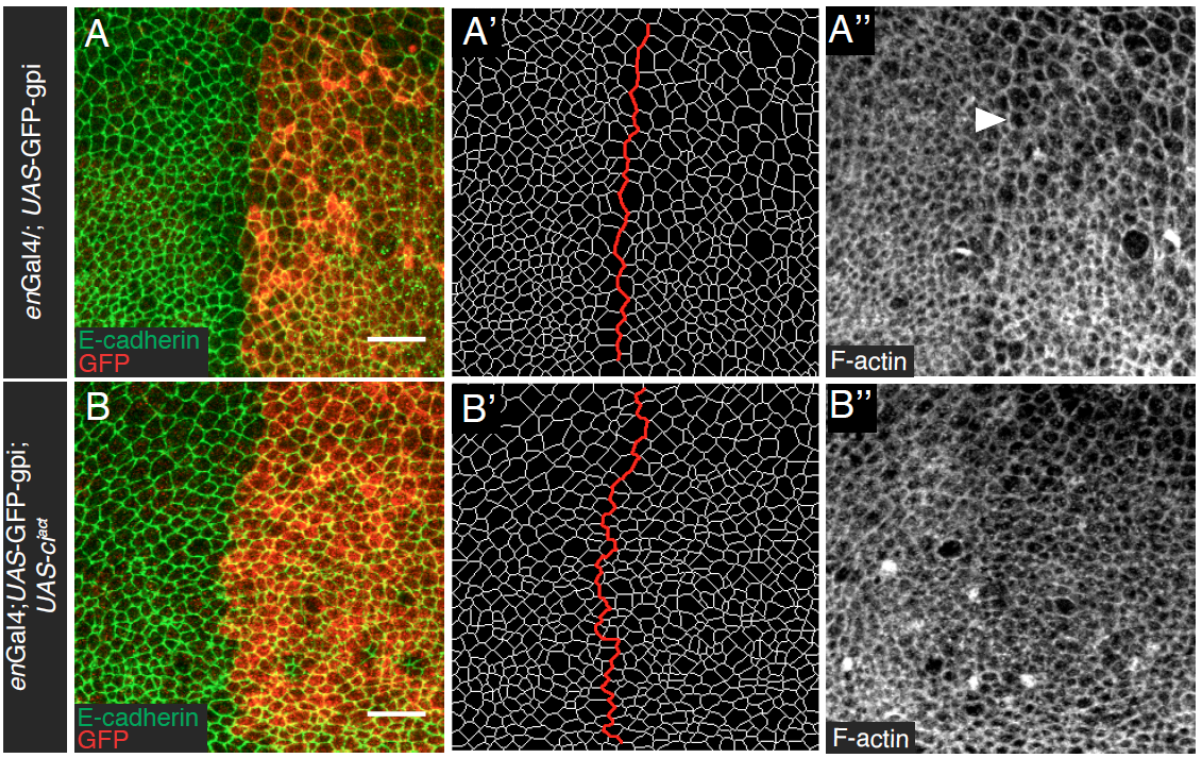

Figure 19: The difference in Hh signal transduction activity is necessary to maintain the straight shape of the A/P boundary.
Cropped confocal images of a control wing disc **(A)** and a wing disc expressing *UAS-ci*^{PKA4} in the posterior compartment **(B)** of wandering-stage larvae. Control and *enGal4 UAS-ci*^{PKA4} expressing larvae were raised at 18˚C. The posterior compartment is marked by expression of *UAS-GFP-gpi* under the control of the *engrailed* promoter and antibody staining against GFP **(A,B;red).** Antibody staining against E-cadherin was used to mark the adherens junctions **(A,B;green)**. The cell bonds on the level of adherens junctions were segmented using Packing Analyzer for quantitative image analysis. The red line marks the A/P boundary **(A',B').** F-actin was labeled using phalloidin **(A'', B'').** Scale bars represent 10µm. **(A, A')** The A/P boundary is straight in control wing discs. **(B,B')** The A/P boundary is more irregular when *ci*^{PKA4} is expressed in the posterior compartment. **(A'')** F-actin is increased at cell junctions along the A/P boundary in control wing discs (arrowhead). **(B'')** F-actin is not increased anymore when Hh signal transduction is increased in the posterior compartment.

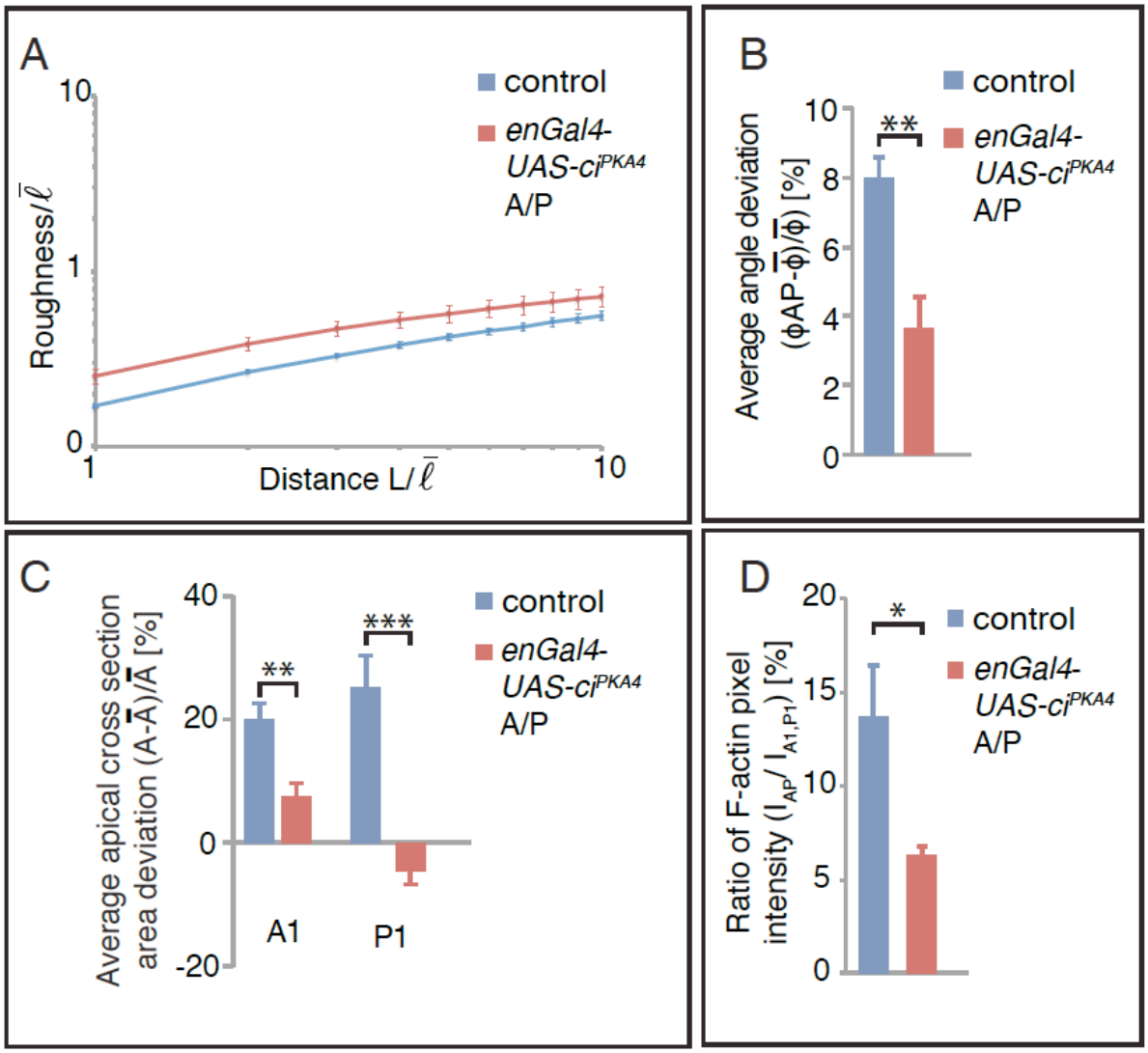

Figure 20: The difference in Hh signal transduction activity is necessary for the straight shape of, and the morphological signatures of the cells along, the A/P boundary

(A) Roughness *w,* normalized to the average cell bond length </> for 1 to 10 average cell bond lengths (L) of the A/P boundary of control (blue) and *enGal4 UAS-ci*^{PKA4} expressing (red) wing discs. Mean and SEM are shown. p<0.01-0.05 for L 1-10, n=6 for control and n=7 for *ci*^{PKA4} expressing wing discs. **(B)** Average deviation of the vertex angle between cell junctions along the A/P boundary (ϕ_{AP}) from the average vertex angle between junctions in the wing disc (<ϕ>=119,8 (Landsberg, Farhadifar et al. 2009)) for control (blue) and Hh mutant (red) wing discs in [%]. Mean and SEM are shown. p<0.01, n= 6 (control), n=7 (*UAS-ci*^{PKA4}). **(C)** Apical cross section area deviation for cells in the first row anterior (A1) and posterior (P1) parallel to the A/P boundary in control (blue) and Hh mutant wing discs (red) from the average apical cross section area of cells in the wing disc (<A>) in [%]. Mean and SEM are shown. A1: p<0.01, n=6 (control), n=5 (*UAS-ci*^{PKA4}). P1: p<0.001, n=6 (control), n=5 (*UAS-ci*^{PKA4}). **(D)** Ratio of F-actin pixel intensity of junctions along the A/P boundary (I_{AP}) compared to cell junctions of A1 and P1 cells ($I_{A1,P1}$) in [%] for control (blue) and *ci*^{PKA4} expressing (red) wing discs. Mean and SEM are shown. p<0.05, n=4 (control), n=5 (Hh mutant wing discs).

8.7 THE DIFFERENCE IN HEDGEHOG SIGNAL TRANSDUCTION ACTIVITY IS NECESSARY FOR THE INCREASE IN MECHANICAL TENSION ALONG THE AP BOUNDARY

To test whether the difference in Hh signal transduction activity between A and P cells is required for the increase in mechanical tension along the AP boundary, laser ablation was performed at the AP boundary and at cell bonds away from it in wild-type (Figure 11 A) and *ci*^{PKA4}expressing wing imaginal discs. The adherens junctions were marked by *ubi-DEcadherin-GFP* and the posterior compartment was marked by *UAS-GFP*-gpi, driven by *engrailed.* In control wing discs the vertex distance increase after ablation of cell bonds along the A/P boundary was larger compared to cuts away from the boundary (Figure 21 A). The vertex distance increase after the ablation was not increased for cuts along the AP boundary compared to cuts between cells of the same compartment in *UAS-ci*^{PKA4} expressing wing discs (Figure 21 A). The initial velocity after ablation of cell bonds along the A/P boundary in control wing discs (3.03µm/s±0.42; n=12) was significantly higher ($p<0.01$) than after cuts along A/A or P/P cell bonds (1.37µm/s±0.23; n=10) (Figure 21 B). Tension is increased by 2.2-fold along the A/P boundary in control wing imaginal discs. The initial velocity for cuts along the AP boundary in *ci*^{PKA4} expressing wing imaginal discs was not increased (1.84µm/s±0.15; n=15) compared to the initial velocity of cuts away from it (1.52µm/s ±0.15; n=14) (Figure 21 B). These results show that the difference in Hh signal transduction activity is necessary for the increase in mechanical tension along the AP compartment boundary.

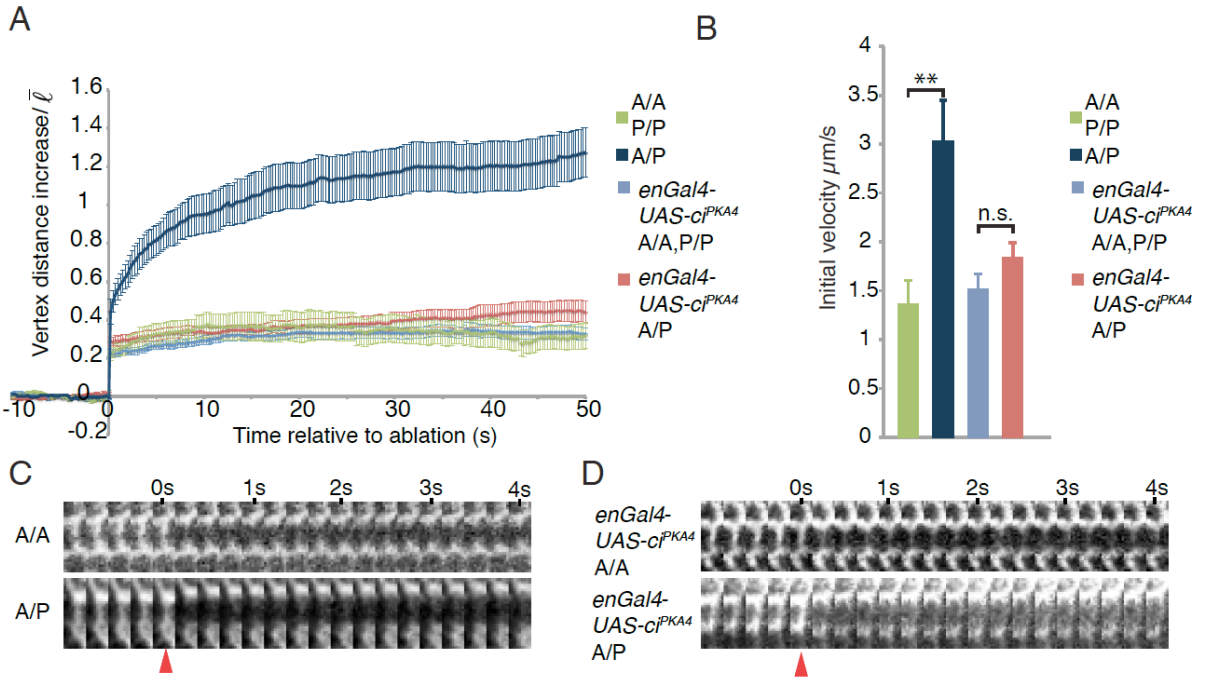

Figure 21: Ectopic expression of Ci in the posterior compartment leads to the loss in mechanical tension along the AP boundary

(A) Vertex distance increase normalized for the average cell bond length in the wing disc (1.7µm (Landsberg, Farhadifar et al. 2009)) as a function of time relative to ablation. Cell bonds between cells of the same compartment (A/A, P/P, light blue and green) and along the A/P boundary (A/P dark blue, red) were ablated in control and ci^{PKA4} expressing wing imaginal discs. Larvae were raised at 25˚C (control) repectively 18˚C (ci^{PKA4}). Vertex displacement was measured every 250ms for 10s before and 50s after the cut. **(A)** Vertex distance increase for cuts in control and ci^{PKA4} expressing wing discs. Mean and SEM are shown. Control: n=10 (A/A, P/P;green), n=12 (A/P;dark blue). *enGal4-UAS-*ci^{PKA4} : n=14 (A/A, P/P;light blue), n=15 (A/P;red) **(B)** Initial velocity [µm/s] of vertex displacement 250ms after ablation for cell bonds between cells of the same compartment (A/A, P/P; green,light blue) and cell bonds along the A/P boundary (A/P; dark blue,red). Mean and SEM are shown. Control: $p<0.01$ n=10 (A/A, P/P;green), n=12 (A/P;dark blue). *enGal4-UAS-*ci^{PKA4} : $p>0.05$ n=14 (A/A, P/P;light blue), n=15 (A/P;red) **(C)** Kymographs for cuts of cell bonds between cells in the anterior compartment (A/A) and along the A/P boundary for control and ci^{PKA4} expressing wing imaginal discs for 4s after the cut. The frame rate is 4 frames/s. The red arrowhead marks the timepoint of the cut.

8.8 THE DIFFERENCE IN HEDGEHOG SIGNAL TRANSDUCTION ACTIVITY IS SUFFICIENT TO MAINTAIN THE MORPHOLOGICAL SIGNATURES OF THE AP BOUNDARY

To test whether the difference in Hh signal transduction activity is sufficient to maintain the straight shape of, and the morphological signatures of the cells along the AP boundary, Hh signal transduction was activated in the posterior compartment only by expressing ci^{PKA4} in posterior cells of a hh^{ts2} mutant wing imaginal disc. Larvae were raised at permissive temperature and shifted to the restrictive temperature for 24-26 h right before dissection. The activation of the Hh signal transduction was confirmed by antibody staining against Patched (Figure 22). The border of the expression domain of Patched co-localized with junctions with increased F-actin pixel intensity. To measure the roughness of the A/P boundary and to analyse the morphological signatures of the cells along the A/P boundary, wing imaginal discs were stained with antibodies against DE-cadherin to label the adherens junctions, against Engrailed to mark the posterior compartment (Figure 23 A) and with phalloidin to label F-actin (Figure 23 D). The boundary was significantly ($p<0.05$) less rough for all L than in hh^{ts2} mutants (Figure 24 B). Quantification of the average deviation of the vertex angle between cells along the AP boundary revealed that angles are significantly ($p<0.05$) widened in wing discs expressing ci^{PKA4} in the posterior compartment only (11.6%±2.9; n=4) compared to hh^{ts2} mutants (2.1%±1.1; n=4) (Figure 24 B). Furthermore, the apical cross section area of A1 cells was significantly ($p<0.001$) larger (77.32%±22.1; n=4) than in hh^{ts2} mutant wing discs (0.9%±7.27; n=8). P1 cells have a larger apical cross section area deviation ($p<0.001$) (68.4%±4; n=4) compared to hh^{ts2} mutants (-2.8%±6.4; n=8) (Figure 24 C). F-actin pixel intensity was increased along the AP boundary in hh^{ts2} mutants that expressed ci^{PKA4} in the posterior compartment (18.8%±5; n=4). The increase of F-actin pixel intensity was significantly ($p<0.01$) higher than in hh^{ts2} mutants (-1.8%±0.5; n=4) (Figure 24 D). These results show that the difference in Hh signal transduction activity is sufficient to

maintain a straight boundary and for the morphological signatures of the AP compartment boundary.

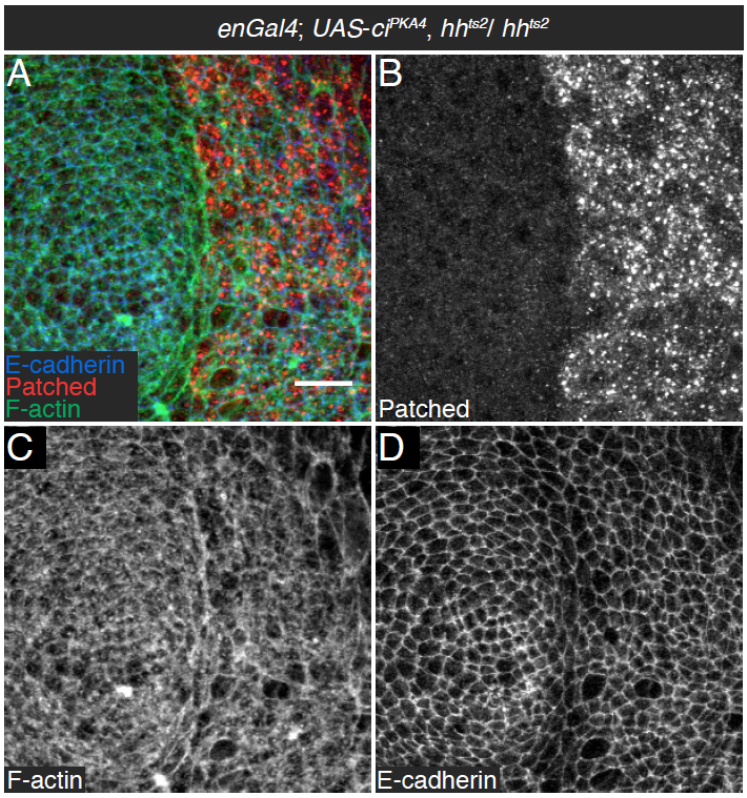

Figure 22: Expression of *ci*^{PKA4} leads to Hh signal transduction activity in the posterior compartment.
(A-D) Cropped confocal images of a wing imaginal disc homozygous for *hh*^{ts2} and expressing *enGal4-UAS-ci*^{PKA4} of wandering-stage larvae. Larvae were raised for 24-26 hrs at restrictive temperature. **(A)** Staining for Patched (red), E-cadherin (blue) and F-actin (green). Scale bar represents 10µm. **(B)** Antibody staining against Patched was used as a readout for Hh signal transduction activity. **(C)** Phalloidin staining for F-actin. (**D)** Antibody staining against E-cadherin.

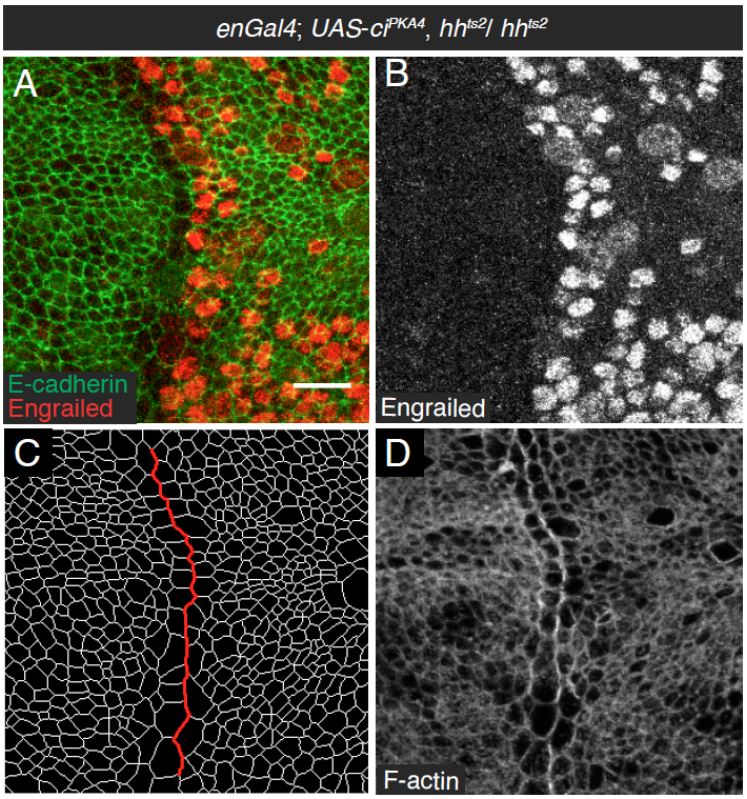

Figure 23: Expression of *ci*^{PKA4} in the posterior compartment is sufficient for the straight shape of, and the morphological signatures along, the A/P boundary.
(A-D) Cropped confocal images of a wing imaginal disc homozygous for *hh*^{ts2} and expressing *enGal4-UAS-ci*^{PKA4} of wandering-stage larvae. Larvae were raised for 24-26 hrs at restrictive temperature. **(A)** Projection of confocal sections showing antibody staining for Engrailed to mark the posterior compartment (red) and E-cadherin to mark the adherens junctions (blue). Apical sections showing the level of adherens junctions (green) was merged with more-basal sections showing the Engrailed protein being localized in the nuclei. Due to this, the Engrailed signal in the nuclei can appear to be localized anterior to the A/P boundary. Scale bar represents 10µm. **(B)** Antibody staining against Engrailed was used to mark the posterior compartment. **(C)** Segmentation on the level of adherens junctions with the Packing Analyzer software. (**D)** Phalloidin staining for F-actin.

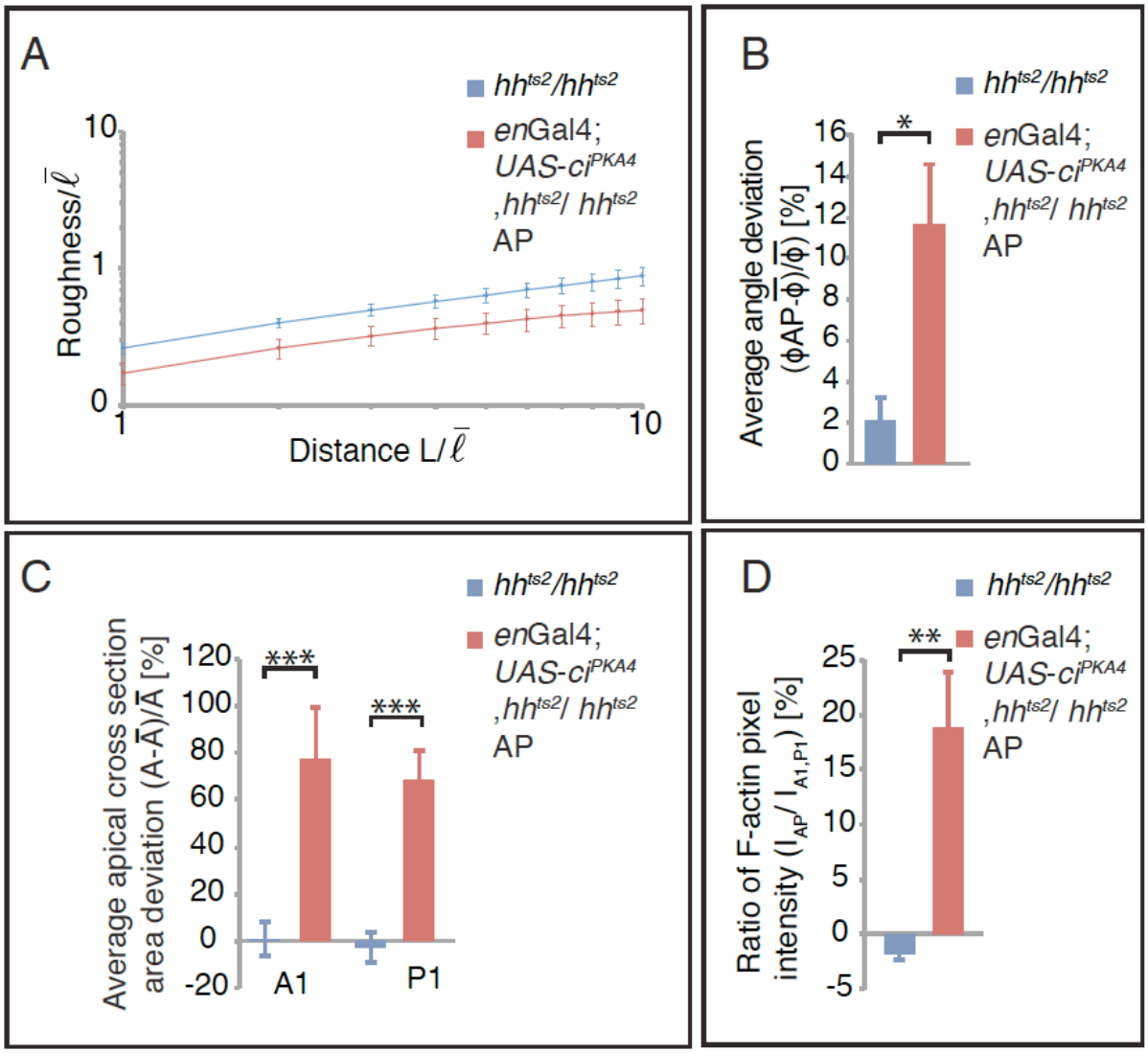

Figure 24: The difference in Hh signal transduction activity along the A/P boundary is sufficient for the straight shape of, and the morphological signatures along, the A/P boundary. **(A)** Roughness *w,* normalized to the average cell bond length </> for 1 to 10 average cell bond lengths (L) of the A/P boundary of hh^{ts2} mutant wing imaginal discs (blue) and hh^{ts2} mutant wing imaginal discs expressing *enGal4-UAS-ci*^{PKA4} (red). Mean and SEM are shown. p<0.05 for L 1-10, n=7 for hh^{ts2} mutant and n=5 for hh^{ts2} mutant *enGal4-UASci*^{PKA4} expressing wing discs. **(B)** Average deviation of the vertex angle between cell junctions along the A/P boundary (ϕ_{AP}) from the average vertex angle between junctions in the wing disc (<ϕ>=119,8 (Landsberg, Farhadifar et al. 2009)) for hh^{ts2} mutant (blue) and hh^{ts2} mutant *enGal4-UASci*^{PKA4} expressing (red) wing imaginal discs in [%]. Mean and SEM are shown. p<0.05, n= 4 (hh^{ts2} mutant), n=4 (*enGal4-UAS-ci*^{PKA4}, hh^{ts2}/hh^{ts2}). **(C)** Apical cross section area deviation for cells in the first row anterior (A1) and posterior (P1) parallel to the A/P boundary in hh^{ts2} mutant (blue) and hh^{ts2} mutant *enGal4-UASci*^{PKA4} expressing (red) wing imaginal discs from the average apical cross section area of cells in the wing disc (<A>) in [%]. Mean and SEM are shown. A1: p<0.001, n=8 (hh^{ts2} mutant), n=4 (*enGal4-UAS-ci*^{PKA4}, hh^{ts2}/hh^{ts2}). P1: p<0.001, n=8 (hh^{ts2} mutant), n=4 (hh^{ts2} mutant). **(D)** Ratio of F-actin pixel intensity of junctions along the A/P boundary (I_{AP}) compared to cell junctions of A1 and P1 cells ($I_{A1,P1}$) in [%] for hh^{ts2} mutant (blue) and hh^{ts2} mutant *enGal4-UASci*^{PKA4} expressing (red) wing imaginal discs. Mean and SEM are shown. p<0.01, n=4 (hh^{ts2} mutant), n=4 (*enGal4-UAS-ci*^{PKA4}, hh^{ts2}/hh^{ts2}).

8.9 THE DIFFERENCE IN HEDGEHOG SIGNAL TRANSDUCTION ACTIVITY IS SUFFICIENT TO INCREASE MECHANICAL TENSION ALONG THE AP BOUNDARY

To test whether the difference in Hh signal transduction activity is sufficient for the increase in mechanical tension along the AP boundary, laser ablation was performed at cell bonds along the AP boundary and away from it in hh^{ts2} mutants, which expressed ci^{PKA4} in the posterior compartment. The vertex distance increase after laser ablation was increased along the AP boundary compared to cuts away from it, similar to the wild-type situation (Figure 25 A). The initial velocity was also significantly ($p<0.001$) increased along the AP boundary (3.4µm/s±0.26; n=14) compared to cuts at cell bonds in the compartments (1.56µm/s±0.14; n=15) (Figure 25 B). Thus, mechanical tension is increased 2-fold along the AP boundary when Hh signal transduction is active exclusively in the posterior compartment. These results show that the difference in Hh signal transduction activity is sufficient to increase mechanical tension along the AP compartment boundary.

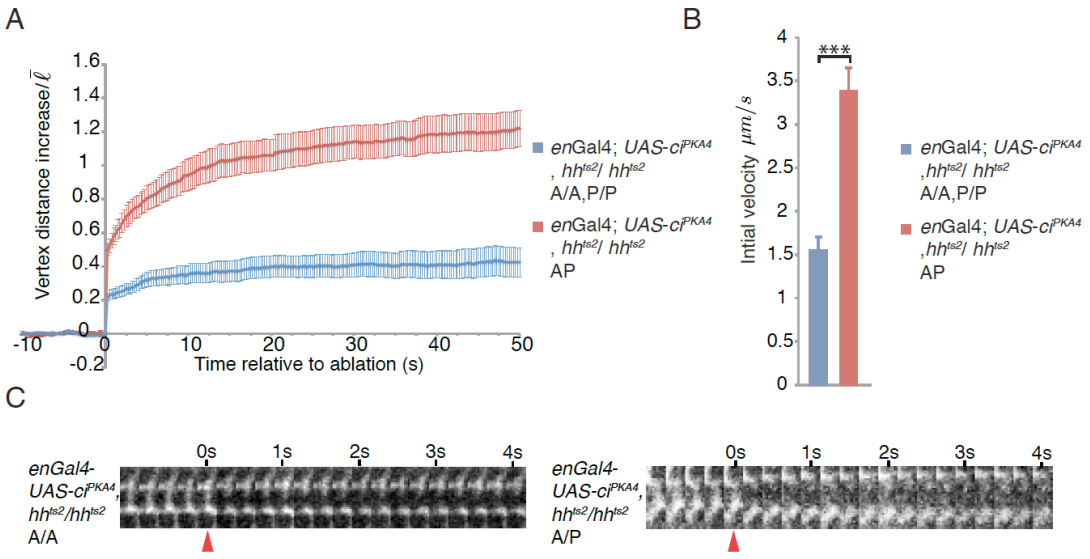

Figure 25: Ectopic expression of Ci in the posterior compartment only leads to an increase in mechanical tension along the AP boundary
(A) Vertex distance increase normalized for the average cell bond length in the wing disc (1.7µm (Landsberg, Farhadifar et al. 2009)) as a function of time relative to ablation. Cell bonds between cells of the same compartment (A/A,P/P, light blue) and along the A/P boundary (A/P, red) were ablated in hh^{ts2} mutant wing imaginal discs expressing *enGal4-UAS-*ci^{PKA4}. Vertex displacement was measured every 250ms for 10s before and 50s after the cut. Mean and SEM are shown: n=14 (A/A, P/P,blue), n=15 (A/P,green). **(B)** Initial velocity [µm/s] of vertex displacement 250ms after ablation for cell bonds between cells of the same compartment (A/A, P/P; blue) and cell bonds along the A/P boundary (A/P; red). Mean and SEM are shown: $p<0.001$ n=14 (A/A, P/P;blue), n=15 (A/P;red) **(C)** Kymographs for cuts of cell bonds between cells in the anterior compartment (A/A) and along the A/P boundary for for 4s after the cut. The frame rate is 4 frames/s. The red arrowhead marks the timepoint of the cut.

8.10 EXPERIMENTAL DESIGN II: ANALYSIS OF ECTOPIC BOUNDARIES

To test whether the increase in mechanical tension correlates with cell sorting events, mosaic analysis was used. Clones of cells with different genetic conditions were generated by the FLP-FRT system and the shape, the morphological signatures and mechanical tension were quantified along their interfaces. The shape of the clones was quantified by measuring clonal roughness, which is defined as the deviation of the contour length s to the length of a straight line between two points (i and j) (Figure 26) (Maryam Aliee, unpublished).

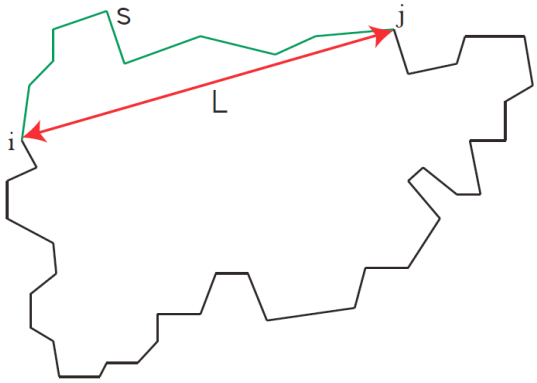

Figure 26: Clonal roughness.
Clonal roughness was measured by quantifying the deviation of the contour length (s) between two points i and j from the length of a straight line between two points i and j for different L (illustration by Maryam Aliee).

The morphological signatures of the cells along the clone borders were quantified like for the AP boundary. Laser ablation of single cell bonds along the clonal interface of control clones and such with altered genetic conditions was performed to measure the relative mechanical tension. To test whether the difference in Hh signal transduction is sufficient to create smooth interfaces and to increase mechanical tension along ectopic interfaces, clones with four different genetic conditions were used. In the control situation, clonal cells were identical to the surrounding cells except that they expressed the clonal marker (Figure 27 A). To test whether the difference in Hh signal transduction activity is sufficient to create smooth boundaries at ectopic interfaces, clones overexpressing ci^{PKA4} were induced (Figure 27 B). To test whether differential expression of Engrailed is sufficient to create smooth interfaces and to increase mechanical tension, we examined the interfaces of *engrailed* mutant clones in the anterior (Figure 27 C) and posterior (Figure 27 D) compartment. In posterior clones the loss of function of Engrailed leads to Hh signal transduction activity as *ci* is no longer repressed by Engrailed. Clones mutant for *engrailed* and *ci* were induced in the anterior (Figure 27 E) and posterior (Figure 27 F) compartment to test whether the difference in Engrailed is sufficient to create smooth boundaries independent of Hh signal transduction

activity. Furthermore, clones ectopically expressing the LRR-protein *capricious* were used to test whether smooth boundaries correlate with the increase in mechanical tension in an Hh independent manner.

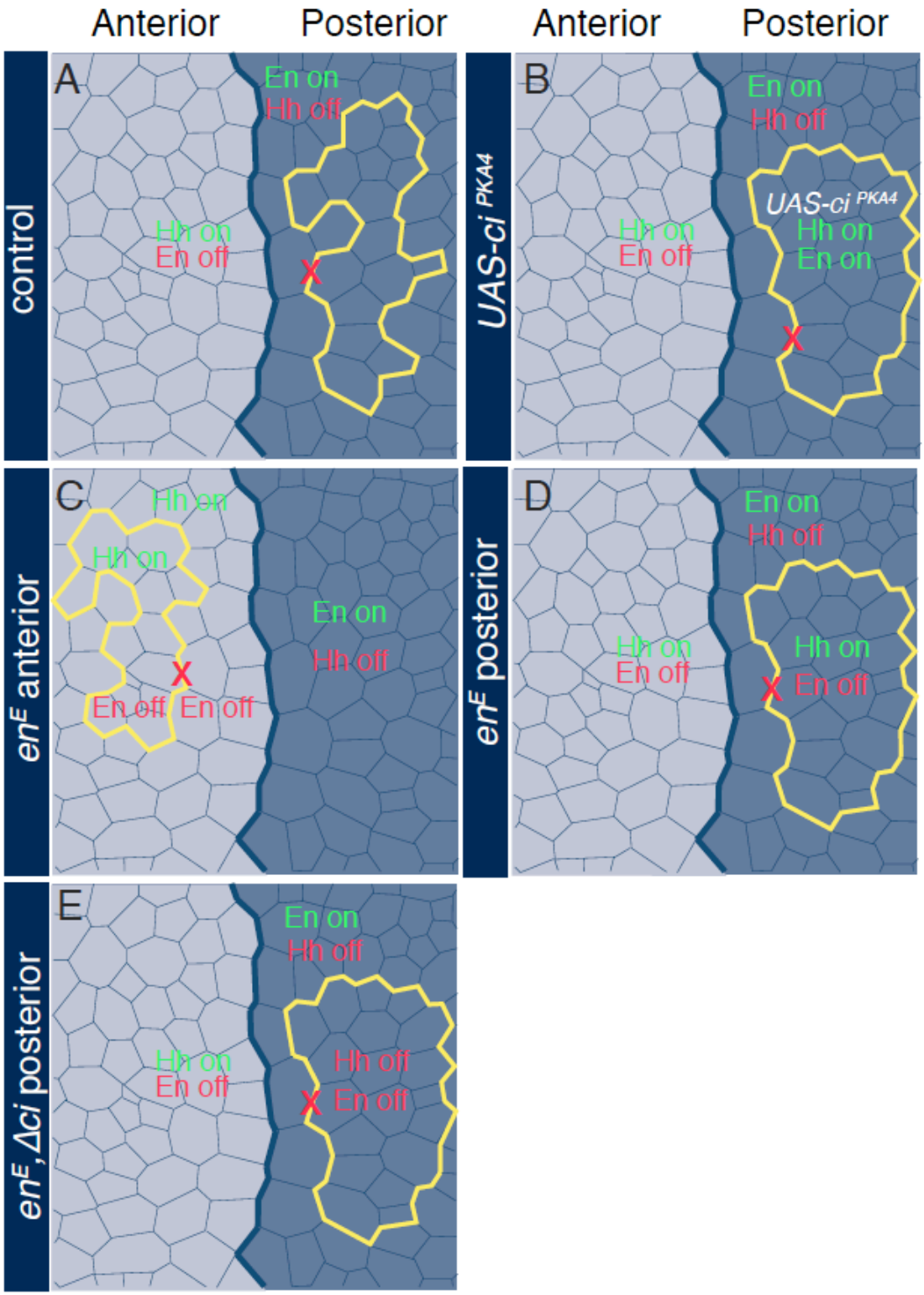

Figure 27: Experimental scenarios for the differences in Hh signal transduction activity and Engrailed along ectopic interfaces.
To test whether the difference in Hh signal transduction and Engrailed are sufficient to induce straight boundaries and to recapitulate the morphological signatures of cells along the A/P boundary at ectopic

interfaces, the following genetic scenarios were induced. Moreover, it was tested whether differences in Hh signal transduction activity and Engrailed are sufficient for the increase in mechanical tension at cell bonds along clonal interfaces in these five scenarios. The yellow line marks the clonal interface. Hh: Hh signal transduction is active (Hh on, green) or inactive (Hh off, red). En: Engrailed is expressed (En on, green) or not expressed (En off, red). The red cross marks the cell bonds which were ablated. **(A)** Control clone in the anterior or, as shown here, posterior compartment of the wing imaginal disc. Cells inside the clone are only different from the surrounding wild-type cells in the expression of a marker protein. **(B)** Clones ectopically expressing *UAS-ci*^{PKA4}. **(C)** Clones mutant for Engrailed (*en*^{E}) in the anterior compartment. Hh signal transduction activity and Engrailed expression are not different between clonal and surrounding anterior wild-type cells. **(D)** Clones mutant for Engrailed (*en*^{E}) in the posterior compartment. Due to the inactivation of Engrailed, expression of *ci* is de-repressed. Thus, cells in *en*^{E} clones differ in the expression of Engrailed and in the Hh signal transduction activity from surrounding posterior wild-type cells. **(E)** Clones mutant for Engrailed (*en*^{E}) and Ci (Δ*ci*^{94}) located in the posterior compartment are different in the expression level of Engrailed from the the surrounding posterior wild-type cells. Illustration modified from (Dahmann, Oates et al. 2011).

8.11 THE DIFFERENCE IN HEDGEHOG SIGNAL TRANSDUCTION ACTIVITY IS SUFFICIENT TO CREATE SMOOTH BORDERS ALONG ECTOPIC INTERFACES

To test whether the difference in Hh signal transduction activity is sufficient to create smooth boundaries and to recapitulate the morphological signatures of cells along the AP boundary at ectopic interfaces, control clones (Figure 27 A) as well as clones overexpressing *ci*^{PKA4} were induced. Antibodies against E-cadherin to label the adherens junctions and CD2 to negatively mark the clonal cells (Figure 29, A,B) were used as well as phalloidin to label F-actin (Figure 29 H,I). The clonal roughness of clones expressing *ci*^{PKA4} was significantly smaller for 2-8.75 L ($p<0.01$-0.05) compared to control clones (Figure 29 C). The deviation of the vertex angles between cells along the clonal interfaces from the average vertex angle in the wing imaginal disc ($<\Phi>=119.8$ (Landsberg, Farhadifar et al. 2009)) was significantly ($p<0.01$) higher along *ci*^{PKA4} expressing clones (8.28%±1.6; n=5) compared to control clones (-0.4%±1.2; n=4) (Figure 29 F). In control clones the average cross section area deviation of cells along the interface inside the clone (C1) was -0.36% (±5.6; n=5) and outside the clone (W1) -6.3% (±4.6; n=5) from the average apical cross section area of cells of the second row surrounding the clone (W2). In *ci*^{PKA4} expressing clones the deviation of the apical cross section area for c1 (17.29%±7.74; n=6) was not larger compared to cells of control clones. W1 cells at the interface of *ci*^{PKA4} expressing clones had a significantly ($p<0.001$) larger apical cross section area deviation (62%±10; n=6) than W1 cells of control clones (Figure 29 G). F-actin pixel intensity was not increased along control clone interfaces (3.64%±0.6; n=7) but along clones expressing *ci*^{PKA4} F-actin pixel intensity was significantly ($p<0.01$) increased (9.5%±1.3; n=7) (Figure 29 J). These results show that the difference in Hh signal transduction activity is sufficient to create smooth interfaces and to recapitulate the morphological signatures of the A/P boundary along ectopic borders.

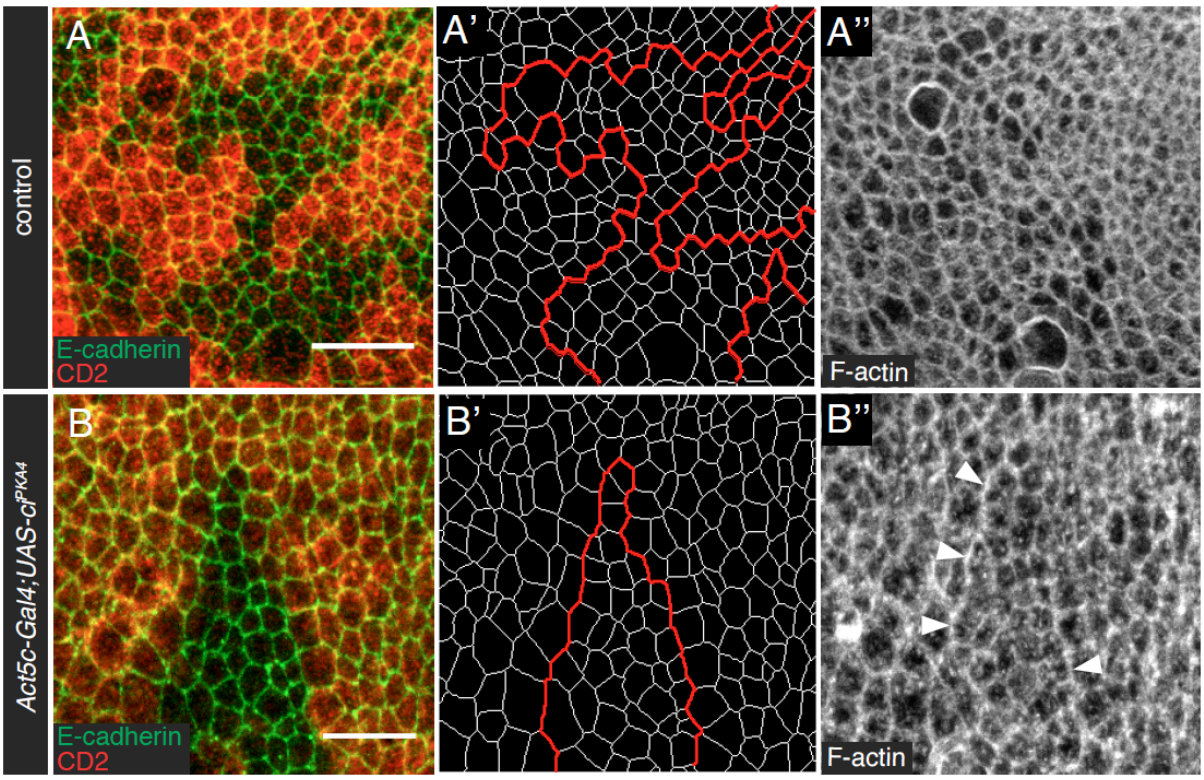

Figure 28: Expression of *ci*^{PKA4} results in straight clone interfaces and to an increase in F-actin at junctions along the clone border.
Cropped confocal images of control clones **(A)** and clones expressing *UAS-ci*^{PKA4} **(B)** of wandering-stage larvae. Recombination was induced by heatshock treatment for 30' at 36˚C, mediated by the FLP-FRT system, to induce CD2-negative control and *UAS-ci*^{PKA4} expressing cells. Larvae were raised for 3 days at 25˚C after heatshock. Clonal cells are marked by the absence of the membrane marker CD2 **(A,B;red).** Antibody staining against E-cadherin was used to mark the adherens junctions **(A,B;green)**. The cell bonds on the level of adherens junctions were segmented using Packing Analyzer for quantitative image analysis. The red line marks the clonal interface **(A',B').** F-actin was labeled using phalloidin **(A'', B'').** Scale bars represent 10µm. **(A, A')** Control clone. **(B,B')** Clone expressing *ci*^{PKA4}. **(A'')** F-actin is not increased at junctions along the control clone interface. **(B'')** F-actin is increased at junctions along *ci*^{PKA4} expressing clones (arrowheads).

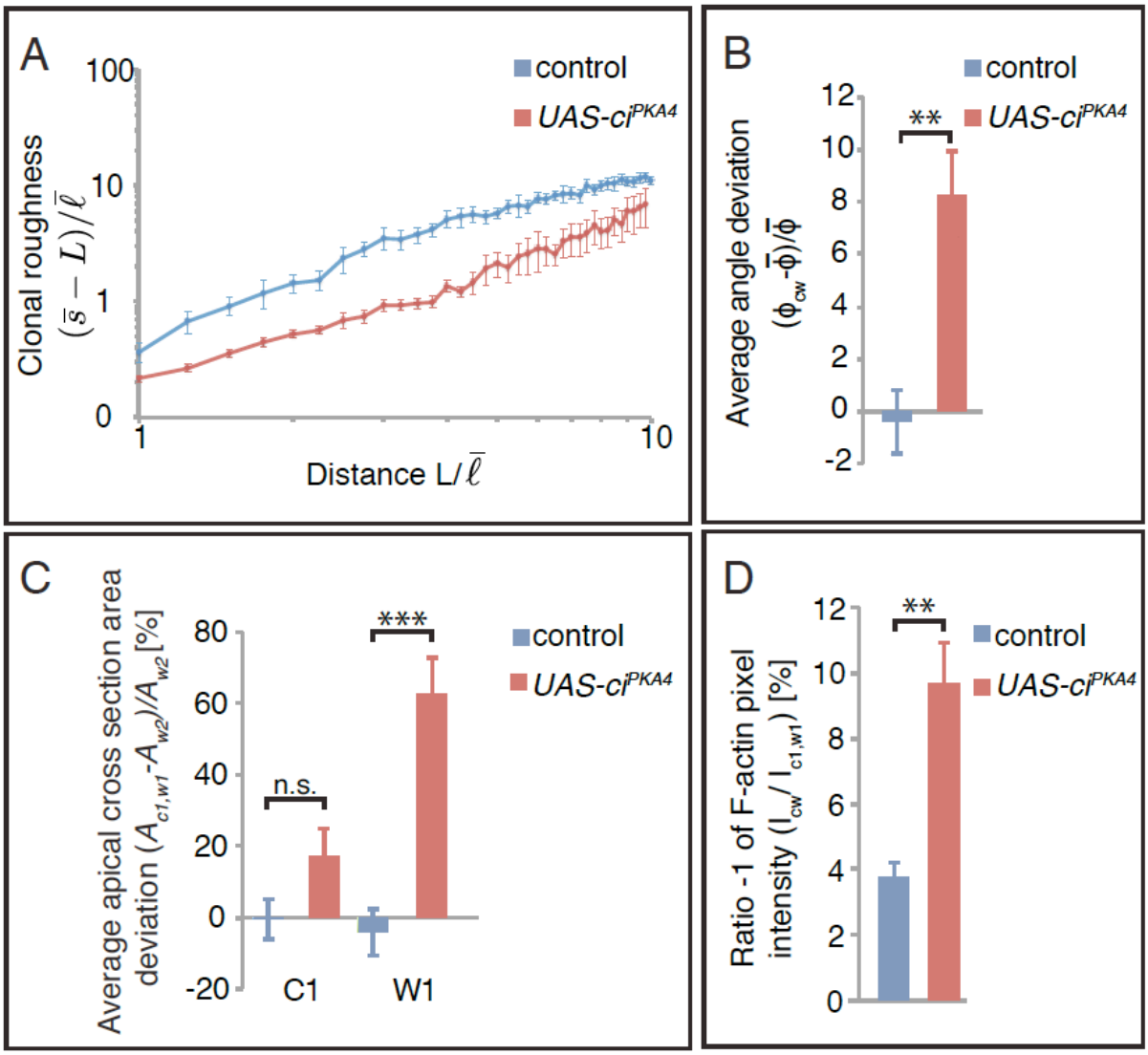

Figure 29: Expression of *ci*^{PKA4} is sufficient to induce smooth clonal interfaces and for the recapitulation of the morphological signatures of cells along the A/P boundary at clone borders.

(A) Clonal roughness, normalized to the average cell bond length </> for 1 to 10 average cell bond lengths (L) of the interface of control (blue) and *ci*^{PKA4} expressing clones (red). Mean and SEM are shown: p<0.01-0.05 for L 2-8.75, n=7 for control and n=6 for *ci*^{PKA4} expressing clones. **(B)** Average deviation of the vertex angle between cell junctions along the clone boundary (ϕ_{CW}) from the average vertex angle between junctions in the wing disc (<ϕ>=119,8 (Landsberg, Farhadifar et al. 2009)) for control (blue) and *ci*^{PKA4} expressing (red) clones [%]. Mean and SEM are shown. p<0.01, n= 5 (control), n=4 (*UAS-ci*^{PKA4}). **(C)** Apical cross section area deviation for cells in the first row inside (C1) and outside (W1) of clones in control (blue) *ci*^{PKA4} expressing (red) clones from the average apical cross section area of cells in the second row around the clone (W2) (<A_{w2}>) in [%]. Mean and SEM are shown. C1: p>0.05, n=5 (control), n=6 (*ci*^{PKA4}). W1: p<0.001, n=5 (control), n=6 (*ci*^{PKA4}) **. (D)** Ratio of F-actin pixel intensity of junctions along the clone boundary (I_{cw}) compared to cell junctions of C1 and W1 cells ($I_{C1,W1}$) in [%] for control (blue) and *ci*^{PKA4} expressing (red) clones. Mean and SEM are shown. p<0.01, n=7 (control), n=7 (*ci*^{PKA4}).

8.12 DIFFERENCES IN HEDGEHOG SIGNAL TRANSDUCTION ACTIVITY LEVELS ARE SUFFICIENT TO INCREASE MECHANICAL TENSION ALONG ECTOPIC INTERFACES

To test whether differences in Hh signal transduction activity are sufficient to increase mechanical tension along ectopic interfaces, laser ablation was performed along borders of control and ci^{PKA4} expressing clones. The adherens junctions were marked by ubi-DE-cadherin-GFP. The FLP-FRT system was used to induce stochastic recombination by heatshock treatment to express flippase. The larvae were raised for 3 days at 25˚C to allow clone growth. Recombination led to the expression of *UAS-GFP-gpi* in clonal cells. The vertex distance increase after laser ablation and the initial velocity were quantified to calculate the relative increase in mechanical tension along the clonal interfaces. Cuts along the control clone interfaces showed a similar vertex distance increase (Figure 30 A) than cuts in the anterior or posterior compartment (compare to Figure 21 A). The interfaces of ci^{PKA4} expressing clones showed a similar vertex distance increase after laser ablation (Figure 30 A) than cuts along the AP boundary (Figure 21 A). The initial velocity of cuts along the clone boundary for the first time point after the cut was 1.32µm/s (±0.13; n=7) and along ci^{PKA4} expressing clones 2.9µm/s (±0.27; n=12). Mechanical tension was increased 2.1-fold along ci^{PKA4} expressing clones compared to control clones ($p<0.05$) and similar compared to cuts along the A/P boundary (Figure 21 B). These results show that the difference in Hh signal transduction activity is sufficient to increase mechanical tension along ectopic boundaries similar to the A/P boundary.

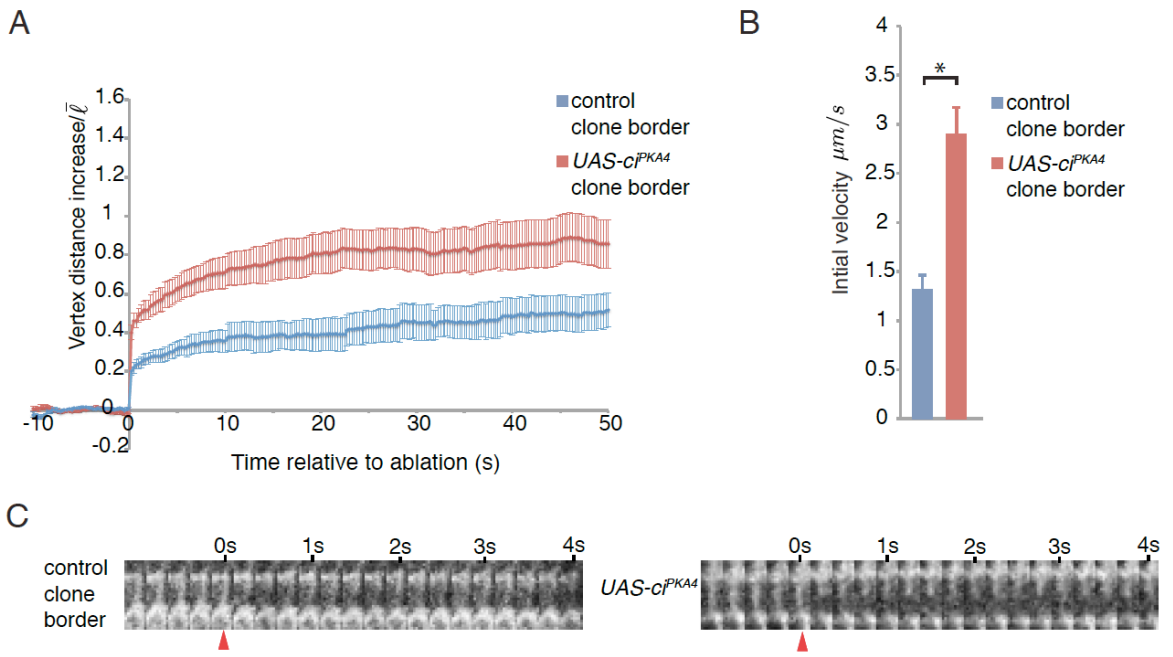

Figure 30: Expression of *ci*^{PKA4} is sufficient for the increase in mechanical tension along ectopic interfaces.
(A) Vertex distance increase normalized for the average cell bond length in the wing disc (1.7µm (Landsberg, Farhadifar et al. 2009)) as a function of time relative to ablation. Cell bonds along control clones (blue) and *ci*^{PKA4} expressing clones (red) were ablated. Vertex displacement was measured every 250ms for 10s before and 50s after the cut. Mean and SEM are shown: n=7 (control), n=12 (*ci*^{PKA4}). **(B)** Initial velocity [µm/s] of vertex displacement 250ms after ablation for cell bonds along control (blue) and *ci*^{PKA4} expressing clones (red). Mean and SEM are shown: p<0.05 n=7 (control, blue), n=12 (*ci*^{PKA4}, red) **(C)** Kymographs for cuts of cell bonds along control and *ci*^{PKA4} expressing clones 4s after the cut. The frame rate is 4 frames/s. The red arrowhead marks the timepoint of the cut.

8.13 THE DIFFERENCE IN ENGRAILED IS SUFFICIENT TO CREATE SMOOTH INTERFACES ALONG ECTOPIC BOUNDARIES

To test whether the difference in Engrailed is sufficient to create smooth interfaces, Engrailed function was reduced using a mutant *engrailed* allele (*en*^{E}) (Gustavson, Goldsborough et al. 1996). Clones mutant for *engrailed* that were located within the anterior compartment served as a control as Engrailed is not expressed in the anterior compartment. The clonal cells were induced by heat-shock and negatively marked for DE-cadherin::GFP. The wing discs were stained with antibodies against DE-cadherin to mark the adherens junctions and against GFP. F-actin was labelled with phalloidin (Figure 31 A,B). Clones located in the posterior compartment had a smoother boundary than anterior clones (p<0.01-0.05 for L=3.75-8.75) (Figure 32 A). The average deviation of the vertex angle between cells along the clonal interface was 1.5% (±1; n=6) for anterior *en*^{E} clones. Along the interface of posterior *en*^{E} clones the deviation of the vertex angle was significantly (p<0.01) increased 7.2% (±1.2; n=10) compared to anterior control clones (Figure 32 B). The

deviation of the apical cross section area of cells in the first row inside the clone (C1) from W2 cells was 19.8% (±9.5, n=6) for anterior en^E clones and 17.6% (±4.2, n=10) for posterior en^E clones. The deviation of the apical cross section area for cells in the first row outside the clone (W1) was 3.23% (±5.6, n=6) for anterior en^E clones and 11.6% (±9.7, n=10) for posterior en^E clones (Figure 32 C). The deviation of the apical cross section area for C1 and W1 cells was similar ($p>0.05$) for anterior and posterior en^E clones. The average of the deviation of the F-actin pixel intensity was significantly ($p<0.05$) increased along posterior en^E (9%±1.8; n=10) compared to anterior clones (3%±0.3; n=6) (Figure 32 D). These results show that the difference in Engrailed is sufficient to create smooth interfaces, and to recapitulate most of the morphological signatures of cells along ectopic boundaries.

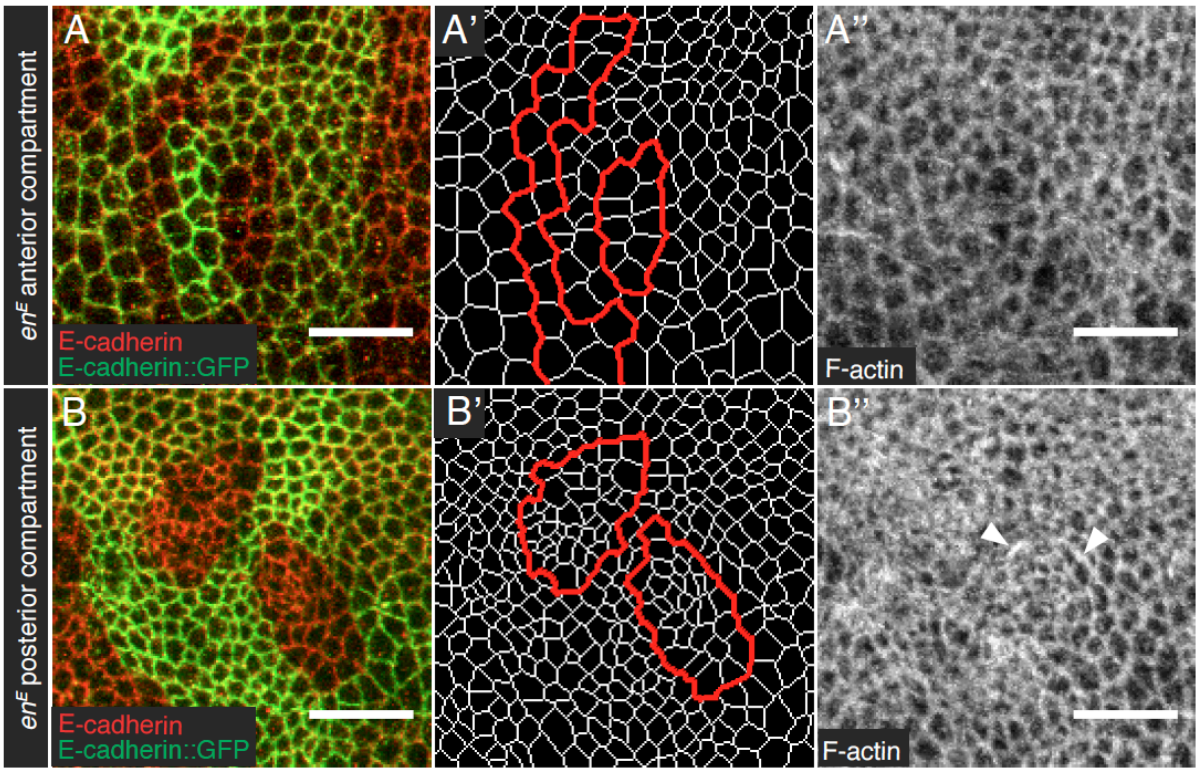

Figure 31: Differential expression of Engrailed induces smooth clonal boundaries and increased levels of F-actin along ectopic interfaces.
Cropped confocal images of en^E clones in the anterior **(A)** and posterior **(B)** compartment in the wing discs of wandering-stage larvae. Recombination was induced by heatshock treatment for 40' at 37˚C, mediated by the FLP-FRT system, to induce en^E mutant clones lacking DE-cadherin::GFP **(A,B; green)**. Larvae were raised for 3 days at 25˚C after heatshock. Antibody staining against E-cadherin was used to mark the adherens junctions **(A,B;red)**. The cell bonds on the level of adherens junctions were segmented using Packing Analyzer for quantitative image analysis. The red line marks the clonal interface **(A',B').** F-actin was labeled using phalloidin **(A'', B'').** Scale bars represent 10µm. **(A-A'')** Engrailed mutant clone in the anterior compartment. **(B-B'')** Engrailed mutant clone in the posterior compartment. **(A'')** F-actin is not increased at junctions along the interface of the en^E mutant clone in the anterior compartment. **(B'')** F-actin is increased at junctions along en^E mutant clones in the posterior compartment (arrowheads).

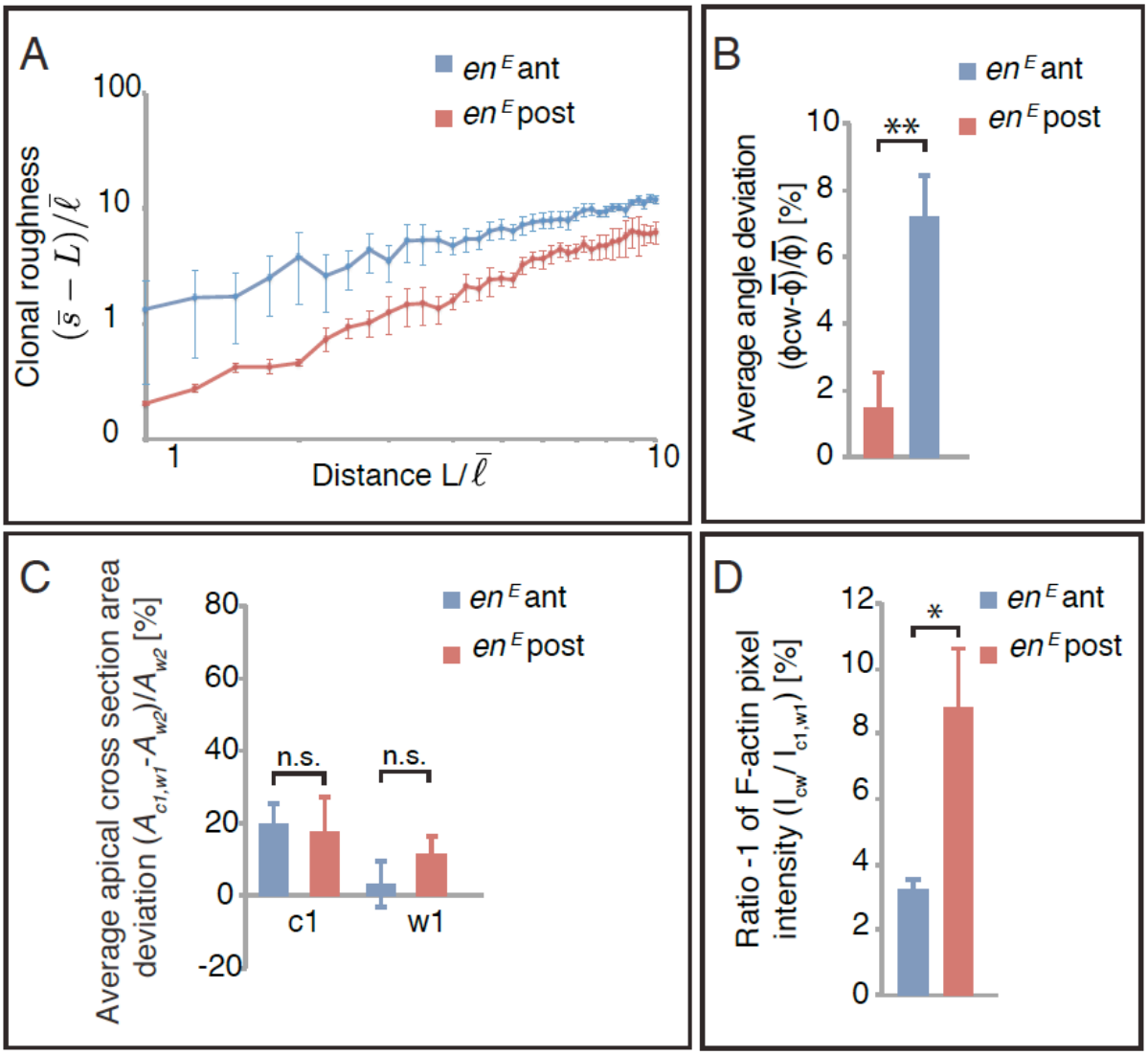

Figure 32: The difference in Engrailed expression is sufficient to recapitulate most of the morphological signatures of cells along the A/P boundary along ectopic interfaces.
(A) Clonal roughness, normalized to the average cell bond length </> for 1 to 10 average cell bond lengths (L) of the interface of anterior en^E (blue) and posterior en^E mutant clones (red). Mean and SEM are shown: p<0.01-0.05 for L 3.75-8.75, n=4 (anterior) and n=6 (posterior). **(B)** Average deviation of the vertex angle between cell junctions along the clone boundary (ϕ_{CW}) from the average vertex angle between junctions in the wing disc (<ϕ>=119,8 (Landsberg, Farhadifar et al. 2009)) for anterior (blue) and posterior (red) clones [%]. Mean and SEM are shown. p<0.01, n= 6 (anterior), n=10 (posterior). **(C)** Apical cross section area deviation for cells in the first row inside (C1) and outside (W1) of clones in anterior (blue) and posterior (red) clones from the average apical cross section area of cells in the second row around the clone (W2) ($<A_{w2}>$) in [%]. Mean and SEM are shown. C1: p>0.05, n=6 (anterior), n=10 (posterior). W1: p>0.05, n=6 (anterior), n=10 (posterior)**. (D)** Ratio of F-actin pixel intensity of junctions along the clone boundary (I_{cw}) compared to cell junctions of C1 and W1 cells ($I_{C1,W1}$) in [%] for anterior (blue) and posterior (red) clones. Mean and SEM are shown. p<0.05, n=6 (anterior), n=10 (posterior).

8.14 THE DIFFERENCE IN ENGRAILED IS SUFFICIENT TO INCREASE MECHANICAL TENSION ALONG ECTOPIC BOUNDARIES

To test whether the difference in Engrailed is sufficient to increase mechanical tension along ectopic interfaces, laser ablation was performed along en^E mutant clones located in the anterior and posterior compartment. The adherens junctions were recognized by DE-cadherin::GFP and the clonal cells were marked by the absence of DE-cadherin::GFP. The vertex distance increase after laser ablation was higher for cuts along interfaces of en^E mutant clones in the posterior compartment compared to clones in the anterior compartment (Figure 33, L). For anterior control clones the initial velocity after the cut was with 1µm/s (±0.07; n=14) significantly ($p<0.001$) lower than for cuts along the interface of en^E mutant clones in the posterior compartment (1.8µm/s±0.18; n=15) (Figure 33, M). Hence, there is a 1.8-fold increase in mechanical tension along en^E mutant clones located in the posterior compartment compared to anterior control clones. These results show that the difference in Hh signal transduction and Engrailed is sufficient to increase mechanical tension along ectopic interfaces.

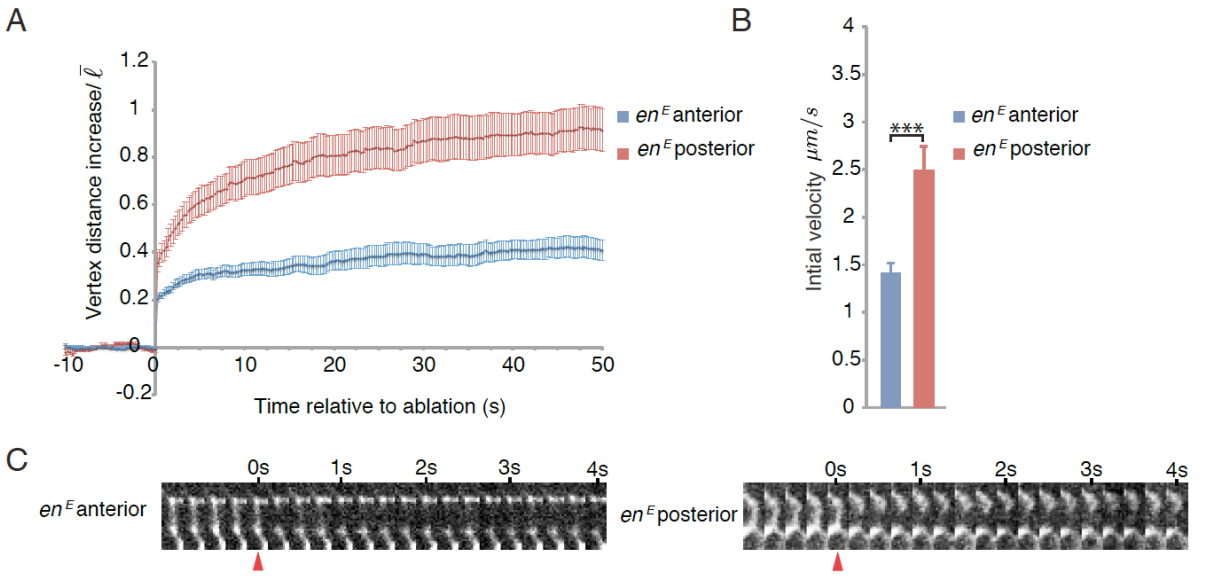

Figure 33: The difference in Engrailed expression is sufficient for the increase in mechanical tension along clonal interfaces.
(A) Vertex distance increase normalized for the average cell bond length in the wing disc (1.7µm (Landsberg, Farhadifar et al. 2009)) as a function of time relative to ablation. Cell bonds along anterior en^E mutant clones (en^E anterior, blue) and posterior en^E mutant clones (en^E posterior, red) were ablated. Vertex displacement was measured every 250ms for 10s before and 50s after the cut. Mean and SEM are shown: n=14 (anterior, blue), n=15 (posterior, red). **(B)** Initial velocity [µm/s] of vertex displacement 250ms after ablation for cell bonds along anterior (blue) and posterior Engrailed mutant clones (red). Mean and SEM are shown: $p<0.001$ n=14 (anterior, blue), n=15 (posterior, red) **(C)** Kymographs for cuts of cell bonds along anterior and posterior Engrailed mutant clones 4s after the cut. The frame rate is 4 frames/s. The red arrowhead marks the timepoint of the cut.

8.15 DIFFERENTIAL EXPRESSION OF ENGRAILED ONLY IS SUFFICIENT TO CREATE SMOOTH INTERFACES

Engrailed represses the expression of *ci* in the posterior compartment (Tabata, Eaton et al. 1992; Zecca, Basler et al. 1995). In posterior en^E mutant clones *ci* is no longer repressed by Engrailed, which leads to Hh signal transduction activity inside the clone and thus to a difference in *engrailed* and Hh signal transduction activity between clonal and surrounding wild-type cells. To test the contribution of the differential expression of Engrailed to the cell sorting processes along clone boundaries, independent of Ci, clones mutant for *engrailed* and *ci* where generated by heat-shock induced mitotic recombination mediated by the FLP-FRT system. The posterior compartment was marked by antibody staining against Engrailed. The clones were marked by the absence of GFP. Antibody staining against DE-cadherin was used to recognize the adherens junctions (Figure 34). The shape of the clones was measured by quantifying clonal roughness. Clones double mutant for Engrailed and Ci (en^- ci^-) had a similar clonal roughness like posterior En mutant clones for lower L and a similar clonal roughness like anterior En mutant clones for larger L. The vertex angle deviation between junctions along the clonal interface was 3.98% (±0.64, n=5). It was ($p>0.05$) not significantly different to the vertex angel between junctions along anterior or posterior en^E mutant clones (Figure 35 B). The average deviation of the apical cross section area of cells in the first rows inside (C1) (3.35% ±6.28, n=5) and outside (W1) (7.37±4.34, n=5) the clone from the clones in the second row around the clone (W2) was not significantly different to the deviation of the apical cross section area of C1 or W1 cells of anterior and posterior Engrailed mutant clones (Figure 35 C). These results show that the difference in Engrailed expression is sufficient for the formation of smooth boundaries along ectopic interfaces, but not to the same extend as Engrailed mutant clones expressing Ci in the posterior compartment.

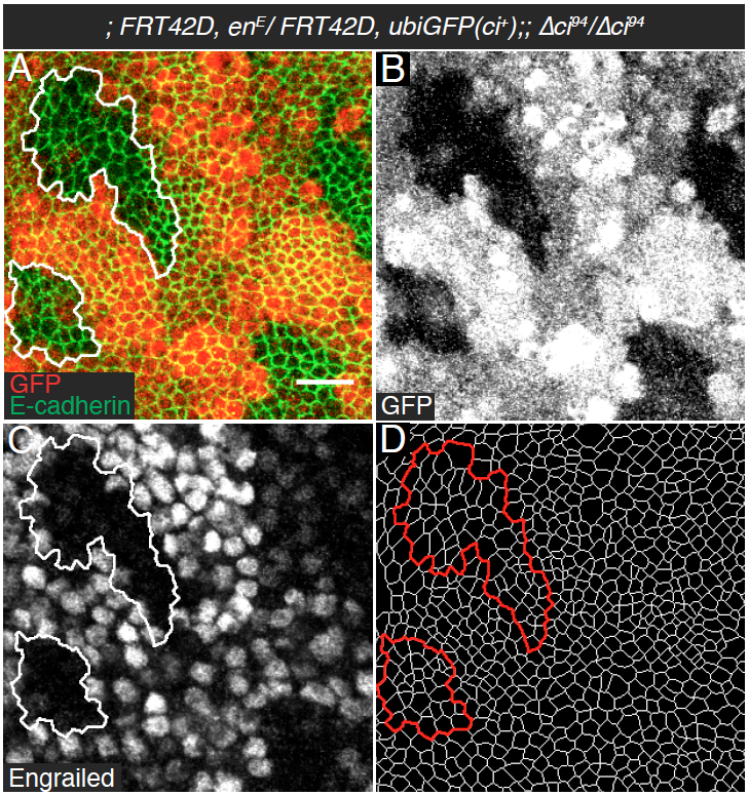

Figure 34: The difference in Engrailed expression only is sufficient to create smooth interfaces.
Cropped confocal images of en^{E}, Δci^{94} clones in the posterior compartment **(A)** in the wing discs of wandering-stage larvae. Mitotic recombination was induced by heatshock treatment for 60' at 37˚C, mediated by the FLP-FRT system, to induce $en^{E},\Delta ci^{94}$ mutant clones lacking ubi-GFP **(A, red, B)**. Larvae were raised for 3 days at 25˚C after heatshock. Antibody staining against E-cadherin was used to mark the adherens junctions **(A, green)**. **(B)** Antibody staining against GFP. **(C)** Antibody staining against Engrailed. **(D)** The cell bonds on the level of adherens junctions were segmented using Packing Analyzer for quantitative image analysis. The red line marks the clonal interface.

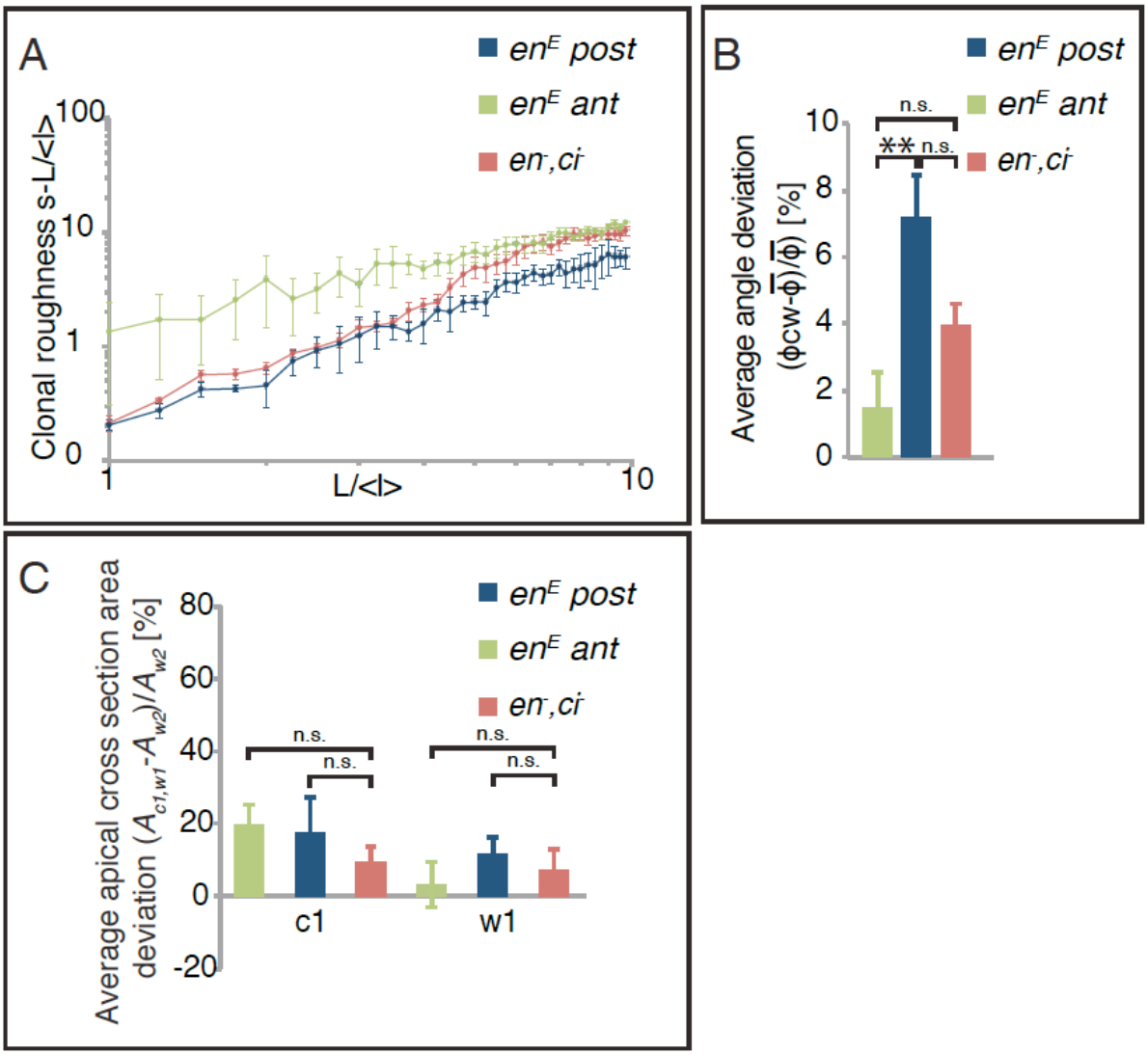

Figure 35: Different levels of Engrailed expression are sufficient to generate smooth interfaces along ectopic interfaces.
(A) Clonal roughness, normalized to the average cell bond length </> for 1 to 10 average cell bond lengths (L) of the interface of anterior en^E (light green), posterior en^E mutant clones (dark blue) and en^E, Δci^{94} mutant clones (en^-, ci^-; red) . Mean and SEM are shown: p>0.05 for L= 0-6.25 and L=8.25-10 (en^E, Δci^{94} compared to posterior en^E mutant clones). p>0.05 for L=4.5-10 (en^E, Δci^{94} compared to anterior en^E mutant clones). **(B)** Average deviation of the vertex angle between cell junctions along the clone boundary (ϕ_{CW}) from the average vertex angle between junctions in the wing disc (<ϕ>=119,8 (Landsberg, Farhadifar et al. 2009)) for anterior (light green), posterior (dark blue) and posterior en^E, Δci^{94} clones (red) [%]. Mean and SEM are shown. p>0.05, n= 6 (anterior), n=10 (posterior), n=5 (en^E, Δci^{94}). **(C)** Apical cross section area deviation for cells in the first row inside (C1) and outside (W1) of clones in anterior (light green), posterior (dark blue) and en^E, Δci^{94} (red) clones from the average apical cross section area of cells in the second row around the clone (W2) (<A_{w2}>) in [%]. Mean and SEM are shown. C1: p>0.05, n=6 (anterior), n=10 (posterior), n=5 (en^E, Δci^{94}). W1: p>0.05, n=6 (anterior), n=10 (posterior), n=5 (en^E, Δci^{94}).

8.16 DIFFERENT EXPRESSION LEVELS OF THE LRR-PROTEIN CAPRICIOUS ARE SUFFICIENT TO CREATE SMOOTH BORDERS AND TO RECAPITULATE THE MORPHOLOGICAL SIGNATURES OF THE A/P BOUNDARY ALONG ECTOPIC BOUNDARIES

Overexpressing the LRR-transmembrane protein Capricious in clones of cells was shown to result in smooth boundaries along clonal interfaces (Milan, Perez et al. 2002). To test whether the different expression of Capricious is sufficient to create smooth borders and to recapitulate the morphological signatures of the AP boundary along ectopic interfaces, *capricious* overexpressing clones were induced. The wing imaginal discs were stained with antibodies against DE-cadherin to mark the adherens junctions and against CD2 to negatively mark the clonal cells (Figure 36 A). Phalloidin staining was used to label F-actin (Figure 36 A''). The clonal roughness of clones overexpressing *capricious* was significantly ($p<0.001$-0.05) lower for L=2.75-10 compared to control clones (Figure 37 B). The vertex angles between cells along the clonal interface were significantly ($p<0.01$) widened along *capricious* expressing clones (8%±1.8; n=5) compared to control clones (-0.4%±1.2; n=4) (Figure 37 D). The average cross section area of cells along the clonal interface were significantly ($p<0.05$) larger compared to cells along control clone borders. The cells along the interface inside the clone (C1) were 30.3% (±10, n=5) and the cells outside the clone (W1) were 26.2% (±6.9; n=5) larger than the cells along control clone interfaces (Figure 37 C). The overexpression of *capricious* also led to an increase in F-actin along the clonal interface. The F-actin pixel intensity along *capricious* clones was significantly ($p<0.01$) enriched (15.2%±3.7; n=4) compared to control clones (Figure 37 D). These results show that the differences in the expression of Capricious is sufficient to induce smooth borders and to recapitulate the morphological signatures of the AP boundary along ectopic interfaces.

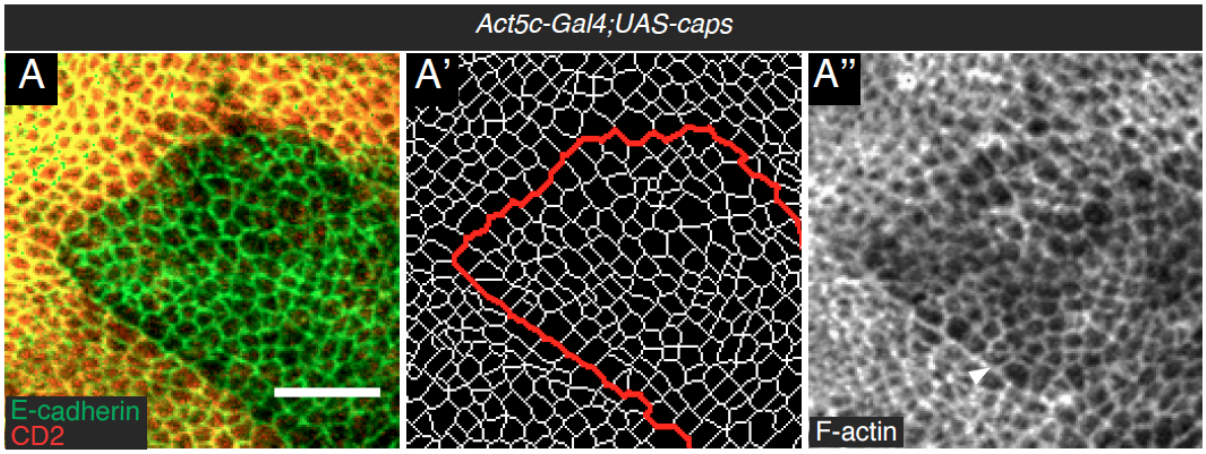

Figure 36: Overexpression of the LRR-transmembrane protein Capricious leads to smooth boundaries along ectopic interfaces.

Cropped confocal image of *UAS-caps* expressing clones **(A)** in wing imaginal discs of wandering-stage larvae. Recombination was induced by heatshock treatment for 30' at 36˚C, mediated by the FLP-FRT system, to induce CD2-negative *UAS-caps* expressing clones. Larvae were raised for 3 days at 25˚C after heatshock. Clonal cells are marked by the absence of the membrane marker CD2 **(A, red).** Antibody staining against DE-cadherin was used to mark the adherens junctions **(A, green)**. The cell bonds on the level of adherens junctions were segmented using Packing Analyzer for quantitative image analysis. The red line marks the clonal interface **(A').** F-actin was labeled using phalloidin **(A'').** Scale bars represent 10µm. **(A'')** F-actin is increased at junctions along *UAS-caps* expressing clones (arrowhead).

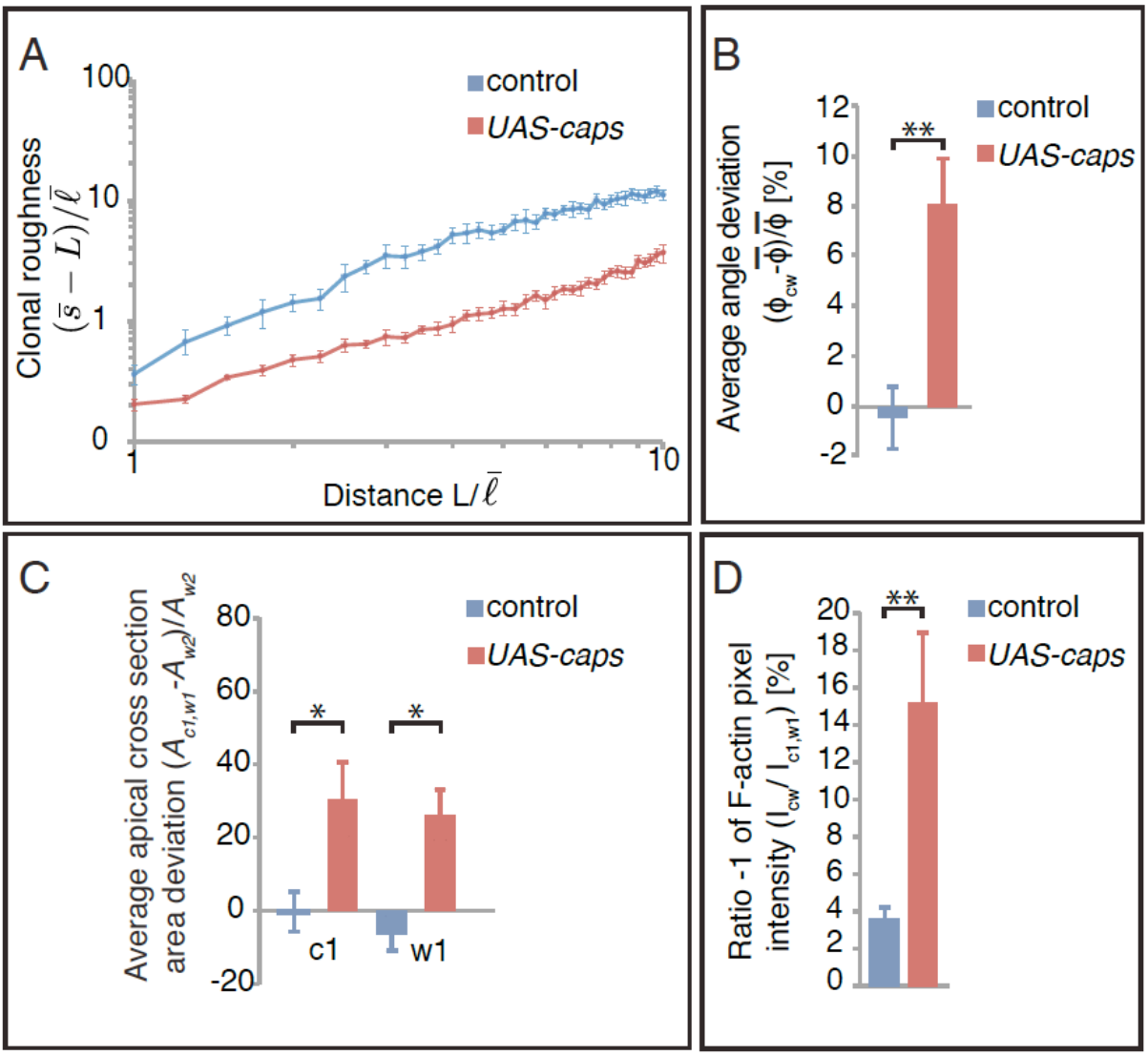

Figure 37: Differential expression of Capricious is sufficient for the formation of smooth boundaries along ectopic interfaces and for the recapitulation of the morphological signatures of cells along the A/P boundary along ectopic interfaces.
(A) Clonal roughness, normalized to the average cell bond length </> for 1 to 10 average cell bond lengths (L) of the interface of control (blue) and *caps* expressing clones (red). Mean and SEM are shown: p<0.001-0.05 for L 2.75-10, n=7 for control and n=5 for *caps* expressing clones. **(B)** Average deviation of the vertex angle between cell junctions along the clone boundary (ϕ_{CW}) from the average vertex angle between junctions in the wing disc (<ϕ>=119,8 (Landsberg, Farhadifar et al. 2009)) for control (blue) and *caps* expressing (red) clones [%]. Mean and SEM are shown. p<0.01, n= 5 (control), n=5 (*UAS-caps*). **(C)** Apical cross section area deviation for cells in the first row inside (C1) and outside (W1) of clones in control (blue) *caps* expressing (red) clones from the average apical

cross section area of cells in the second row around the clone (W2) (<A_{w2}>) in [%]. Mean and SEM are shown. C1: p<0.05, n=5 (control), n=5 (*caps*). W1: p<0.05, n=5 (control), n=5 (*caps*) **. (D)** Ratio of F-actin pixel intensity of junctions along the clone boundary (I_{cw}) compared to cell junctions of C1 and W1 cells ($I_{C1,W1}$) in [%] for control (blue) and *caps* expressing (red) clones. Mean and SEM are shown. p<0.01, n=7 (control), n=7 (*caps*).

8.17 DIFFERENT EXPRESSION LEVELS OF THE LRR PROTEIN CAPRICIOUS LEAD TO AN INCREASE IN MECHANICAL TENSION ALONG ECTOPIC INTERFACES

To test whether the differential expression of Capricious is sufficient to increase mechanical tension along ectopic boundaries, laser ablation was performed along *capricious* overexpressing clones to measure the relative increase in mechanical tension. The adherens junctions were marked by ubi-DE-cadherin-GFP and the clonal cells were marked by GFP-gpi. The vertex distance increase after laser ablation was increased for cuts along *capricious* expressing clones compared to cuts along control clone interfaces (Figure 38 A). The initial velocity of vertex displacement 250ms after the cut along *capricious* overexpressing clones was 2.6µm/s (±0.24; n=11) (Figure 38 B). Thus, mechanical tension is increased 1.9-fold (p<0.01) along *capricious* overexpressing clones compared to control clones. These results show that the differential expression of Capricious is sufficient to increase mechanical tension along ectopic interfaces.

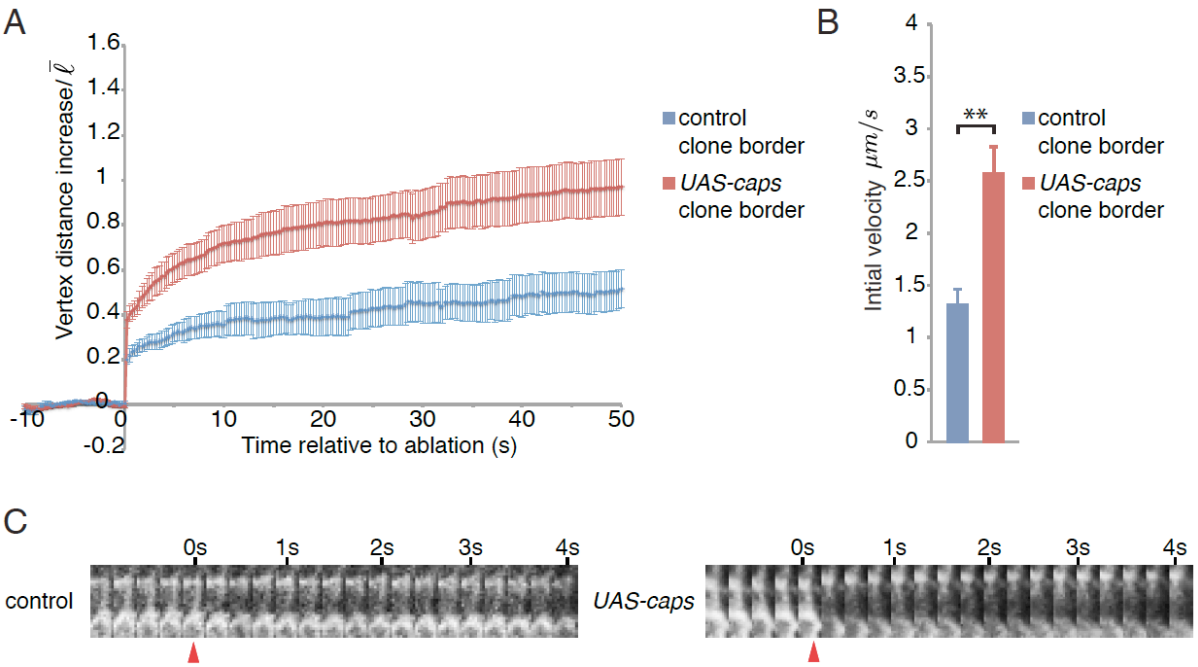

Figure 38: Differential expression of the LRR-protein Capricious is sufficient to increase mechanical tension at cell bonds along ectopic boundaries.
(A) Vertex distance increase normalized for the average cell bond length in the wing disc (1.7µm (Landsberg, Farhadifar et al. 2009)) as a function of time relative to ablation. Cell bonds along control clones (blue) and *caps* expressing clones (red) were ablated. Vertex displacement was measured every 250ms for 10s before and 50s after the cut. Mean and SEM are shown: n=7 (control), n=11

(ci^{PKA4}). **(B)** Initial velocity [µm/s] of vertex displacement 250ms after ablation for cell bonds along control (blue) and *caps* expressing clones (red). Mean and SEM are shown: p<0.01 n=7 (control, blue), n=11 (*caps*, red) **(C)** Kymographs for cuts of cell bonds along control and *caps* expressing clones 4s after the cut. The frame rate is 4 frames/s. The red arrowhead marks the timepoint of the cut.

8.18 MECHANICAL TENSION IS INCREASED LOCALLY AT EACH CELL BOND ALONG THE AP BOUNDARY

It was previously proposed that the cortical actomyosin meshwork at junctions along the A/P boundary would form a “fence” (Major and Irvine 2005; Major and Irvine 2006) or supracellular cable (Monier, Pelissier-Monier et al. 2010). This would mean that tension is transmitted between junctions along the A/P boundary by such a cable. To test whether the increase in mechanical tension is transmitted between junctions along the AP boundary, laser ablation at two neighboring cell bonds was performed. The first cell bond was cut, and after 20s the next but one was ablated (Figure 39 A,B). The vertex distance increase after ablation was similar for the first and the second cut (Figure 39 C). The initial velocity of vertex displacement directly after the cut was similar as well for the first (2.67µm/s ±0.3; n=14) and the second cut (2.69µm/s ±0.3; n=14) (Figure 39 D). These results show that the increase in mechanical tension is not transmitted between junctions but rather generated locally at each cell bond.

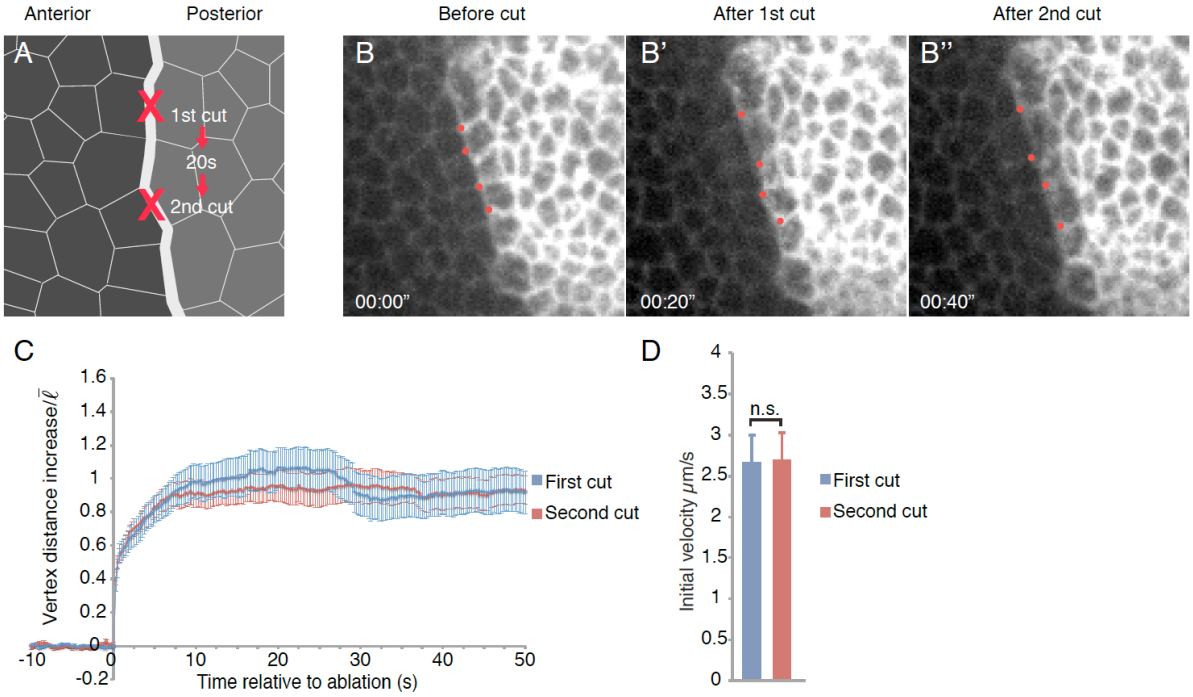

Figure 39: The increase in mechanical tension along the A/P boundary is not transmitted between the junctions along the A/P boundary

(A) Scheme of the experimental strategy. Two neighbouring cell bonds, separated by one cell bond, were cut 20s after each other. **(B-B'')** Time course of vertex displacement before **(B)**, after the first cut **(B')** and after the second cut (**B'').** The red dots mark the verticies of the cell bonds that are cut. **(C)** Vertex distance increase normalized for the average cell bond length in the wing disc (1.7µm (Landsberg, Farhadifar et al. 2009)) as a function of time relative to ablation. 2 neighbouring cell bonds along the A/P boundary were ablated wing imaginal discs of wandering stage larvae. Vertex displacement was measured every 250ms for 10s before and 50s after the cut. Mean and SEM are shown: n=14 (first cut, blue), n=14 (seond cut, red). **(D)** Initial velocity [µm/s] of vertex displacement 250ms after ablation for cell bonds between cell bonds along the A/P boundary. Mean and SEM are shown: $p>0.05$ n=14 (first cut, blue), n=14 (second cut, red)

9 DISCUSSION

9.1 BIOCHEMICAL SIGNALS REGULATE MECHANICAL PROCESSES ALONG THE A/P COMPARTMENT BOUNDARY IN THE *DROSOPHILA* WING IMAGINAL DISC

The formation of a complex organism with various specialized tissues and organs that arises from a single cell requires, amongst others, cell communication and cell sorting. Biochemical signals transmitted between cells provide information about a cell's identity. Based on their identity, groups of cells have to be segregated by mechanical processes into distinct tissues and organs. Furthermore, subdividing tissues into groups of cells with different identities is important for setting up organizer structures and therefore for appropriate growth and pattern formation. The wing imaginal disc of *Drosophila melanogaster* larvae provides an excellent model to study cell sorting during development. The wing imaginal disc tissue is subdivided into two groups of cells, the anterior and posterior compartments, which are separated by the A/P compartment boundary. This boundary is important for the proper patterning and morphogenesis of the wing imaginal disc tissue, so that it can form a functional adult wing of the correct size and shape. It is established by biochemical signals. The selector gene *engrailed* and the Hedgehog signaling pathway, which is induced by Engrailed, regulate cell segregation between the anterior and posterior compartment (Basler and Struhl 1994; Rodriguez and Basler 1997; Methot and Basler 1999; Dahmann and Basler 2000). Recent studies provide experimental evidence for mechanical processes being involved in the A/P boundary formation (Landsberg, Farhadifar et al. 2009; Aliee, Roper et al. 2012). Landsberg et al. showed that mechanical tension at cell bonds along the A/P boundary is increased 2.5-fold, compared to cell bonds away from it. Mechanical tension is increased as well at cell bonds along the D/V boundary, separating the dorsal and ventral compartment of the wing imaginal disc (Aliee, Roper et al. 2012). However, it remained unclear whether and how biochemical signals and mechanical processes act together to maintain a straight and functional A/P boundary. Here I show that Engrailed and the Hedgehog signaling pathway regulate the morphological signatures of, and the increase in mechanical tension along the A/P compartment boundary in the developing *Drosophila melanogaster* wing. I generated three different scenarios of Hh signal transduction activity patterns along the A/P compartment boundary and examined their impact on the morphological signatures, the shape of, and the increase in mechanical tension along the boundary. I show that the difference in Hh signal transduction activity along the A/P boundary is necessary and

sufficient for maintaining the shape, the morphological signatures and the increase in mechanical tension to ensure the formation of a functional A/P boundary. Furthermore, I show that the difference in Hh signal transduction activity is sufficient to induce smooth borders, to recapitulate the morphological signatures of boundary cells and to increase mechanical tension along ectopic boundaries. These morphological signatures and the increase in mechanical tension are also induced by the differential expression of the LRR-transmembrane protein Capricious along ectopic boundaries. These results indicate that the formation of smooth interfaces and the increase in mechanical tension could be a general feature of cell sorting events. Moreover, I provide experimental evidence that the increase in mechanical tension along the A/P boundary is not due to an "actomyosin-cable", as previously proposed (Major and Irvine 2005; Major and Irvine 2006; Monier, Pelissier-Monier et al. 2010), but rather generated locally at each cell bond. My results provide new insights into the interplay between biochemical signals and mechanical processes regulating cell sorting along tissue interfaces in developing animals.

9.2 DIFFERENCES IN HEDGEHOG SIGNAL TRANSDUCTION ACTIVITY AND ENGRAILED ARE IMPORTANT FOR THE FORMATION OF SMOOTH INTERFACES

The difference in Hh signal transduction activity along the A/P compartment boundary in the wing imaginal disc is due to the ability of anterior cells only to transduce the Hh signaling pathway. Posterior cells lack the receptor Patched and therefore cannot transduce the Hh signal. It has previously been shown that *smoothened* mutant clones, which cannot transduce the Hh signal, sort out from anterior cells and mix with posterior cells (Rodriguez and Basler 1997). According to this, Hh signal transduction activity is necessary for cell sorting between anterior and posterior cells. My results now show that the difference in Hh signal transduction activity along the A/P boundary is not only necessary, but also sufficient for the straight shape of the A/P boundary. Similar levels of Hh signal transduction activity in anterior and posterior cells lead to an increase in the roughness of the A/P boundary. In contrast, high Hh signal transduction activity in either the anterior or posterior compartment is sufficient to maintain the straight shape of the A/P boundary. Both, inactivating Hh in the whole tissue and increasing Hh signal transduction activity in the posterior compartment result in a rougher A/P boundary. However, no cell mixing was observed in both cases. Inactivating Hh in the whole tissue by using a temperature-sensitive *hh* allele and raising the larvae at restrictive temperature for 24-26h lowers the level of the Hh-target gene *dpp*. Dpp acts as a growth factor. Thus, inactivating Hh signaling presumably leads to less cell proliferation in the wing disc tissue. This is consistent with the observation, that inactivating Hh signaling leads to smaller wing discs compared to controls. Thus, the absence of cell

mixing along the compartment boundary could be due to less cell proliferation and the short time of Hh inactivation since it is assumed that cell proliferation could lead to cell mixing (Figure 8). However, elevation of Hh signal transduction activity via Engrailed-dependent expression of *ci* in the posterior compartment did not lead to cell mixing. In the latter case *ci* was expressed throughout development and Dpp was still expressed (Figure 18). Thus, a further reason for the absence of cell mixing in the experiments is that cell mixing does not occur at all or only very rarely during normal growth of the wing imaginal disc tissue. Live imaging of cultured wing imaginal discs followed by quantitative image analysis and cell tracking could reveal whether and if yes, how frequently cells of the same compartment intermingle. The absence of cell mixing along the A/P boundary when Hh signal transduction activity was equal between the anterior and posterior compartment could be also due to the differential expression of Engrailed in posterior cells, which could be sufficient to prevent cell mixing. The role of the differential expression of Engrailed could be tested by partly inactivating Engrailed in larval wing discs using a hypomorphic allele.

I was able to show as well that a difference in Hh signal transduction activity is sufficient to create smooth boundaries along ectopic interfaces. Overexpressing a constitutively active form of *ci* in a clone was sufficient to create a smooth clonal boundary. Furthermore, clones mutant for *engrailed* formed smooth interfaces towards surrounding posterior cells probably because of differential expression of *ci.* Expression of *ci* in posterior cells is inhibited by Engrailed. Thus, a loss in Engrailed leads to expression of *ci.* Nevertheless, Engrailed can mediate cell sorting in an Hh independent way since posterior clones mutant for *engrailed* and *ci* sort out from posterior cells and form smooth boundaries (Dahmann and Basler 2000) (Figure 35). The boundaries of clones double mutant for *engrailed* and *ci,* however, were not as smooth as the boundaries of *ci* overexpressing or *engrailed* mutant clones. Thus, the differential expression of Engrailed along clonal boundaries is sufficient to form smooth boundaries, but not to the same extend as the differential expression of Ci. Taken together, my results show that the difference in Hh signal transduction activity is necessary and sufficient to maintain a straight A/P compartment boundary. Additionally, the difference in Engrailed may mediate cell sorting in an Hh independent manner.

9.3 THE DIFFERENCE IN HEDGEHOG SIGNAL TRANSDUCTION ACTIVITY IS NECESSARY AND SUFFICIENT TO MAINTAIN THE MORPHOLOGICAL SIGNATURES OF THE AP BOUNDARY

In addition to the straight shape of the A/P boundary, boundary cells show distinct morphological signatures. The cells in the first row next to the A/P boundary of each compartment (A1,P1) show an increased apical cross section area and widened vertex angles between cell junctions compared to cells in the bulk of the tissue (Landsberg, Farhadifar et al. 2009). Widened vertex angles between junctions were shown to correlate with an increase in mechanical tension (Landsberg, Farhadifar et al. 2009). I now show that the difference in Hh signal transduction activity is necessary and sufficient for these morphological signatures. When the levels of Hh signal transduction activity between the anterior and posterior compartment are similar the apical cross section area of the boundary cells is no longer increased. Neither are the vertex angles between junctions along the A/P boundary. However, if Hh signal transduction activity is high in the posterior compartment only, the apical cross section area and the vertex angles are increased again. Cells along the interface of clones overexpressing Ci show an increase in apical cross section area and vertex angles as well. The differential expression of Engrailed along the A/P boundary is not sufficient for the increase in apical cross section area when the levels of Hh signal transduction activity were similar between anterior and posterior cells. Different levels of Engrailed are neither sufficient to induce an increase in apical cross section area of boundary cells along clonal interfaces. However, cells at the interface between *engrailed* mutant clones and posterior cells have increased vertex angles. This could be due to the de-repression of *ci* in the *engrailed* mutant clones or an Hh independent function of Engrailed. Boundary cells at the interface of *engrailed* and *ci* double mutant clones show values of vertex angles that lie in between the values of *engrailed* mutant and wild-type clones, indicating that this effect is mediated by Engrailed in an Hh-dependent and Hh–independent manner. Widened vertex angles correlate with the straight shape of the A/P boundary as well as with smooth clonal interfaces.

How the apical cross section area of cells along the A/P boundary is increased in response to the difference in Hh signal transduction activity and whether this is important for the shape and function of the A/P boundary is currently not understood. However, it indicates that the boundary cells have different mechanical properties from the cells away from the boundary.

9.4 THE DIFFERENCE IN HEDGEHOG SIGNAL TRANSDUCTION ACTIVITY IS NECESSARY AND SUFFICIENT FOR THE INCREASE IN F-ACTIN ALONG THE A/P BOUNDARY AND ALONG CLONAL INTERFACES

F-actin was found to be increased at cell junctions along the A/P and D/V compartment boundaries (Major and Irvine 2005; Major and Irvine 2006; Landsberg, Farhadifar et al. 2009). It was proposed that this increase in F-actin could physically prevent cell mixing along the A/P boundary by forming a "fence" (Major and Irvine 2005; Major and Irvine 2006; Monier, Pelissier-Monier et al. 2010). However, it was not clear how F-actin is up-regulated along the A/P boundary. My results show that a difference in Hh signal transduction activity is required and sufficient for the increase in F-actin along the A/P boundary. When the level of Hh signal transduction activity is similar in the first cell rows of the anterior and posterior compartment F-actin is not increased anymore. The differential expression of Engrailed which persists under these conditions is therefore not sufficient to increase F-actin along the A/P boundary. Increased levels of Hh signal transduction activity either in the anterior or posterior compartment are sufficient for the increase in F-actin along the A/P boundary. A differential expression of *ci* along clonal interfaces is sufficient as well for the increase of F-actin along clone borders. It will be interesting to identify the mechanisms by which the difference in Hh signal transduction activity regulates the increase of F-actin along the A/P boundary. It is also not completely understood whether the increase in F-actin is required for the shape of the A/P boundary and the increase in mechanical tension along the compartment boundaries. Even though F-actin is not increased anymore along the D/V boundary in late 3rd instar wing discs (Major and Irvine 2005; Major and Irvine 2006) mechanical tension is still increased (Aliee, Roper et al. 2012). Lowering the amount of F-actin without altering the levels of Hh signal transduction activity could help to understand whether the increase in F-actin along the compartment boundaries or clonal interfaces is required for the increase in mechanical tension.

9.5 THE DIFFERENCE IN HEDGEHOG SIGNAL TRANSDUCTION ACTIVITY IS NECESSARY AND SUFFICIENT TO INCREASE MECHANICAL TENSION ALONG THE A/P BOUNDARY

Mechanical tension is increased along the A/P compartment boundary in the *Drosophila* wing imaginal disc (Landsberg, Farhadifar et al. 2009). However, the role of the differential activity of the Hh signaling pathway for the increase in mechanical tension remained unclear. Here I show that the difference in Hh signal transduction activity along the A/P compartment

boundary is necessary and sufficient for the 2-fold increase in mechanical tension. Similarly high or low levels of Hh signal transduction activity between anterior and posterior cells result in the loss of increased mechanical tension along the boundary, whereas high Hh signal transduction activity in the posterior compartment only is sufficient for the 2-fold increase in mechanical tension. The differential expression of Engrailed has an indirect influence on the increase in mechanical tension along the A/P boundary via inducing the difference in Hh signal transduction activity between A and P cells. It is, however, not sufficient to increase mechanical tension along the A/P boundary. When the levels of Hh signal transduction activity are similar between anterior and posterior cells the relative mechanical tension at junctions along the A/P boundary is similar to the tension at junctions between cells of the same compartment. Differential expression of Ci along clonal boundaries is also sufficient to increase mechanical tension at such interfaces. Mechanical tension is increased as well along the interfaces of *engrailed* mutant clones in the posterior compartment, but this could be due to the additional difference in *ci* expression between the clonal cells and the surrounding posterior cells. It will be interesting to test whether the differential expression of Engrailed is sufficient to increase mechanical tension along clonal interfaces in an Hh-independent manner. To test this, measuring mechanical tension along clones unable to transduce the Hh signal, which abut the A/P boundary could be performed.

9.6 DIFFERENCES IN HEDGEHOG SIGNALING REGULATE THE STRAIGHT SHAPE, THE MORPHOLOGICAL SIGNATURES AND THE INCREASE IN MECHANICAL TENSION ALONG THE A/P COMPARTMENT BOUNDARY IN THE *DROSOPHILA* WING IMAGINAL DISC

Maintaining the straight shape of the A/P compartment boundary and preventing cell mixing between the adjacent compartments is crucial for the appropriate growth and development of the adult wing structure. The increase in mechanical tension, induced by Hedgehog signaling seems to be an effective boundary mechanism. Based on my results I propose a model in which differences in Hedgehog signal transduction activity regulate mechanical processes through Ci-mediated transcriptional response along the A/P boundary. Different levels of Hh signal transduction activity directly influence morphological signatures of, and the increase in mechanical tension along the A/P boundary (Figure 40). Differential expression of Engrailed along the A/P boundary leads to differential Hh signal transduction activity between the anterior and posterior compartment. The cells of the first row each in the anterior and posterior compartment appear to measure the differential Hh signal transduction activity via an unknown mechanism. This induces the boundary cells to enrich F-actin locally along the junctions facing the cells of the adjacent compartment. The increase

in F-actin subsequently results in an increase in mechanical tension along the junctions at the A/P boundary. The increase in F-actin always correlated with an increase in mechanical tension in my experiments. The increase in mechanical tension influences the shape of the boundary and the morphological signatures of the cells along the A/P boundary. An increase in mechanical tension always correlated with a straight boundary. When mechanical tension was not increased anymore, the boundary became more rough. Computer simulations already showed that the increase in mechanical tension could be sufficient to maintain a straight A/P boundary (Landsberg, Farhadifar et al. 2009) and, by that, eventually prevent cell mixing between the anterior and posterior compartment. The differential expression of Engrailed could also be important to maintain the straight shape of the boundary to some degree in an Hh independent manner (Dahmann and Basler 2000) (Figure 35). The increase in mechanical tension not only correlates with the straight shape of the boundary but also with widened vertex angles at cell junctions along the A/P boundary. However, it is not clear how the increase in mechanical tension leads to these morphological signatures and to what extend they correlate with each other.

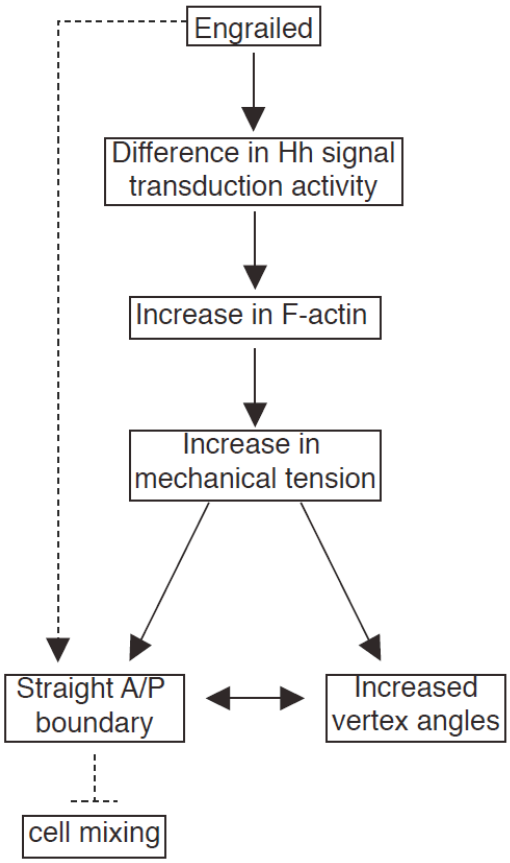

Figure 40: Model of how differences in Hh signal transduction activity between anterior and posterior cells could regulate mechanical tension along the A/P compartment boundary.
Expression of Engrailed in the posterior compartment induces differences in Hh signal transduction activity between anterior and posterior cells. Hh signal transduction is inhibited in the posterior compartment by Engrailed and therefore only anterior cells are able to transduce the Hh signal. The apposition of anterior cells with high and posterior cells with low levels of Hh signal transduction

activity along the A/P boundary leads to an increase in F-actin at the junctions along the A/P boundary via an unknown mechanism. The increase in F-actin mediates the local increase in mechanical tension at junctions along the A/P boundary, which leads to a straight shape of the boundary via increased vertex angles at cell junctions along the A/P boundary. Engrailed could also have a direct, Hh-independent effect on the straight shape of the A/P boundary (dashed line). Maintaining a straight A/P compartment boundary via the differential expression of Engrailed and the increase in mechanical tension mediated by the difference in Hh signal transduction activity between A and P cells eventually could be important to prevent cell mixing between cells of the anterior and posterior compartments (dashed line).

Moreover, it remains unclear how the difference in Hh signal transduction activity leads to an increase in mechanical tension along the A/P boundary. Schilling, Basler and von Mering proposed a model based on studies *in silico*, which could explain the increase in mechanical tension due to transcriptional response to the Hh pathway along the A/P compartment boundary (Schilling, Willecke et al. 2011). The Hh signaling pathway is active in several cell rows in the anterior compartment, and so is the transcriptional response displayed by *ptc* and *dpp* expression. However, mechanical tension is increased locally at cell junctions along the A/P boundary. Based on the vertex model (Farhadifar, Roper et al. 2007; Landsberg, Farhadifar et al. 2009) they coupled Hh production, diffusion and signal transduction to the physical properties of the cells in the tissue in their simulations. Schilling, Basler and van Mering suggested two possible scenarios in which the increase in tension along the A/P boundary is mediated either via heterotypic or homotypic binding of transmembrane proteins between adjacent anterior and posterior cells, mediated by an Hh dependent transcriptional response. The expression of different transmembrane proteins along the boundary would depend on anterior and posterior identities of the cells. The boundary cells would measure this heterotypic binding, which would lead to increased mechanical tension (Schilling, Willecke et al. 2011). However, they state that this model would not explain the sorting behaviour of anterior clones mutant for *smoothened* because their identity is not changed from anterior to posterior. They evaluated the possibility of the differential expression of one unknown transmembrane molecule, TMx, which forms homotypic bindings, which would be a direct target of the Hh pathway, but not part of it. The intracellular domain of such a protein could regulate the cortical actomyosin meshwork and by that increase in mechanical tension dependent on the amount of homotypic bindings at one cell bond compared to the other bonds of the cell. Therefore, the ratio and not the total level of TMx would lead to an increase in tension (Schilling, Willecke et al. 2011). They propose that when posterior cells with a low amount of TMx molecules are adjacent to anterior cells with many TMx molecules, the TMx molecules on the other bonds of the posterior cell will be recruited to the bond at the interface. The ratio of TMx distribution in the posterior cell would be measured and would eventually lead to an increase in mechanical tension in the posterior cells only (Schilling, Willecke et al. 2011). When implementing this into their model, they were able to

recapitulate the sorting of *smoothened* mutant clones *in silico.* My results are consistent with their model where it states, that a sudden difference in Hh signal transduction activity between two groups of cells is required for the increase in mechanical tension. The increase in mechanical tension at posterior cell bonds along the A/P boundary only would consequently mean that F-actin and Myosin II are also enriched only along the bonds of the posterior cells at the A/P boundary. Monier et. al. showed that Myosin II is enriched along anterior and posterior bonds along the parasegment boundary in the *Drosophila* embryo (Monier, Pelissier-Monier et al. 2010). We assume that this is also the case along the A/P boundary in the wing imaginal disc. However, the image resolution was not sufficient to confirm this assumption. Even though the Hh dependent differential expression of a single transmembrane protein along the A/P boundary could serve as an explanation for the Ci mediated increase in mechanical tension *in silico* no molecule is known so far which could take over this part *in vivo*. The cadherin Cad99C was found to be expressed along the A/P boundary in an Hh dependent manner, however the loss of Cad99C did not disrupt the compartment boundary (Schlichting, Demontis et al. 2005).

9.7 TENSION IS NOT TRANSMITTED BY AN ACTOMYOSIN CABLE

It was proposed that the actomyosin meshwork forms a “fence” or a “cable” along compartment boundaries to prevent cell mixing (Major and Irvine 2005; Major and Irvine 2006; Monier, Pelissier-Monier et al. 2010). If such a supra-cellular cable would exist, then tension should be transmitted between junctions along the A/P boundary. My results show that the increase in mechanical tension at cell bonds along the A/P boundary is generated locally at each cell bond and not transmitted between junctions along the A/P boundary. Thus, F-actin and Myosin II do not build up a fence or cable to prevent cell mixing along the A/P compartment boundary. However, it remains unclear how the increase in mechanical tension could prevent cell mixing along the A/P boundary. It will be interesting to test whether cell rearrangements are locally regulated by the increase in mechanical tension after cell division to prevent cell mixing.

9.8 DIFFERENTIAL EXPRESSION OF CAPRICIOUS IS SUFFICIENT TO CREATE SMOOTH INTERFACES, TO INDUCE MORPHOLOGICAL SIGNATURES AND TO INCREASE MECHANICAL TENSION ALONG ECTOPIC INTERFACES

The LRR-transmembrane protein Capricious was shown to be involved in the formation of the D/V boundary (Milan, Weihe et al. 2001). My results show that the differential expression of Capricious is sufficient to recapitulate all signatures of the A/P boundary at clonal interfaces. Clones overexpressing Caps had a smooth interface (Milan, Weihe et al. 2001) (Figure 37) and F-actin was enriched along clonal boundaries. The vertex angles at junctions between cells along the clone boundary were increased, as was the apical cross section area of wild-type boundary cells along the clonal interface. Furthermore, I could show that mechanical tension is increased along *capricious* overexpressing clones. Thus, the differential expression of this transmembrane protein is sufficient to create smooth interfaces and to increase mechanical tension. The differential expression of this transmembrane protein could thus mediate the increase in mechanical tension along the D/V compartment boundary.

9.9 CELL SORTING AT RHOMBOMERIC BOUNDARIES IN THE VERTEBRATE BRAIN

The heterotypic binding of Eph receptors to *ephrin* ligands was shown to mediate cell sorting in vertebrate brain development (Mellitzer, Xu et al. 1999; Xu, Mellitzer et al. 1999). Cell sorting along rhombomere boundaries in the hindbrain was proposed to be regulated either via repulsive interactions between EphA and ephrin B expressing cells (Mellitzer, Xu et al. 1999; Xu, Mellitzer et al. 1999) or via differential adhesive properties of cells of different rhombomeric identity (Cooke, Kemp et al. 2005; Kemp, Cooke et al. 2009). Recent studies show that F-actin and Myosin are enriched along rhombomeric boundaries in an Eph-ephrin signaling dependent manner (Calzolari, Terriente et al. 2014). They propose that EphA4a expression in odd rhombomers leads to the formation of the cable and that this actomyosin cable is required to prevent cell mixing along rhombomeric boundaries. Considering these results, it would be very interesting to test whether mechanical tension is increased at rhombomeric boundaries in the vertebrate hindbrain. This could tell whether the increase in mechanical tension mediated via the actomyosin meshwork is an evolutionary conserved mechanism to prevent cell mixing during animal embryonic development. However, it has to be tested as well whether an actomyosin cable is formed or whether mechanical tension is increased locally at the cell bonds along the rhombomeric boundaries. These results could also help to understand the increase in mechanical tension along the A/P and D/V

compartment boundary. It would be interesting to test whether Eph-ephrin signaling plays a role in compartment boundary formation in the *Drosophila* wing imaginal disc.

9.10 INTERPLAY BETWEEN BIOCHEMICAL SIGNALS AND MECHANICAL PROCESSES DURING ANIMAL DEVELOPMENT

Uncovering the interplay between biochemical signals and mechanical processes is crucial to understand morphogenetic processes during animal development (reviewed in Heisenberg and Bellaiche 2013). However, there are only a few examples where biochemical signaling pathways have been identified to regulate mechanical processes. In vertebrates the Wnt/Fz-PCP pathway was shown to regulate cell intercalations during germ-layer morphogenesis (reviewed in Roszko, Sawada et al. 2009)reviewed in Roszko, Sawada et al. 2009). Recent studies showed that Wnt/Fz mediated planar cell polarity is also involved in cell rearrangements during neural tube formation (Nishimura, Honda et al. 2012). The Fat/Ds-PCP pathway in *Drosophila* polarizes the myosin Dachs and thereby regulates tissue morphogenesis (Ambegaonkar, Pan et al. 2012; Bosveld, Bonnet et al. 2012; Brittle, Thomas et al. 2012). Another example for the interplay between biochemical signals and cellular mechanics is the process of axon guidance in the developing brain (reviewed by Dickson 2002). The growth cone, a special structure at the tip of axons and dendrites can be attracted or reppelled by extracellular signals. The growth cone is a highly motile structure, which forms actin-driven filopodia to move and to orientate itself (Bentley and Toroian-Raymond 1986; Chien, Rosenthal et al. 1993; Zheng, Wan et al. 1996; reviewed by Dickson 2002). It has been shown that Rho-GTPases regulate actomysoin dynamcis during axon guidance (Luo 2000; Lundquist, Reddien et al. 2001; Hakeda-Suzuki, Ng et al. 2002; Kishore and Sundaram 2002; Ng, Nardine et al. 2002). Moreover, Eph-signaling (Shamah, Lin et al. 2001) and regulation of Abl downstream of Slit-Robo signaling (Wong, Ren et al. 2001) were found to be involved in actin dynamics during axon guidance. However, my results provide the first evidence for the Hedgehog signaling pathway regulating mechanical processes along the A/P compartment boundary in the *Drosophila* wing imaginal disc to prevent cell mixing.

9.11 UNDERSTANDING CELL SORTING IS IMPORTANT FOR KNOWLEDGE ABOUT GENERATION OF DISEASES

Sorting of cells with different identities is not only important during animal development but also for preventing tumor growth and forming of metastases in adult organisms (reviewed in Batlle and Wilkinson 2012). The change of mechanical properties of cells plays an important role in tumor formation. In order to segregate from the tissue they originated from and to spread into other tissues and organs, tumor cells have to exclude themselves from the

integration inside the tissue. This process, called epithelial-to-mesenchymal transition (EMT), requires the loss of adhesive forces between the tumor cell and the surrounding tissue, which often involves the deregulation of E-cadherin (Thiery, Acloque et al. 2009). Metastatic cells were for example found to be more deformable than healthy cells (Cross, Jin et al. 2007). Attempts exist already to use this knowledge for clinical diagnosis (Remmerbach, Wottawah et al. 2009). Moreover, it has been shown that Eph-ephrin signaling plays a role in preventing colorectal, prostate and breast cancer (reviewed in Batlle and Wilkinson 2012) by maintaining tissue boundaries and therefore preventing the invasion of tumorous cells of a certain identity into an adjacent territory. The results of this thesis contribute to the understanding of the interplay between biochemical signals and mechanical processes during animal development. And thereby may help to examine medically relevant processes, like tumor formation and metastasis.

10 ACKNOWLEDGEMENTS

First of all, I would like to thank my supervisor Prof. Dr. Christian Dahmann for offering this exciting project to me. His support and input on all aspects of my project were always a great help and made the successful outcome of my project possible. I also would like to thank him for giving me the opportunity to present my results at several meetings of the scientific community.

Moreover, I would like to express my gratitude to Prof. Dr. Frank Jülicher for his great and valuable input on my project and for the numerous fruitful discussions.

I would like to thank Maryam Aliee for developing the algorithm to analyze the clonal roughness and for performing numerous simulations (not included in this thesis). I very much enjoyed the fruitful discussions with her.

I thank Prof. Dr. Stephan Grill and Peter Groß for kindly providing access to their laser ablation device. I thank Benoit Aigouy for sharing the Packing Analyzer software, that made the various image analyses possible. I thank Marco Milan for providing fly stocks.

I would like to thank the former lab members Jens-Christian Röper for introducing me to the laser ablation analysis, Ria Zengler for her great help and friendship and most of all, Daiki Umetsu for the uncountable discussions, his ideas, input, support and for his friendship.
Thanks to all of my colleagues for providing such a warm and motivating working atmosphere in our lab. I thank Franziska Aurich, Liyuan Sui, Cagdas Göktas, Katharina Landsberg, Veronika Faltin and Marcus Michel for their critical comments on my project, their support and friendship.

Moreover, I would like to thank my friends and my family for supporting and believing in me throughout the time of the project and during the writing process. Many thanks to Armine, Anke and Deborah for critical comments on the manuscript. Particularly, I thank my parents for their unconditional support, care and love.
Last but not least, I thank Stefan, who went with me through all the ups and downs during the last 10 years for his love, friendship and unlimited support.

11 REFERENCES

Aigouy, B., R. Farhadifar, et al. (2010). "Cell flow reorients the axis of planar polarity in the wing epithelium of Drosophila." Cell **142**(5): 773-786.

Alexandre, C., A. Baena-Lopez, et al. (2014). "Patterning and growth control by membrane-tethered Wingless." Nature **505**(7482): 180-185.

Alexandre, C., A. Jacinto, et al. (1996). "Transcriptional activation of hedgehog target genes in Drosophila is mediated directly by the cubitus interruptus protein, a member of the GLI family of zinc finger DNA-binding proteins." Genes & Development **10**(16): 2003-2013.

Aliee, M., J. C. Roper, et al. (2012). "Physical mechanisms shaping the Drosophila dorsoventral compartment boundary." Current biology : CB **22**(11): 967-976.

Ambegaonkar, A. A., G. Pan, et al. (2012). "Propagation of Dachsous-Fat planar cell polarity." Current biology : CB **22**(14): 1302-1308.

Baena-Lopez, L. A., X. Franch-Marro, et al. (2009). "Wingless promotes proliferative growth in a gradient-independent manner." Science signaling **2**(91): ra60.

Basler, K. and G. Struhl (1994). "Compartment boundaries and the control of Drosophila limb pattern by hedgehog protein." Nature **368**(6468): 208-214.

Batlle, E. and D. G. Wilkinson (2012). "Molecular mechanisms of cell segregation and boundary formation in development and tumorigenesis." Cold Spring Harbor perspectives in biology **4**(1): a008227.

Bentley, D. and A. Toroian-Raymond (1986). "Disoriented pathfinding by pioneer neurone growth cones deprived of filopodia by cytochalasin treatment." Nature **323**(6090): 712-715.

Bershadsky, A. (2004). "Magic touch: how does cell-cell adhesion trigger actin assembly?" Trends in cell biology **14**(11): 589-593.

Blair, S. S. (1992). "Engrailed expression in the anterior lineage compartment of the developing wing blade of Drosophila." Development **115**(1): 21-33.

Blair, S. S. (1993). "Mechanisms of compartment formation: evidence that non-proliferating cells do not play a critical role in defining the D/V lineage restriction in the developing wing of Drosophila." Development **119**(2): 339-351.

Blair, S. S. (1995). "Compartments and appendage development in Drosophila." BioEssays : news and reviews in molecular, cellular and developmental biology **17**(4): 299-309.

Blair, S. S. and A. Ralston (1997). "Smoothened-mediated Hedgehog signalling is required for the maintenance of the anterior-posterior lineage restriction in the developing wing of Drosophila." Development **124**(20): 4053-4063.

Bosveld, F., I. Bonnet, et al. (2012). "Mechanical control of morphogenesis by Fat/Dachsous/Four-jointed planar cell polarity pathway." Science **336**(6082): 724-727.

Brand, A. H. and N. Perrimon (1993). "Targeted gene expression as a means of altering cell fates and generating dominant phenotypes." Development **118**(2): 401-415.

Briscoe, J. and P. P. Therond (2013). "The mechanisms of Hedgehog signalling and its roles in development and disease." Nature reviews. Molecular cell biology **14**(7): 416-429.

Brittle, A., C. Thomas, et al. (2012). "Planar polarity specification through asymmetric subcellular localization of Fat and Dachsous." Current biology : CB **22**(10): 907-914.

Brodland, G. W. (2002). "The Differential Interfacial Tension Hypothesis (DITH): a comprehensive theory for the self-rearrangement of embryonic cells and tissues." Journal of biomechanical engineering **124**(2): 188-197.

Brodland, G. W. and H. H. Chen (2000). "The mechanics of heterotypic cell aggregates: insights from computer simulations." Journal of biomechanical engineering **122**(4): 402-407.

Calzolari, S., J. Terriente, et al. (2014). "Cell segregation in the vertebrate hindbrain relies on actomyosin cables located at the interhombomeric boundaries." The EMBO journal **33**(7): 686-701.

Capdevila, J. and I. Guerrero (1994). "Targeted expression of the signaling molecule decapentaplegic induces pattern duplications and growth alterations in Drosophila wings." The EMBO journal **13**(19): 4459-4468.

Chen, Y., S. Li, et al. (2010). "G protein-coupled receptor kinase 2 promotes high-level Hedgehog signaling by regulating the active state of Smo through kinase-dependent and kinase-independent mechanisms in Drosophila." Genes & Development **24**(18): 2054-2067.

Chien, C. B., D. E. Rosenthal, et al. (1993). "Navigational errors made by growth cones without filopodia in the embryonic Xenopus brain." Neuron **11**(2): 237-251.

Cooke, J. E., H. A. Kemp, et al. (2005). "EphA4 is required for cell adhesion and rhombomere-boundary formation in the zebrafish." Current biology : CB **15**(6): 536-542.

Couso, J. P., S. A. Bishop, et al. (1994). "The wingless signalling pathway and the patterning of the wing margin in Drosophila." Development **120**(3): 621-636.

Couso, J. P., E. Knust, et al. (1995). "Serrate and wingless cooperate to induce vestigial gene expression and wing formation in Drosophila." Current biology : CB **5**(12): 1437-1448.

Couso, J. P. and A. Martinez Arias (1994). "Notch is required for wingless signaling in the epidermis of Drosophila." Cell **79**(2): 259-272.

Cross, S. E., Y. S. Jin, et al. (2007). "Nanomechanical analysis of cells from cancer patients." Nature nanotechnology **2**(12): 780-783.

Dahmann, C. and K. Basler (1999). "Compartment boundaries: at the edge of development." Trends in genetics : TIG **15**(8): 320-326.

Dahmann, C. and K. Basler (2000). "Opposing Transcriptional Outputs of Hedgehog Signaling and Engrailed Control Compartmental Cell Sorting at the Drosophila A/P Boundary." Cell **100**(4): 411-422.

Dahmann, C., A. C. Oates, et al. (2011). "Boundary formation and maintenance in tissue development." Nature reviews. Genetics **12**(1): 43-55.

Denef, N., D. Neubuser, et al. (2000). "Hedgehog induces opposite changes in turnover and subcellular localization of patched and smoothened." Cell **102**(4): 521-531.

Diaz-Benjumea, F. J. and S. M. Cohen (1993). "Interaction between dorsal and ventral cells in the imaginal disc directs wing development in Drosophila." Cell **75**(4): 741-752.

Diaz-Benjumea, F. J. and S. M. Cohen (1995). "Serrate signals through Notch to establish a Wingless-dependent organizer at the dorsal/ventral compartment boundary of the Drosophila wing." Development **121**(12): 4215-4225.

Dickson, B. J. (2002). "Molecular mechanisms of axon guidance." Science **298**(5600): 1959-1964.

Doherty, D., G. Feger, et al. (1996). "Delta is a ventral to dorsal signal complementary to Serrate, another Notch ligand, in Drosophila wing formation." Genes & Development **10**(4): 421-434.

Eaton, S. and T. B. Kornberg (1990). "Repression of ci-D in posterior compartments of Drosophila by engrailed." Genes & Development **4**(6): 1068-1077.

Farhadifar, R., J. C. Roper, et al. (2007). "The influence of cell mechanics, cell-cell interactions, and proliferation on epithelial packing." Current biology : CB **17**(24): 2095-2104.

Foty, R. A. and M. S. Steinberg (2005). "The differential adhesion hypothesis: a direct evaluation." Developmental biology **278**(1): 255-263.

Fraser, S., R. Keynes, et al. (1990). "Segmentation in the chick embryo hindbrain is defined by cell lineage restrictions." Nature **344**(6265): 431-435.

Gale, N. W. and G. D. Yancopoulos (1997). "Ephrins and their receptors: a repulsive topic?" Cell Tissue Res **290**(2): 227-241.

Garcia-Bellido, A. (1975). "Genetic control of wing disc development in Drosophila." Ciba Found Symp **0**(29): 161-182.

Garcia-Bellido, A. and J. Moscoso del Pradio (1979). "Genetic analysis of maternal information in Drosophila." Nature **278**(5702): 346-348.

Garcia-Bellido, A., P. Ripoll, et al. (1973). "Developmental compartmentalisation of the wing disk of Drosophila." Nat New Biol **245**(147): 251-253.

Garcia-Bellido, A., P. Ripoll, et al. (1976). "Developmental compartmentalization in the dorsal mesothoracic disc of Drosophila." Developmental biology **48**(1): 132-147.

Gates, J. and M. Peifer (2005). "Can 1000 reviews be wrong? Actin, alpha-Catenin, and adherens junctions." Cell **123**(5): 769-772.

Gilbert, S. F. (2000). Developmental Biology.6th edition, Sunderland (MA), Sinauer Associates.

Giraldez, A. J. and S. M. Cohen (2003). "Wingless and Notch signaling provide cell survival cues and control cell proliferation during wing development." Development **130**(26): 6533-6543.

Godt, D. and U. Tepass (1998). "Drosophila oocyte localization is mediated by differential cadherin-based adhesion." Nature **395**(6700): 387-391.

Golic, K. G. (1991). "Site-specific recombination between homologous chromosomes in Drosophila." Science **252**(5008): 958-961.

Golic, K. G. and S. Lindquist (1989). "The FLP recombinase of yeast catalyzes site-specific recombination in the Drosophila genome." Cell **59**(3): 499-509.

Gustavson, E., A. S. Goldsborough, et al. (1996). "The Drosophila engrailed and invected genes: partners in regulation, expression and function." Genetics **142**(3): 893-906.

Hakeda-Suzuki, S., J. Ng, et al. (2002). "Rac function and regulation during Drosophila development." Nature **416**(6879): 438-442.

Harris, A. K. (1976). "Is Cell sorting caused by differences in the work of intercellular adhesion? A critique of the Steinberg hypothesis." Journal of theoretical biology **61**(2): 267-285.

Heisenberg, C. P. and Y. Bellaiche (2013). "Forces in tissue morphogenesis and patterning." Cell **153**(5): 948-962.

Hidalgo, A. (1994). "Three distinct roles for the engrailed gene in Drosophila wing development." Current biology : CB **4**(12): 1087-1098.

Hooper, J. E. and M. P. Scott (1989). "The Drosophila patched gene encodes a putative membrane protein required for segmental patterning." Cell **59**(4): 751-765.

Irvine, K. D. and C. Rauskolb (2001). "Boundaries in development: formation and function." Annual review of cell and developmental biology **17**: 189-214.

Irvine, K. D. and E. Wieschaus (1994). "fringe, a Boundary-specific signaling molecule, mediates interactions between dorsal and ventral cells during Drosophila wing development." Cell **79**(4): 595-606.

Jafar-Nejad, H., A. C. Tien, et al. (2006). "Senseless and Daughterless confer neuronal identity to epithelial cells in the Drosophila wing margin." Development **133**(9): 1683-1692.

Jamora, C. and E. Fuchs (2002). "Intercellular adhesion, signalling and the cytoskeleton." Nature cell biology **4**(4): E101-108.

Jiang, J. and M. Levine (1993). "Binding affinities and cooperative interactions with bHLH activators delimit threshold responses to the dorsal gradient morphogen." Cell **72**(5): 741-752.

Kalderon, D. (2004). "Hedgehog signaling: Costal-2 bridges the transduction gap." Current biology : CB **14**(2): R67-69.

Kalo, M. S. and E. B. Pasquale (1999). "Signal transfer by eph receptors." Cell Tissue Res **298**(1): 1-9.

Kemp, H. A., J. E. Cooke, et al. (2009). "EphA4 and EfnB2a maintain rhombomere coherence by independently regulating intercalation of progenitor cells in the zebrafish neural keel." Dev Biol **327**(2): 313-326.

Kemp, H. A., J. E. Cooke, et al. (2009). "EphA4 and EfnB2a maintain rhombomere coherence by independently regulating intercalation of progenitor cells in the zebrafish neural keel." Developmental biology **327**(2): 313-326.

Kim, J., K. D. Irvine, et al. (1995). "Cell recognition, signal induction, and symmetrical gene activation at the dorsal-ventral boundary of the developing Drosophila wing." Cell **82**(5): 795-802.

Kishore, R. S. and M. V. Sundaram (2002). "ced-10 Rac and mig-2 function redundantly and act with unc-73 trio to control the orientation of vulval cell divisions and migrations in Caenorhabditis elegans." Developmental biology **241**(2): 339-348.

Klein, T. and A. M. Arias (1998). "Interactions among Delta, Serrate and Fringe modulate Notch activity during Drosophila wing development." Development **125**(15): 2951-2962.

Kornberg, T., I. Siden, et al. (1985). "The engrailed locus of Drosophila: in situ localization of transcripts reveals compartment-specific expression." Cell **40**(1): 45-53.

Landsberg, K. P., R. Farhadifar, et al. (2009). "Increased cell bond tension governs cell sorting at the Drosophila anteroposterior compartment boundary." Current biology : CB **19**(22): 1950-1955.

Langenberg, T. and M. Brand (2005). "Lineage restriction maintains a stable organizer cell population at the zebrafish midbrain-hindbrain boundary." Development **132**(14): 3209-3216.

Lawrence, P. A. (1973). "Maintenance of boundaries between developing organs in insects." Nat New Biol **242**(114): 31-32.

Lawrence, P. A. and G. Struhl (1982). "Further studies of the engrailed phenotype in Drosophila." The EMBO journal **1**(7): 827-833.

Lawrence, P. A. and G. Struhl (1996). "Morphogens, compartments, and pattern: lessons from drosophila?" Cell **85**(7): 951-961.

Lecuit, T. and P. F. Lenne (2007). "Cell surface mechanics and the control of cell shape, tissue patterns and morphogenesis." Nature reviews. Molecular cell biology **8**(8): 633-644.

Lee, J. J., D. P. von Kessler, et al. (1992). "Secretion and localized transcription suggest a role in positional signaling for products of the segmentation gene hedgehog." Cell **71**(1): 33-50.

Li, S., Y. Chen, et al. (2012). "Hedgehog-regulated ubiquitination controls smoothened trafficking and cell surface expression in Drosophila." PLoS biology **10**(1): e1001239.

Lundquist, E. A., P. W. Reddien, et al. (2001). "Three C. elegans Rac proteins and several alternative Rac regulators control axon guidance, cell migration and apoptotic cell phagocytosis." Development **128**(22): 4475-4488.

Luo, L. (2000). "Rho GTPases in neuronal morphogenesis." Nature reviews. Neuroscience **1**(3): 173-180.

Ma, C., Y. Zhou, et al. (1993). "The segment polarity gene hedgehog is required for progression of the morphogenetic furrow in the developing Drosophila eye." Cell **75**(5): 927-938.

Major, R. J. and K. D. Irvine (2005). "Influence of Notch on dorsoventral compartmentalization and actin organization in the Drosophila wing." Development **132**(17): 3823-3833.

Major, R. J. and K. D. Irvine (2006). "Localization and requirement for Myosin II at the dorsal-ventral compartment boundary of the Drosophila wing." Developmental dynamics : an official publication of the American Association of Anatomists **235**(11): 3051-3058.

Major, R. J. and K. D. Irvine (2006). "Localization and requirement for Myosin II at the dorsal-ventral compartment boundary of the Drosophila wing." Dev Dyn **235**(11): 3051-3058.

Martinez Arias, A. (2003). "Wnts as morphogens? The view from the wing of Drosophila." Nature reviews. Molecular cell biology **4**(4): 321-325.

Martinez-Arias, A. and P. A. Lawrence (1985). "Parasegments and compartments in the Drosophila embryo." Nature **313**(6004): 639-642.

Maschat, F., N. Serrano, et al. (1998). "engrailed and polyhomeotic interactions are required to maintain the A/P boundary of the Drosophila developing wing." Development **125**(15): 2771-2780.

McNeill, H. (2000). "Sticking together and sorting things out: adhesion as a force in development." Nature reviews. Genetics **1**(2): 100-108.

Mellitzer, G., Q. Xu, et al. (1999). "Eph receptors and ephrins restrict cell intermingling and communication." Nature **400**(6739): 77-81.

Methot, N. and K. Basler (1999). "Hedgehog controls limb development by regulating the activities of distinct transcriptional activator and repressor forms of Cubitus interruptus." Cell **96**(6): 819-831.

Methot, N. and K. Basler (2000). "Suppressor of fused opposes hedgehog signal transduction by impeding nuclear accumulation of the activator form of Cubitus interruptus." Development **127**(18): 4001-4010.

Milan, M., L. Perez, et al. (2002). "Short-range cell interactions and cell survival in the Drosophila wing." Developmental cell **2**(6): 797-805.

Milan, M., U. Weihe, et al. (2001). "The LRR proteins capricious and Tartan mediate cell interactions during DV boundary formation in the Drosophila wing." Cell **106**(6): 785-794.

Mohler, J. and K. Vani (1992). "Molecular organization and embryonic expression of the hedgehog gene involved in cell-cell communication in segmental patterning of Drosophila." Development **115**(4): 957-971.

Monier, B., A. Pelissier-Monier, et al. (2010). "An actomyosin-based barrier inhibits cell mixing at compartmental boundaries in Drosophila embryos." Nature cell biology **12**(1): 60-65; sup pp 61-69.

Morata, G. and P. A. Lawrence (1975). "Control of compartment development by the engrailed gene in Drosophila." Nature **255**(5510): 614-617.

Nakano, Y., I. Guerrero, et al. (1989). "A protein with several possible membrane-spanning domains encoded by the Drosophila segment polarity gene patched." Nature **341**(6242): 508-513.

Neumann, C. J. and S. M. Cohen (1997). "Long-range action of Wingless organizes the dorsal-ventral axis of the Drosophila wing." Development **124**(4): 871-880.

Ng, J., T. Nardine, et al. (2002). "Rac GTPases control axon growth, guidance and branching." Nature **416**(6879): 442-447.

Ng, M., F. J. Diaz-Benjumea, et al. (1996). "Specification of the wing by localized expression of wingless protein." Nature **381**(6580): 316-318.

Nishimura, T., H. Honda, et al. (2012). "Planar cell polarity links axes of spatial dynamics in neural-tube closure." Cell **149**(5): 1084-1097.

Nolo, R., L. A. Abbott, et al. (2000). "Senseless, a Zn finger transcription factor, is necessary and sufficient for sensory organ development in Drosophila." Cell **102**(3): 349-362.

Oswald, F. (2010). A precise and rapid UV laser ablation system for cell biology. Institut für Biophysik, Prof. Petra Schwille, Fak. Mathematik und Naturwissenschaften. Dresden, TU Dresden. **Dipl.Physicist**.

Padgett, R. W., R. D. St Johnston, et al. (1987). "A transcript from a Drosophila pattern gene predicts a protein homologous to the transforming growth factor-beta family." Nature **325**(6099): 81-84.

Panin, V. M., V. Papayannopoulos, et al. (1997). "Fringe modulates Notch-ligand interactions." Nature **387**(6636): 908-912.

Price, S. R., N. V. De Marco Garcia, et al. (2002). "Regulation of motor neuron pool sorting by differential expression of type II cadherins." Cell **109**(2): 205-216.

Remmerbach, T. W., F. Wottawah, et al. (2009). "Oral cancer diagnosis by mechanical phenotyping." Cancer research **69**(5): 1728-1732.

Robbins, D. J., K. E. Nybakken, et al. (1997). "Hedgehog elicits signal transduction by means of a large complex containing the kinesin-related protein costal2." Cell **90**(2): 225-234.

Rodriguez, I. and K. Basler (1997). "Control of compartmental affinity boundaries by hedgehog." Nature **389**(6651): 614-618.

Roszko, I., A. Sawada, et al. (2009). "Regulation of convergence and extension movements during vertebrate gastrulation by the Wnt/PCP pathway." Seminars in cell & developmental biology **20**(8): 986-997.

Ruel, L., A. Gallet, et al. (2007). "Phosphorylation of the atypical kinesin Costal2 by the kinase Fused induces the partial disassembly of the Smoothened-Fused-Costal2-Cubitus interruptus complex in Hedgehog signalling." Development **134**(20): 3677-3689.

Rulifson, E. J. and S. S. Blair (1995). "Notch regulates wingless expression and is not required for reception of the paracrine wingless signal during wing margin neurogenesis in Drosophila." Development **121**(9): 2813-2824.

Sanicola, M., J. Sekelsky, et al. (1995). "Drawing a stripe in Drosophila imaginal disks: negative regulation of decapentaplegic and patched expression by engrailed." Genetics **139**(2): 745-756.

Sato, A., T. Kojima, et al. (1999). "Dfrizzled-3, a new Drosophila Wnt receptor, acting as an attenuator of Wingless signaling in wingless hypomorphic mutants." Development **126**(20): 4421-4430.

Schilling, S., M. Willecke, et al. (2011). "Cell-sorting at the A/P boundary in the Drosophila wing primordium: a computational model to consolidate observed non-local effects of Hh signaling." PLoS computational biology **7**(4): e1002025.

Schindelin, J., I. Arganda-Carreras, et al. (2012). "Fiji: an open-source platform for biological-image analysis." Nature methods **9**(7): 676-682.

Schlichting, K., F. Demontis, et al. (2005). "Cadherin Cad99C is regulated by Hedgehog signaling in Drosophila." Developmental biology **279**(1): 142-154.

Shamah, S. M., M. Z. Lin, et al. (2001). "EphA receptors regulate growth cone dynamics through the novel guanine nucleotide exchange factor ephexin." Cell **105**(2): 233-244.

Shen, J. and C. Dahmann (2005). "The role of Dpp signaling in maintaining the Drosophila anteroposterior compartment boundary." Developmental biology **279**(1): 31-43.

Shi, Q., S. Li, et al. (2011). "The Hedgehog-induced Smoothened conformational switch assembles a signaling complex that activates Fused by promoting its dimerization and phosphorylation." Development **138**(19): 4219-4231.

Shishido, E. (1998). "Drosophila Synapse Formation: Regulation by Transmembrane Protein with Leu-Rich Repeats, CAPRICIOUS." Science **280**(5372): 2118-2121.

Shishido, E., M. Takeichi, et al. (1998). "Drosophila synapse formation: regulation by transmembrane protein with Leu-rich repeats, CAPRICIOUS." Science **280**(5372): 2118-2121.

Sivasankaran, R., M. Calleja, et al. (2000). "The Wingless target gene Dfz3 encodes a new member of the Drosophila Frizzled family." Mechanisms of development **91**(1-2): 427-431.

Steinberg, M. S. (1963). "Reconstruction of tissues by dissociated cells. Some morphogenetic tissue movements and the sorting out of embryonic cells may have a common explanation." Science **141**(3579): 401-408.

Tabata, T., S. Eaton, et al. (1992). "The Drosophila hedgehog gene is expressed specifically in posterior compartment cells and is a target of engrailed regulation." Genes & Development **6**(12B): 2635-2645.

Tabata, T. and T. B. Kornberg (1994). "Hedgehog is a signaling protein with a key role in patterning Drosophila imaginal discs." Cell **76**(1): 89-102.

Tabata, T., C. Schwartz, et al. (1995). "Creating a Drosophila wing de novo, the role of engrailed, and the compartment border hypothesis." Development **121**(10): 3359-3369.

Taniguchi, H., E. Shishido, et al. (2000). "Functional dissection of drosophila capricious: its novel roles in neuronal pathfinding and selective synapse formation." Journal of neurobiology **42**(1): 104-116.

Thiery, J. P., H. Acloque, et al. (2009). "Epithelial-mesenchymal transitions in development and disease." Cell **139**(5): 871-890.

Townes, P. L. and J. Holtfreter (1955). "Directed movements and selective adhesion of embryonic amphibian cells." J Exp Zoolog A: Comp Exp Biol **128**: 53-120.

Uehata, M., T. Ishizaki, et al. (1997). "Calcium sensitization of smooth muscle mediated by a Rho-associated protein kinase in hypertension." Nature **389**(6654): 990-994.

Weigmann, K., R. Klapper, et al. (2003). "FlyMove--a new way to look at development of Drosophila." Trends Genet **19**(6): 310-311.

Williams, J. A., S. W. Paddock, et al. (1993). "Pattern formation in a secondary field: a hierarchy of regulatory genes subdivides the developing Drosophila wing disc into discrete subregions." Development **117**(2): 571-584.

Winter, C. G., B. Wang, et al. (2001). "Drosophila Rho-associated kinase (Drok) links Frizzled-mediated planar cell polarity signaling to the actin cytoskeleton." Cell **105**(1): 81-91.

Wong, K., X. R. Ren, et al. (2001). "Signal transduction in neuronal migration: roles of GTPase activating proteins and the small GTPase Cdc42 in the Slit-Robo pathway." Cell **107**(2): 209-221.

Xia, R., H. Jia, et al. (2012). "USP8 promotes smoothened signaling by preventing its ubiquitination and changing its subcellular localization." PLoS biology **10**(1): e1001238.

Xu, Q., G. Mellitzer, et al. (1999). "In vivo cell sorting in complementary segmental domains mediated by Eph receptors and ephrins." Nature **399**(6733): 267-271.

Zecca, M., K. Basler, et al. (1995). "Sequential organizing activities of engrailed, hedgehog and decapentaplegic in the Drosophila wing." Development **121**(8): 2265-2278.

Zecca, M., K. Basler, et al. (1996). "Direct and long-range action of a wingless morphogen gradient." Cell **87**(5): 833-844.

Zhang, W., Y. Zhao, et al. (2005). "Hedgehog-regulated Costal2-kinase complexes control phosphorylation and proteolytic processing of Cubitus interruptus." Developmental cell **8**(2): 267-278.

Zhang, Y., F. Mao, et al. (2011). "Transduction of the Hedgehog signal through the dimerization of Fused and the nuclear translocation of Cubitus interruptus." Cell research **21**(10): 1436-1451.

Zhao, Y., C. Tong, et al. (2007). "Hedgehog regulates smoothened activity by inducing a conformational switch." Nature **450**(7167): 252-258.

Zheng, J. Q., J. J. Wan, et al. (1996). "Essential role of filopodia in chemotropic turning of nerve growth cone induced by a glutamate gradient." The Journal of neuroscience : the official journal of the Society for Neuroscience **16**(3): 1140-1149.

Zhou, Q. and D. Kalderon (2011). "Hedgehog activates fused through phosphorylation to elicit a full spectrum of pathway responses." Developmental cell **20**(6): 802-814.

Hiermit versichere ich, dass ich die vorliegende Arbeit ohne unzulässige Hilfe Dritter und ohne Benutzung anderer als der angegebenen Hilfsmittel angefertigt habe; die aus fremden Quellen direkt oder indirekt übernommenen Gedanken sind als solche kenntlich gemacht. Die Arbeit wurde bisher weder im Inland noch im Ausland in gleicher oder ähnlicher Form einer anderen Prüfungsbehörde vorgelegt.

Die Dissertation wurde unter der wissenschaftlichen Betreuung von Prof. Dr. Christian Dahmann am Lehrstuhl für Systembiologie und Genetik, Institut für Genetik, an der Fakultät Mathematik und Naturwissenschaften der TU Dresden angefertigt.

Ich erkenne die Promotionsordnung der Fakultät Mathematik und Naturwissenschaften der TU Dresden an.

Dresden, den 11.06.2014

Katrin Rudolf